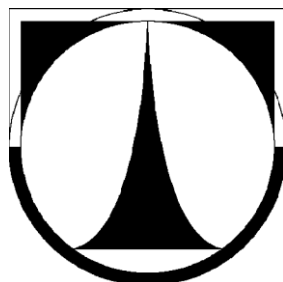


TECHNICKÁ UNIVERZITA V LIBERCI

Faculta textilní



Studijní program: Textilní inženýrství

Studijní obor: Textilní technika

**NEW METHODS IN THE STUDY OF ROLLER
ELECTROSPINNING MECHANISM**

Author: MSc. Fatma Yener

Supervisor Prof. RNDr. Oldřich Jirsák, CSc.

DOKTORSKÁ PRÁCE

2014

Název disertační :	New methods in the study of roller electrospinning mechanism
Autor:	MSc. Fatma Yener
Obor doktorského studia:	Textilní technika
Forma studia:	Full-time
Školící pracoviště:	Department of Nonwoven and Nanofibrous Materials
Školitel:	RNDr. Oldřich Jirsák, CSc.
Počet stránek textu:	136
Počet obrázků:	77
Počet tabulek	22

NEW METHODS IN THE STUDY OF ROLLER ELECTROSPINNING MECHANISM

Acknowledgement

Foremost, I would like to express my deepest gratitude to my supervisor Prof. Oldrich JIRSAK for the continuous support of my Ph.D study and research, for his excellent guidance, patience, caring, motivation, enthusiasm, providing me with an excellent atmosphere for doing research and immense knowledge. His guidance helped me in all the time of research and writing of this thesis.

I want to thank Nonwoven Department of Textile Engineering Faculty, Technical University of Liberec in Czech Republic for providing work conditions such as laboratory, devices etc. I would like to thank all very open, kind and friendly people in the department for their helps. I would like to thank Baturalp YALCINKAYA, who as a good friend was always willing to help and give his best suggestions. Last, but not the least I want to thank all of my family back in Turkey.

Declaration by the author

"I hereby declare that this submission is my own work and that, to the best of my knowledge and belief, it contains no material previously published or written by another person nor material which has been accepted for the award of any other degree or diploma of the university or other institute of higher learning, except where due acknowledgment has been made in the text.

Liberec

07.04.2014

MSc. Fatma YENER

Certificate from supervisor

This is to certify that the thesis entitled “NEW METHODS IN THE STUDY OF ROLLER ELECTROSPINNING MECHANISM” submitted by Fatma Yener to Technical university of Liberec for the award of the degree of Doctor of Philosophy is a bona fide record of the research work carried out by her under my supervision and guidance. The content of the thesis, in full or parts have not been submitted to any other Institute or University for the award of any other degree or diploma.

Liberec

07.04.2014

Prof. Oldrich JIRSAK

Anotace

Ve srovnání s jehlovým elektrostatickým zvlákňováním je bezjehlové zvlákňování novější technologií; z toho důvodu nebyly dosud parametry bezjehlového zvlákňování v celé šíři identifikovány a definovány. Některé závislé parametry byly definovány v předešlých pracích. Teoreticky i experimentálně byly také studovány vztahy mezi vybranými nezávislými a závislými parametry, jak je popsáno v teoretické části práce. Některé parametry však dosud nebyly studovány, jako například: geometrie zvlákňovacího zařízení a vlastnosti a rychlost otáčení válcové zvlákňovací elektrody. Ze závislých parametrů byly definovány pouze některé (zvlákňovací výkon, průměry vláken a jejich distribuce, kvalita nanovlákněné vrstvy

V této práci byly definovány a studovány další parametry procesu elektrostatického zvlákňování, zejména elektrický proud protékající zařízením a jednotlivými polymerními tryskami, rychlost rotace válcové zvlákňovací elektrody, síla působící na polymerní trysku, vzdálenost mezi polymerními tryskami, zvlákňovací plocha na elektrodě, délka polymerních trysek a čas jejich formování, přičemž tyto parametry byly studovány na dvou různých polymerních roztocích – vodném roztoku polyetylenoxidu (PEO) a nevodném roztoku polyuretanu (PU). Byly použity dva typy solí – tetraethylamoniumbromid (TEAB) a chlorid lithný (LiCl).

Experimentální část práce sestává ze tří dílů. V prvním dílu jsou studovány vztahy mezi elektrickými proudy při jehlovém, tyčovém a válcovém elektrostatickém zvlákňování. Při jehlovém elektrostatickém zvlákňování elektrický proud nezávisí na relativní vlhkosti okolního vzduchu v širokém intervalu 20-80 %. U válcového zvlákňování ovlivňuje relativní vlhkost vzduchu v zařízení zvlákňovací výkon, zvláště četnost polymerních trysek na zvlákňovací ploše, a tím i celkový elektrický proud. Bylo rovněž zjištěno, že při jehlovém zvlákňování se elektrický proud zvyšuje s rostoucí délkou vysunutí jehly z nabitě elektrody vlivem intenzivnější tvorby plasmových částic na delším úseku jehly. Byly stanoveny vztahy pro proud připadající na jednu polymerní trysku a pro vzdálenost mezi tryskami.

V druhém dílu experimentální části byly stanoveny hranice koncentrací polymeru a solí pro hlavní experimenty. Pro PEO byla vybrána koncentrace polymeru 6 %. U PU byla akceptována optimální koncentrace 17.5 % popsána v literatuře. Stanovena zde však byla maximální koncentrace LiCl 0.056 mol na litr. Vzhledem k tomu, že obsah solí zvyšuje viskozitu roztoku polyuretanu a tím i průměr vytvořených vláken, byla volena takto nízká maximální koncentrace.

Ve třetím dílu experimentální části byly studovány vztahy mezi vybranými nezávislými a závislými parametry elektrostatického zvlákňování. Z nezávislých parametrů byly vybrány rychlost rotace zvlákňovací válcové elektrody a obsah solí v polymerních roztocích. Bylo zjištěno, že rychlost rotace zvlákňovací elektrody a tím daná rychlost dávkování roztoku do zvlákňovacího pole ovlivňuje produktivitu procesu i kvalitu vytvořených vláken. Dále byla studována zvlákňovitost roztoků PU a PEO a jejich chování při zvlákňování s ohledem na obsah solí. Bylo zjištěno, že přídavek solí snižuje zvlákňovací výkon PEO, zatímco zvyšuje zvlákňovací výkon u roztoku polyuretanu. Tyto rozdíly byly vysvětleny na základě interakcí jednotlivých polymerů se solemi a na základě “leaky” dielektrického modelu.

Klíčová slova: Elektrostatické zvlákňování, polyuretan, polyetylenoxid, závislé parametry, nezávislé parametry, rychlost otáčení válce, elektrický proud

Abstract

Needleless roller electrospinning is a new technique when compared with needle electrospinning; therefore, parameters of needleless electrospinning have not yet been fully identified and defined. Some dependent parameters were defined in previous works. Relations between selected independent and selected dependent parameters were studied, as it is shown in theoretical part, both experimentally and theoretically. Not all the parameters were defined and studied yet, such as: spinner geometry, roller properties, roller velocity. Only few dependent parameters were defined (throughput, fiber diameter and diameter distribution, quality of nanofiber layer and some others).

It is the aim of this work to continue in study of relations between independent and dependent parameters of needleless electrospinning and to enlarge the knowledge of its mechanism. To reach the goal, further independent and dependent process parameters will be defined and the methods of their measurement developed. The relations between selected parameters will be studied.

In this work, the parameters such as current, current per jet, rotating roller speed, force acting on a jet, distance between jets, spinning area on the roller surface, length of jets and launching time of jets were studied for the aqueous polymer solution of polyethylene oxide (PEO) and for the non-aqueous solution of polyurethane (PU). Two various kinds of salts such as tetraethylene ammonium bromide (TEAB) and lithium chloride (LiCl) were used to determine the effects of salts on the process.

The experimental part of this thesis consists of three chapters. In the first chapter, the relations between the current measurements in the needle-, rod- and roller electrospinning are studied. In the needle electrospinning process, the current does not depend on the relative humidity of the surrounding air within broad limits of 20–80%. In the case of roller electrospinning, the relative humidity inside the spinning device affects the spinning performance, especially the number of jets per spinning area, and therefore also the total current. It was also found that in the needle electrospinning, the current increases with increasing needle protrusion length due to more intensive creation of plasma particles. The relations for current per one jet and for the distance between jets were determined.

In the second chapter, the limits of polymer concentrations and salt concentrations in the polymer solutions were determined for the main group of experiments in the chapter three.

6 wt. % was selected as optimum concentration of PEO solution. In the case of PU, the optimum polymer concentration 17.5 wt. % was accepted from literature. In this case, the amount of salt was determined. 0.056 mol per liter LiCl was chosen as the upper limit for PU because the viscosity of PU solution as well as the diameter of produced fibers increases with increasing salt content. For this reason, low amounts of salt were used for PU solutions.

In the third part, the relations between selected independent and dependent electrospinning parameters described in theoretical part are studied. The velocity of spinning roller and the content of salts in the solutions were chosen as independent process parameters. It was found that the velocity of rotating roller which is related to the feed rate, affects the spinning performance as well as the quality of fibers. The spinnability and spinning behavior of PU and PEO solutions depending on the salt content were also studied. It was found that adding salt decreases spinning performance of PEO solution whereas it increases spinning performance of PU solution. These differences were explained by interactions of polymers with salts and by the “leaky” dielectric model.

Keywords: Electrospinning, polyurethane, poly (ethylene oxide), dependent parameters, independent parameters, roller speed, electric current.

CONTENT

Anotace.....	4
Abstract	5
LIST OF SYMBOLS	8
LIST OF FIGURES.....	15
LIST OF TABLES	20
1. INTRODUCTION.....	22
1.1. HISTORY.....	23
1.2. APPLICATIONS OF NANOFIBERS	24
1.3. AIM OF THE WORK	25
2. THEORETICAL PART.....	26
2.1. PRINCIPLES OF ELECTROSPINNING.....	26
2.2. TECHNOLOGIES OF NANOFIBER PRODUCTION.....	27
2.2.1. Needle Electrospinning.....	27
2.2.2. Meltblown system.....	28
2.2.3. Centrifugal electrospinning.....	29
2.2.4. Bi-component fibers	30
2.2.5. Drawing method	31
2.2.6. Roller electrospinning.....	31
2.2.7. Stationary wire electrospinning	32
2.3. PARAMETERS OF ELECTROSPINNING.....	33
2.3.1. PARAMETERS DESCRIBED IN LITERATURE	34
2.3.1.1. Independent Parameters.....	34
2.3.1.1.1. Concentration/Molecular Weight /Viscosity	34
2.3.1.1.2. Surface Tension.....	39
2.3.1.1.3. Conductivity and permittivity.....	39
2.3.1.1.4. Applied voltage	41
2.3.1.1.5. Distance between electrodes.....	42
2.3.1.1.6. Ambient conditions	43
2.3.1.1.7. Velocity of take-up fabric.....	43
2.3.1.1.8. Geometry of electrodes.....	43

2.3.1.1.9. Geometry and conductivity of collector electrode.....	45
2.3.1.2. Dependent parameters.....	46
2.3.1.2.1. Number of cones.....	46
2.3.1.2.2. Jet length.....	46
2.3.1.2.3. Spinning performance and spinning performance per jet	47
2.3.1.2.4. Fiber diameter and fiber diameter distribution	48
2.3.1.2.5. Non-fibrous area.....	48
2.3.1.2.6. Life time of a jet	49
2.3.1.2.7. Measurement of current.....	49
2.3.1.2.8. Launching time of jet.....	51
2.3.2. THE NEW PARAMETERS INTRODUCED BY AUTHOR	51
2.3.2.1. Independent parameters	51
2.3.2.1.1. Velocity of rotating roller and related quantities (Secondary independent parameters).....	51
2.3.2.1.1.1. Thickness of layer on the surface of roller	52
2.3.2.1.1.2. Feeding rate of polymer solution	57
2.3.2.2. Dependent Parameters	59
2.3.2.2.1. Average current and current per jet	59
2.3.2.2.2. Parameters measured using camera records	60
Spinning area and positions of jets.....	60
Number of Taylor's cones per spinning area/Distance between neighbouring jets	62
2.3.2.3. Theoretical considerations concerning the new parameters.....	62
2.3.2.3.1. Throughput per Taylor's Cone	62
Relationships between thickness of polymer layer, viscosity of polymer solution, Coulombian force and throughput per one Taylor's cone [139].....	62
2.4. PROPERTIES OF POLYURETHANE AND POLYETHYLENE OXIDE AND THEIR ELECTROSPINNING	65
2.4.1. Polyurethane	65
Application areas of PU nanofibers	67
2.4.2. Polyethylene Oxide.....	68
Application areas of PEO nanofibers.....	71
2.5. SUMMARY OF THEORETICAL PART AND OBJECTIVE SETTINGS	71
3. EXPERIMENTAL PART AND RESULTS	72
Survey of experiments.....	72
3.1. On the measured current in needle- and needleless electrospinning [33]	73
Needle electrospinning	76
Rod electrospinning.....	79
Roller electrospinning	82
3.2. Determining optimum concentration of solutions.....	83
Polyethylene Oxide	83
Polyurethane.....	86

3. 3. Effect of roller velocity and salt concentration on the electrospinning process.....	88
3.3.1. Nomenclature and symbols of solutions	89
3.3.2. Methods and results	89
Spinning conditions	89
4. DISCUSSION	99
4.1. On the Measured Current in Needle- and Needleless Electrospinning	99
4.2. Determining optimum concentration of solutions.....	101
Polyethylene Oxide	101
Polyurethane	101
4.3. Effect of roller velocity and salt on electrospinning process	101
5. CONCLUSIONS	110
Future works	111
6. REFERENCES	113
7. APPENDIX	122
Appendix A: SEM pictures of samples	122
PUT1 in various rpm:	122
PUT2 in various rpm:	123
PUT3 in various rpm:	124
PUL1 in various rpm:	126
PUL2 in various rpm:	127
PUL3 in various rpm:	129
PEOT1 in various rpm:	131
PEOT2 in various rpm:	132
PEOT3 in various rpm:	133
PEOL1 in various rpm:	134
PEOL2 in various rpm:	135
PEOL3 in various rpm:	136

LIST OF SYMBOLS

Symbols	Long Name	Units
\dot{Q} , Q	mass flow rate	kg/s
D	diameter of cone	m
f	force per volume	kgm/s ²

p	pressure	Pa
ν	– kinematic viscosity	m^2/s
	– flory index	
	– linear velocity of the roller surface	m/s
ρ	density	kg/m^3
μ	– dynamic viscosity	$\text{Pa}\cdot\text{s}$
	– Avr. Nanofiber diameter	nm
V	– volume flow rate	m^3/s
	– applied voltage	kV
R	maximal radius of area from which the fluid is pumped	m
F	total force per Taylor cone (jet)	newton
ES	electrospinning	
PU	polyurethane	
PEO	polyethylene oxide	
LCD	liquid-crystal display	
P_e	electric pressure	volt
P_c	capillary pressure	volt
Γ	dimensionless electrospinning number	
K	– conductivity	$\mu\text{S}\cdot\text{cm}^{-1}$
	– dimensionless wavenumber	
	– Mark–Houwink coefficient	
	– dimensionless number	
K_1	principal curvatures 1	m
K_2	principal curvatures 2	m

R_s	radius of sphere	m
γ, σ	surface tension	mN/m
E	electric field strength	kV
ϵ, ϵ_0	permittivity of surrounding gas	F/m
\$	US dollar	
RJS	rotary jet-spinning	
PET	polyethylene terephthalate	
PP	polypropylene	
PA-6	polyamide 6	
c	concentration of solution	g/ml
c^*	overlap concentration	g/ml
M_w, M_e	molecular weight	g/mol
η	intrinsic viscosity	ml/g
a	Mark–Houwink coefficient	
c^{**}	critical concentration	ml/g
M_c	critical molecular weight	g/mol
ξ	screening length, blob size	m
η_r	relative viscosity	
η_{solv}	viscosity of solvent	Pa.s
η_{sp}	specific viscosity	
η_{red}	reduced viscosity	ml/g
η_I	inherent viscosity	ml/g
G_N^0	plateau modulus of the melt	Pa
τ_e	longest relaxation time in the rouse mode	

wt	weight	g
PAN	polyacrylonitrile	
t_f	characteristic times of fluid flow, hydrodynamic time	s
t_c	charge relaxation time	s
$\epsilon^?$	dielectric permittivity of vacuum	$C^2 N^{-1} m^{-2}$
h_0	nozzle diameter	m
PVA	polyvinyl alcohol	
E_c	critical electric strength	volt
g	gravitational acceleration	m/s^2
α	capillary length	m
k	average inter-jet distance	m
λ	wavelength	m
PSF	polysulfone	
DMF	dimethylformamide	
N, Nc	– number of elements – number of cones	
SP	spinning performance	g/min/m
SP/jet	spinning performance per one taylor's cone	g/h
D	density of cones	$1/m^2$
G	area weight of nanofibers	g/m^2
v	– velocity of running collected fabric – absolute speed of roller	m/min m/s
L_f	the width of nanofibers membrane	m
σ	standard deviation	

ξ	nanofibers diameter	nm
NFA	non-fibrous area	m^2
SEM	scanning electron microscope	
rpm	speed of roller	r/min
θ_0	immersion angle of roller in solution	radian
ω	angular speed	Hz
V	dimensionless velocity of fluid in azimuthal direction	
u^*	characteristic velocity	m/s
H	dimensionless thickness of solution	
h	– thickness of solution on roller, – film thickness	m
h^*	Characteristic thickness	m
R	– radius of roller – resistance	m ohm
MSLs	maximum-supportable loads	
d	roller diameter	m
ℓ, L_r	roller length	m
\dot{v}	voluminous feed rate of solution on roller	m^3/s
TC	Taylor's cone	
T	relaxation time	s
A	– spinning area on roller surface – growth factor – amper	m^2 1/s amp
W_0	dimensionless squares of the angular frequency	

O_h	Ohnesorge number	
I	current	amper
CPJ	current per one jet	amper
TAC	total average current	amper
TEAB	tetraethylammonium bromide	
TA	total surface area of roller	m^2
x	average distance between adjoining taylor cones	m
n	number of jets	
LiCl	lithium chloride	
Li	lithium	
Mg	magnesium	
H ₂ O	water	
THF	tetrahydrofuran	
Et ₄ N ⁺	tetraethylammonium ion	
Me ₄ N ⁺	tetramethylammonium ion	
k_d	the dissociation of the ion pair into the charged ions	
k_r	removal of free ions by the recombination into ion pairs	
H ₃ O ⁺	hydroxonium kation	
OH ⁻	hydroxide anion	
kDA	kilodalton	
AgNPs	silver nanoparticles	
CMCTS	carboxymethyl chitosan	
KCl	potassium chloride	
NaCl	Sodium chloride	

Pa	Pascal	
S	Simens	
mN	mili newton	
RH	Relative humidity	%
temp	temperature	C ⁰
π	pi number	

LIST OF FIGURES

Fig. 2.1. Diagram of needle electrospinning system.....	28
Fig. 2.2. Schematic drawing of the MB process [45].....	29
Fig. 2.3. Centrifugal spinning head and a pilot production line by Dienes/Reiter [46].....	29
Fig. 2.4. Diagram of the rotary-jet spinning process device [48].	30
Fig. 2.5. Cross-section and separation process between sea and island [49].....	30
Fig. 2.6. Illustration of the basic production process of nanofibers by drawing from droplet of the polymer [12].....	31
Fig. 2.7. Diagram of roller electrospinning system.....	32
Fig. 2.8. Stationary wire electrode [52].	33
Fig. 2.9. Classification of polymer solutions in terms of concentration and molecular weight (Graessley, 1980) [61].....	35
Fig. 2.10. Dependence of viscosity on the shear rate for a Newtonian liquid and a non-Newtonian pseudoplastic polymer solution [32].	37
Fig. 2.11. (A) At high viscosity, the solvent molecules are distributed over the entangled polymer molecules. (B) With a lower viscosity, the solvent molecules tend to congregate under the action of surface tension.....	39
Fig. 2.12. Electric field intensity profiles of cylinder, disc, and spiral coil spinnerets [95]	44
Fig. 2.13. Schematic summary of needleless rotating spinnerets (electrospinning direction along the red arrow).	45
Fig. 2.14. Number of cones on the roller surface.....	46
Fig. 2.15. Radial movement of ions in a jet.	47

Fig. 2.16. Non-fibrous area of a nanofiber layer.....	49
Fig. 2.17. Overall system geometry [119].	53
Fig. 2.18. Graph of dimensionless thickness (H) as a function of immersion angle θ [119].....	54
Fig. 2.19. Thickness of PU solutions layer as a function of roller rpm and viscosity; (a) comparison of measurement results (points) and theoretical (lines) calculation, (b) measurement result of thickness (dot lines represent connection of points).	56
Fig. 2.20. Thickness of PEO solutions layer as a function of roller rpm and viscosity; (a) comparison of measurement results (points) and theoretical (lines) calculation, (b) measurement result of thickness (dot lines represent connection of points).	57
Fig. 2.21. Feed rate of PU solution.	58
Fig. 2.22. Feed rate of PEO solution with standart deviation.	59
Fig. 2.23. Spinning area on the roller surface	60
Fig. 2.24. Surface of roller	61
Fig. 2.25. Spinning of low (a), optimum (b) and high (c) roller rpm.....	61
Fig. 2.26. Schematic diagram of Taylor's cone. f – electric force, h – thickness of fluid layer, D – diameter of the base of Taylor's cone	63
Fig. 2.27. Chemical interaction between polyurethane (PU) and Lithium chloride (LiCl).	66
Fig. 2.28. Conductivity of TEAB and LiCl solutions in DMF. Dash lines indicate connection of points.	67
Fig. 2.29. Dependence of water solution conductivity on the concentration of LiCl and TEAB. Dash lines indicate connection of points.	69
Fig. 2.30. Multiple fluid jets using plane-plane electrode configuration without capillaries.	70
Fig. 3.1. Needle electrospinning system	74

Fig. 3.2. Rod electrospinning system	75
Fig. 3.3. Roller electrospinning system.....	75
Fig. 3.4. Effect of humidity on current.	76
Fig. 3.5. Current vs. protrusion length in needle electrospinning system.....	77
Fig. 3.6. Jet current vs. applied voltage at various feed rates – needle diameter 0.8 mm.....	78
Fig. 3.7. Jet current vs. applied voltage at various feed rates – needle diameter 0.6 mm.....	78
Fig. 3.8. Jet current vs. applied voltage at various feed rates – needle diameter 0.4 mm.....	79
Fig. 3.9. Plot of current vs. EQ0.5K0.4 at various needle diameters with a feed rate of 0.2 ml/h.....	79
Fig. 3.10. Time course of current and number of jets in the rod electrospinning process. Solution of PEO with 0.1 mol/L NaCl.....	81
Fig. 3.11. Time course of current and number of jets in rod electrospinning. Solution of PEO with 0.1 mol/L KCl	82
Fig. 3.12. Current vs. time in roller electrospinning	82
Fig. 3.13. Camera record of roller electrospinning	82
Fig. 3.14. (a) SP and, (b) SP/Jet vs. viscosity of PEO solutions.	84
Fig. 3.15. Fiber diameter vs. concentration of PEO solutions	85
Fig. 3.16. SEM image of PEO solutions (a) 5 % PEO with 0.062 M TEAB, (b) 6 % PEO with 0.062 M TEAB, (c) 7 % PEO with 0.062 M TEAB, (d) 8 % PEO with 0.062 M TEAB, (e) 9 % PEO with 0.062 M TEAB, (e) 10 % PEO with 0.062 M TEAB.....	85
Fig. 3.17. (a) spinning performance, (b) SP/jet vs. viscosity of PU solution	87
Fig. 3.18. Fiber diameter vs. concentration of PU solutions.....	87

Fig. 3.19. SEM image of PU solutions (a) 17.5% PU, (b) 17.5% PU with 0.056 M LiCl, (c) 17.5% PU with 0.014 M LiCl, (d) 17.5% PU with 0.28 M LiCl, (e) 17.5% PU with 0.45 M LiCl, (e) 17.5% PU with 0. 56 M LiCl.	88
Fig. 3.20. Effect of nonsolvent on chain entanglements of macromolecules.	89
Fig. 3.21. Fiber bundles and unevenness on the take up fabric surface	90
Fig. 3.22. Surface tension of polymer solutions	91
Fig. 3.23. Viscosity of polymer solutions	91
Fig. 3.24. Conductivities of polymer solutions with content of salts (dot lines indicate connection of points).	91
Fig. 3.25. Diagram of roller electrospinning system.....	92
Fig. 3.26. Wire between roller and collector (distance of the tip of wire from roller surface is 95mm).	92
Fig. 3.27. Launching time of PU solutions	93
Fig. 3.28. Launching time of PEO solutions.....	94
Fig. 3.29. Launching time of selected PEO solutions.....	95
Fig. 3.30. Number of jets on the roller.....	95
Fig. 3.31. Spinning area	95
Fig. 3.32. Measurement of current on roller electrospinning system.....	96
Fig. 3.33. Total current vs. roller speed	96
Fig. 3.34. Current/jet vs. roller speed.....	97
Fig. 3.35. Distance between jets vs. roller speed	97

Fig. 3.36. Spinning performance of PU and PEO nanofibers in various rpm.....	97
Fig. 3.37. SP/jet of PU and PEO nanofibers in various rpm.....	98
Fig. 3.38. Fiber diameter vs. roller speed (a) PU with TEAB salt, (b) PU with LiCl salt, (c) PEO with TEAB salt, (d) PEO with LiCl salt.....	98
Fig. 3.39. Non-fibrous area vs. roller speed (a) PU, (b) PEO nanofibers	99
Fig. 3.40. Length of jets vs. molar ratio of salt	99
Fig. 4.1. Computed structure of the tetramethylammonium ion and lithium ion complexed to four N,N-dimethylformamide molecules [145].	103
Fig. 4.2. Chemical interaction of LiCl salt with PU polymer.	103
Fig. 4.3. The shielding effect of rods in different length.	105
Fig. 4.4. Length of jets vs. Distance between jets at 3 rpm roller speed.....	105
Fig.4.5. Average total current vs. spinning performance (PU).....	108
Fig. 4.6. Current per jet vs. spinning performance per jet (PU).....	108
Fig. 4.7. Movement of roller and position of jets.	109

LIST OF TABLES

Table 2.1. Dependent and independent parameters of needleless electrospinning system (described in literature)	34
Table 3.1. Needle diameters	74
Table 3.2. Viscosity, conductivity, and surface tension of PEO polymer solutions.	76
Table 3.3 Spinning conditions in Experiment 1.3.	77
Table 3.4. Spinning conditions – rod electrospinning experiments	80
Table 3.5. Number of jets, total current, and current per jet in the rod spinning process. Solution of PEO with 0.1 mol/L NaCl.....	81
Table 3.6. Number of jets, total current, and current per jet in the rod spinning process. Solution of PEO with 0.1 mol/L KCl	81
Table 3.7. Spinning conditions of PEO polymer solutions in roller spinning.....	82
Table 3.8. Number of jets, total current, and current per jet in roller electrospinning	83
Table 3.9. Properties of PEO solutions.....	83
Table 3.10. Spinning conditions of PEO polymer solution on roller ES.....	84
Table 3.11. Polymer solution properties of PU.	86
Table 3.12. Spinning conditions of PU solutions on roller ES.....	86
Table 3.13. Spinning conditions of PEO solutions on roller ES	90
Table 3.14. Spinning conditions of PU solutions on roller ES.....	90
Table 3.15. Launching time of cones for PU polymer solutions (in second).	93

Table 3.16. Launching time of cones for PEO polymer solutions (in second).....93

Table 3.17. Launching time of jet with the grounded wire (in seconds).....94

Table 4.1. Shielding angle of PU jets105

Table 4.2. Shielding angle of PEO jets.....105

Table 4.3. Inter-jet distance of PU solution.....106

Table 4.4. Inter-jet distance of PEO solution106

1. INTRODUCTION

The European commission defined the nanomaterials as those containing particles with one or more external dimensions in the size range 1 – 100 nm. In the field of fibrous materials, the fibers with diameters smaller than 1000 nm are called nanofibers.

One of the aims of researchers is to use nanofibers in the industrial application area. Nanotechnology has gained an interest of the global research and development support over the last few years. Nanotechnology literally means any technology performed on a nanoscale that has applications in the real world [1,2,3,4,5,6,7,8,9,10,11]. It has also a vast application area in the textile field.

Several techniques were reported in early literature for the laboratory preparation of nanofibers [12,13]. Recent research developed methods to prepare polymer nanofibres by a number of processing techniques such as drawing, template synthesis, phase separation, self-assembly, etc. Under certain conditions and drawing, self-assembly of polymer melts can produce small samples of polymer nanofibers.

Nowadays, the electrospinning remains the most convenient and scalable technique for nanofiber production. In the electrospinning method, a polymer solution is placed in a syringe and a high voltage is applied to polymer solution coming out of a needle tip which highly electrifies the solution droplet at the needle tip. As a result, the solution droplet at the needle tip is drawn itself toward the opposite electrode and deforming into a conical shape which is called as “Taylor’s cone” (Taylor, 1969) [14]. If electrostatic force overcomes the surface tension, a jet is formed from the Taylor’s cone. The charged jet subjected to a high electrostatic field elongates and forms nanofibers. During electrospinning, the solvent evaporates and dry fibers can be obtained.

There are many factors affecting the electrospinning process and fiber properties. Viscosity, concentration, surface tension, molecular weight, conductivity and dielectric properties of polymer solution are classified as system parameters of electrospinning. Voltage, feed rate of polymer solution, distance between collector and needle tip, temperature of solution and ambient parameters are in the group of process parameter. Each parameter plays a role in the electrospinning. Additives to polymer solutions also play an important role in the fiber formation process. However, nanofibers cannot be generated in high quantities using the needle electrospinning.

On the other side, there is another method which is called as ‘roller electrospinning’, able to produce nanofibers in a continuous process (Fig. 2.7). Hundreds of jets can be formed simultaneously in the roller spinning electrode. Parameters of the roller electrospinning process will be discussed in theoretical part.

1.1. HISTORY

In the late 1500s, Sir William Gilbert observed that when a suitably electrically charged piece of amber was brought near a droplet of water it would form a cone shape and small droplets would be ejected from the tip of the cone. This phenomenon is called as electrospraying [15].

In 1882, Lord Rayleigh [16] predicted the spontaneous deformation and eventual break up of perfectly conducting liquid droplets charged electrically beyond a certain critical value, now known as the 'Rayleigh limit'.

In 1888, C. V. Boys used electrical spinning stable fiber to measure torsion balance. In Boys' apparatus for electrospraying consisted of a small dish insulated and connected with an electrical machine [17].

The preparation of polymeric nanofibers was firstly patented in 1902 by Cooley and Morton [18,19], but the fibrous layer was too weak for practical uses. These patents describe a deposition of fine fibers produced from a viscous polymer solution on a charged electrode held close to an electrode of opposite charge to obtain electrostatic spinning.

In 1914, Zeleny studied the behavior of fluid droplets at the end of capillaries and also found a method to evaluate surface charge intensity by recording the pressure change in a liquid reservoir [20]. He measured the effect of geometry of a pointed cylindrical electrode and atmosphere (humidity, temperature and pressure) on the discharge current [21] and concluded that the diameter of the electrode was the principal factor, rather than the shape of its end.

Later in 1934, Formhals patented an improved version of the electrospraying process and apparatus. His first patents on electrospraying of cellulose acetate from acetone used a fiber collection system that could be moved, allowing some degree of fiber orientation during spinning. By 1944, Formhals [22,23,24,25,26] had filed four more patents on improved processes and claimed methods to electrospin even multi-component webs that contained more than one type of nanofiber. In this patent he designed a device to produce continuous fibers.

WA Macky studied effect of strong electrical fields on the deformation of water droplets in flight and indicated that filaments of fluid were drawn from experimental drops, and that the drop size is a limiting factor in this phenomenon. His results indicate that for a breaking drop, the flow of current is due to ionised gas or vapour particles rather than the flight of charged liquid particles [27,28].

In 1936, the electrospraying of the melt solution which used an air-blast to assist fiber formation was patented by Northon [29].

Between 1964 and 1969, Sir Geoffrey Ingram Taylor produced a significant advance in the theory of electrospraying by modelling the shape of the cone formed by the fluid droplet under the influence of an electric field [30]; the Taylor cone. His work plays a role on electrospraying by mathematical modelling the shape of this cone under the effect of an electric field. He also studied "leaky dielectric model" for semi-conducting fluids [31].

Nowadays, Nanospider is one of the commercial equipments to produce nanofibers-web via needleless electrospinning technology. This technology was patented by Jirsak et. al. from Technical university of Liberec, and then it was developed by the Czech company Elmarco, Liberec as an industrial device to produce nanofibers. This equipment can produce membranes consisting of fibers in a range from 100 to 800 nm in diameter. Such materials are widely utilized in many fields, as filtration, healthcare, building construction, automotive industries, industry, cosmetics and many others. Elmarco produced the pilot manufacturing line for nanofiber production in 2004, and in 2006 offered the first models for industrial production. Recent models of Nanospiders have production rate up to 30 m/min with the fabric width bigger than 1 m [32].

1.2. APPLICATIONS OF NANOFIBERS

There are many patents and publications describing nanofiber applications. Nanofibers have extremely high specific surface area and are a base for highly porous membranes. Therefore, they are good candidates for specific fabrics. Using additives and special polymers special surfaces can be produced. The unique characteristics plus the functionalities from the polymers themselves impart the nanofibers many excellent properties for advanced applications. Some potential application area is listed below:

Tissue engineering scaffolds

- Porous membrane for skin
- Tubular shapes for blood vessels and nerve regenerations
- 3D scaffolds for bone and cartilage regenerations

Wound healing

- Structure and functions of human skin
- Wound on human skin and healing process
- Wound management and wound dressing

Drug release control

- Water soluble
- Poor-water soluble
- Water-insoluble

Filtration

- Liquid filtration
- Gas filtration
- Molecular filtration

Sensors

- Thermal sensors
- Optical sensors
- Biological sensors
- Piezoelectric sensors
- Chemical sensors
- Electrical sensors
- Gas sensors

Military protective clothing

- Minimal impedance to air
- Efficiency in trapping aerosol particles
- Anti-biochemical gases

Other industrial applications

- Catalyst and enzyme carriers
- Cosmetic skin mask
- Photovoltaic devices
- LCD devices
- Ultra-lightweight spacecraft materials
- Micro/nano electronic devices
- Electromagnetic interference shielding

1.3. AIM OF THE WORK

Needleless roller electrospinning is a new technique when compared with needle electrospinning; therefore, parameters of needleless electrospinning have not yet been fully identified and defined. Some dependent parameters were defined in previous works [32]. Relations between selected independent and selected dependent parameters were studied, as it will be shown in theoretical part, both experimentally and theoretically. Not all of them were defined and studied, such as: spinner geometry, roller properties, roller velocity. Only few dependent parameters were defined (throughput, fiber diameter and diameter distribution, quality of nanofiber layer and some others).

It is the aim of present work to continue in the study of relation between independent and dependent parameters and to contribute to the knowledge of needleless electrospinning mechanism. To reach this aim, some more independent and dependent parameters will be defined and the methods for their measurement developed.

2. THEORETICAL PART

In this part, firstly we will discuss the principle of electrospinning mainly with regard to the mechanism of free surface electrospinning. Then, alternative nanofiber production methods will be discussed. The parameters of roller electrospinning are discussed as presented in previous works. Some new roller electrospinning parameters introduced by author are defined and the methods of their measurement described. Finally, some theoretical considerations concerning the new parameters are presented. The corresponding chapter (2.3.2) contains the first part of the author's contribution to the study of roller electrospinning.

2.1. PRINCIPLES OF ELECTROSPINNING

Electrospinning is a simple and cost effective process for the producing of the polymeric fibers with diameters in a micro and nanometer range using an electrostatic field. Up to now, two ways to produce nanofibers using high voltage are known. Those are needle electrospinning and needle-less electrospinning from a free surface. Both the spinning techniques were explained in previous work [33]. Herein roller electrospinning system was studied. However, there are some new alternative systems of nanofiber production developed recently [34,35,36,37,38].

Tonks [39] studied that a possible mechanism for the onset of aperiodic instability ($\omega^2 < 0$) of surface when subjected on a strong electric field. The initial perturbation of the surface causes a local-field increase which determines the further growth of the perturbation. The critical field is determined directly from the corresponding dispersion equation [40];

$$\omega^2 = \frac{k}{\rho} \left(\sigma k^2 + \rho g - \frac{E^2}{4\pi} k \right) \quad (2.1)$$

Where g is the gravitational acceleration, σ is the surface tension, ρ is the density, and $k = 2\pi/\lambda$ is the wave number.

The mechanism of the fast forming instability was explained by Lukas et. al.[35]. In this analysis, it is supposed that electrohydrodynamics of a liquid surface may conveniently be analysed with the capillary waves running on an one-dimensional approximation of the fluid surface, oriented along the horizontal axis, say, of the Cartesian system of coordinates. The wave's vertical displacement along the z -axis is described using the periodic real part of a complex quantity, $\xi = A \exp[i(kx - \omega t)]$, where k denotes wave number and ω is angular frequency. The relationship between wave number k and wave length λ is, $k = 2\pi/\lambda$, while angular frequency ω is related to period T as $\omega = 2\pi/T$.

The relationships $\omega = f(k)$ between spatial and time-dependant parameters k and ω of waves undergoing various force fields that are called dispersion laws. For gravity waves, $\omega^2 = gk$, where g is gravity acceleration. By adding surface tension:

$$\omega^2 = (\rho g + \gamma k^2 - \epsilon E_0^2 k) \frac{k}{\rho} \quad (2.2)$$

where ρ is liquid mass density, γ is linear force of surface tension, k is wave number, ϵ is permittivity, E_0 is field strength, t is time, h is the thickness of layer on the surface.

Lukas also gives out a new concept that is dimensionless electrospinning number Γ [41]. This is the ratio of electric pressure (P_e) to capillary pressure (P_c). So we have, $\Gamma = P_e / P_c$.

Capillary pressure (P_c) caused by an arbitrarily curved liquid surface is a product of the surface tension and a sum of two principal curvatures K_1 and K_2 , so $P_c = \gamma(K_1 + K_2)$.

In the case of the sphere with a radius R_s in a gravitational acceleration field, both principal curvatures K_1 and K_2 are of the same value and are equal to $1/R_s$, so $P_c = 2\gamma/R_s$.

Electric pressure (P_e) is another basic concept in electrospinning and it is calculated according to the equation

$$P_e = (\epsilon E^2)/2 \quad (2.3)$$

where E is the strength of electric field and ϵ is the permittivity of surrounding air.

So, the phenomenon of electrospinning only occurs when the dimensionless electrospinning number is bigger or at least equal to 1 ($\Gamma \geq 1$ or $P_e \geq P_c$). The principle of roller electrospinning is explained in sub-chapter 2.2.6.

In the needle electrospinning, the polymer solution is drawn into fibres in electrostatic field arranged between a needle tip and a collector. Polymer solution stretches into fibres while the solvent is evaporating. Fibers in nano or micro range are collected on a collector. Fibre quality and morphology depends on several factors. The morphology of nanostructures formed on the collector varies with parameters of the spinning device and process parameters.

The parameters of roller electrospinning are discussed below.

Dao et. al. divided electrospinning processes into three stages. In the first stage, polymer solution is fed by a roller from container or by pump in the needle spinning process. High electric potential inserted in the solution leads to the formation of jets. The jets (jet) are discharged from roller's surface or from droplet on needle tip. This causes the jets to steadily accelerate and thin out along an axis aligned with the general direction of electric field. This is an important stage because the stability and results of it controls all its subsequent stages and, in the final analysis, the desired properties of the finished fiber. The second stage consists of several simultaneously occurring processes. In it, the fluctuations of the electric lines of force, caused by time and space variation of the bulk density of electrical charges, causes jets to turn transversely to the field direction and to be decelerated by the constantly increasing drag force of the gas. This produces a cloud that expands toward the collector by action of the same-polarity charges. At the same time, the rate of vaporization of the solvent that started already at the first stage of the process is steeply intensified, the jet solidifies and the resulting fibrous cloud drifts in the applied electric field onto collector. At this stage the jet may still undergo a sequence of splitting resulting in the formation of an unsteady bulk fiber-mesh structure. The following, third stage also consists of two simultaneous processes: the first consisting of random deposition of fibers into a layer on collector and the second of a gas spark discharge between collector and the fiber layer formed on it, that closes the electric circuit [32].

2.2. TECHNOLOGIES OF NANOFIBER PRODUCTION

2.2.1. Needle Electrospinning

Needle electrospinning is the most common method to produce nanofibers as shown in Fig. 2.1. In the needle electrospinning method, a polymer solution or melt is placed in a syringe and fed

out of syringe through a hollow needle. A high voltage source is linked with the needle or with the solution. If the electric force overcomes the surface tension of polymer solution, a cone appears on the droplet and jet is formed and stretched under the electrostatic field creating very fine fibers. These are transported towards a collector electrode and create a nanofiber layer on its surface.

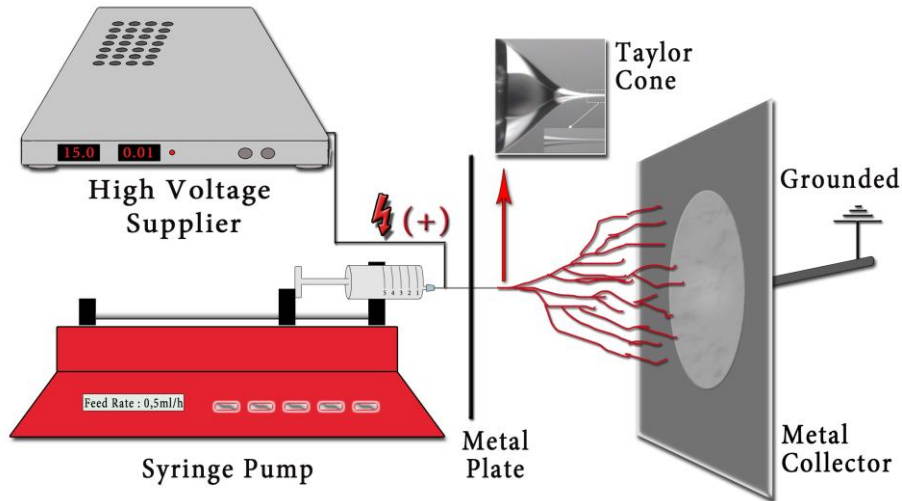


Fig. 2.1. Diagram of needle electrospinning system

Viscosity, concentration, surface tension, molecular weight, conductivity and dielectric properties of polymer solution are called solution parameters of electrospinning. Voltage, feed rate of polymer solution, distance between the collector and the needle tip, temperature of solution and ambient parameters are the main process parameters. Each parameter influences the electrospinning process as well as the fiber and fiber layer quality. Additives also affect fiber morphology.

Commercial applications of the needle electrospinning are limited due to its extremely low throughput (production rate). This system is just suitable for laboratory works.

2.2.2. Meltblown system

Another technique to produce polymeric nanofibers has been introduced by Nanofiber Technology Inc. of Aberdeen, NC. [42,43,44]. Nanofibers are produced by melt blowing a polymer melt using a modified spinning die. The sizes of fibers are a mixture of both micron and submicron fibers with average fiber diameter ranging between 1 and 2 μm . Using this method, thermoplastic polymers can be processed. The method eliminates utilization of solvents. Production rate is very high. The technique does appear to have the potential to make large quantities of polymeric nanofibers at a cost less than \$10 per kilogram.

A melt blowing processes was originally developed to produce microfibers. A molten polymer is spun into a stream of high velocity hot air. A layer of self-bonded fibers is formed on a surface of moving collector as shown in Fig. 2.2 [45].

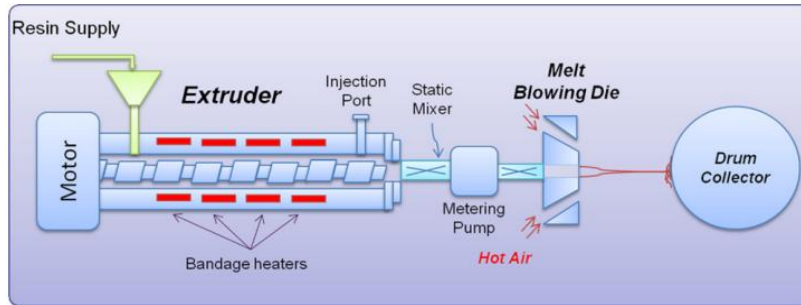


Fig. 2.2. Schematic drawing of the MB process [45].

Meltblown webs are known for their high thermal insulation value, high surface area per unit weight, and high barrier properties. The application area is very large such as protective apparel, quality filters, surgical drapes and gowns, diaper leg cuff. However, there are still several concerns. One concern is the broad range of fiber diameter distribution and the other is the cost of spinning equipment versus the production rate.

2.2.3. Centrifugal electrospinning

In 2008, Dauner et al [46] developed centrifugal system for forming liquid polymer into thin fibers (Fig. 2.3). Potential application areas are filtration, protective clothing, medical materials, cleaning devices, solar and battery technology.



Fig. 2.3. Centrifugal spinning head and a pilot production line by Dienes/Reiter [46].

Despite the high productivity (up to $1000 \text{ cm}^3/\text{m}\cdot\text{hr}$), the fiber diameter distribution and homogeneity of the deposited nanofiber layer are not at the levels achieved by electrospinning.

Rotary jet-spinning (RJS) is a new and cost-effective method which was improved at the Harvard University (Fig. 2.4). A polymer solution flows through a high-speed rotating nozzle to form a jet. The jet thins due to centrifugal forces, solvent evaporates and the fiber solidifies. The fibers are collected in a reservoir of an arbitrary shape and the container dictates the form of the final fiber assembly [47].

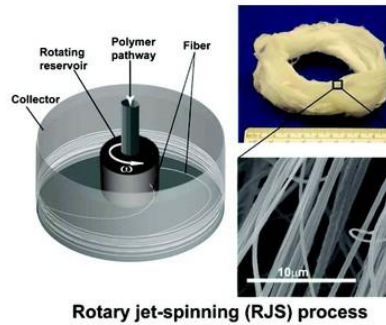


Fig. 2.4. Diagram of the rotary-jet spinning process device [48].

Possible application areas are tissue engineering, surgery, in vitro analytical systems, reinforcing small cavities, military applications and drug delivery. The advantage of this method is its ability to spin protein fibers.

2.2.4. Bi-component fibers

Another technique that can be used to produce nanofibers is spinning bicomponent islands-in-the-sea fibers that, after spinning, are submitted to dissolution of the matrix (Fig. 2.5). PET, PP and PA-6 were used as island-part of the bi-component fiber and polyethylene, poly (vinyl alcohol), polystyrol or modified polyester used as sea-part of that. The resultant fiber diameter is around 300 nm. The production rate was approximately 5 kilograms per hour. When compared with other production principles, the fiber diameter distribution is narrower [38].

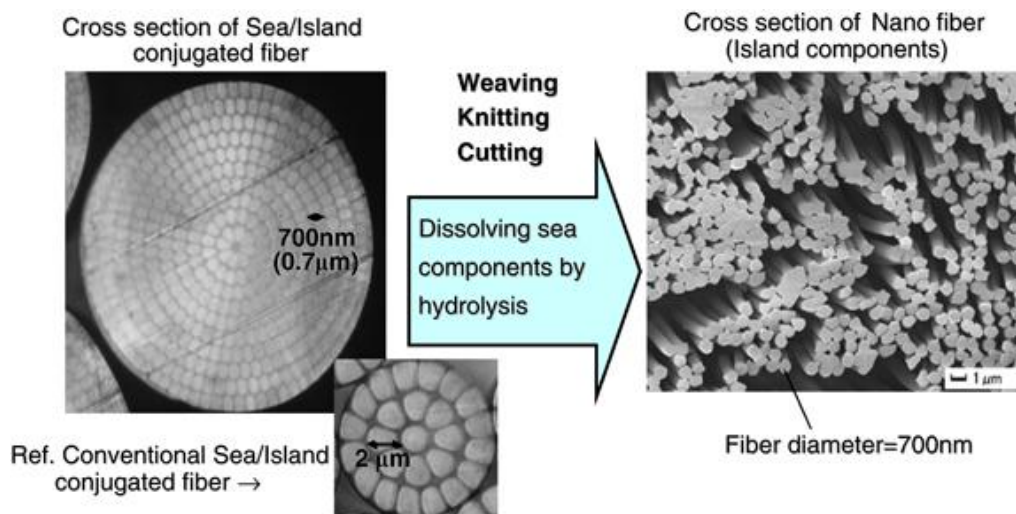


Fig. 2.5. Cross-section and separation process between sea and island [49].

Splittable bicomponent fibers can be produced in a melt spinning process [50]. The number of segments should be sixteen or more and the best approach might be to use a water soluble polymer in a small ratio along with PET or PP. The ultimate approach are fibers that contain > 600 island fibrils that would have diameters as low as 50 nm and which act as a regular melt blown fiber through fabric formation after which the sea polymer is dissolved and only the nanofibers are left [44]. Another described technology is based on production of spunbond material composed of segmented bi-component fibers and following splitting of the fibers in the spun-laced process.

2.2.5. Drawing method

Nanofibers can be produced by a process of drawing using a micropipette with a diameter of a few micrometers. The micropipette is dipped into the droplet near the contact line using a micromanipulator as shown in Fig. 2.6 [12]. In the drawing process, the fibers are fabricated by contacting a previously deposited polymer solution droplet with a sharp tip and drawing it as a liquid fiber. Fiber is then solidified by rapid evaporation of the solvent due to the high surface area. The drawn fiber can be connected to another previously deposited polymer solution droplet thus forming a suspended fiber [51]. Drawing process can be considered as dry spinning at a molecular level.

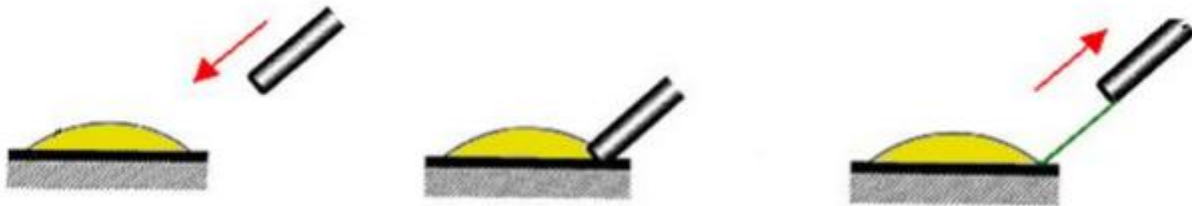


Fig. 2.6. Illustration of the basic production process of nanofibers by drawing from droplet of the polymer [12]

The predeposition of droplets significantly limits the ability to extend this technique, especially in free dimensional configurations and hard to access spatial geometries. Drawing a fiber requires a viscoelastic material that can undergo strong deformations while being cohesive enough to support the stresses developed during pulling. Furthermore, there is a specific time in which the fibers can be pulled. Viscosity of the droplet continuously increases with time due to solvent evaporation from the deposited droplet. The continual shrinkage in the volume of the polymer solution droplet affects the diameter of the fiber drawn and limits the continuous drawing of fibers [51]. Productivity is low due to production of only one yarn per one pipette.

2.2.6. Roller electrospinning

The needleless (roller) electrospinning which is suitable for industrial application has been developed and patented at the Technical University of Liberec in 2003 [13].

In the roller electrospinning technology (Fig. 2.7), a rotating roller placed in a solution tank is the spinning electrode. A supporting material (nonwoven web, paper, etc.) moves along the collector electrode. A high voltage is applied to the rotating roller. If the electric force overcomes the surface tension of the polymer solution, many jets develop on the surface of the roller. A nanofiber layer covers the supporting material. As a result, a continuous nanoweb is formed.

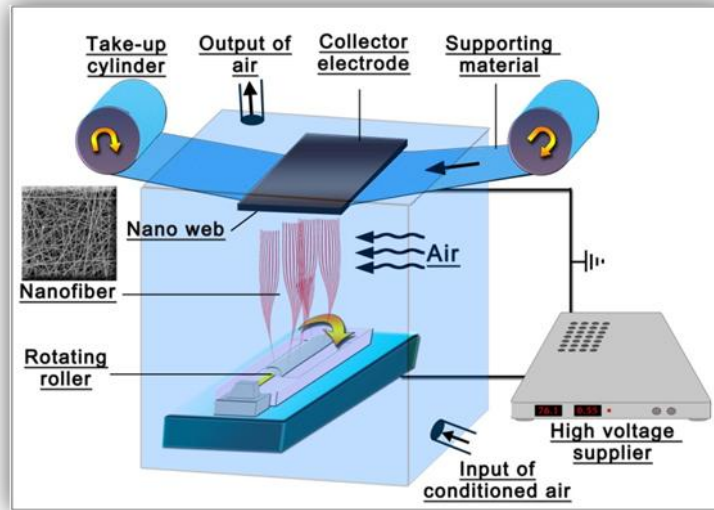


Fig. 2.7. Diagram of roller electrospinning system.

This system is highly productive when compared with other electrospinning methods. Nevertheless, its productivity is still low in comparison with processes yielding planar fibrous materials and the price of nanofiber layers is correspondingly high. Therefore, further development based on the knowledge of process is necessary to improve quality, regularity and price of nanofibers. This commercial method for production of polymeric nanofibers is used in industrial range and it is a simple and versatile method for production of ultrathin fibers from a variety of materials. In addition, the roller ES has the ability to process a wide range of polymers in diameters of 50–800 nm with acceptable narrow fiber diameter distribution into nonwoven webs.

2.2.7. Stationary wire electrospinning

There is a quite new technology to produce nanofibers without any nozzle system. This system was developed by Elmarco Company in the Czech Republic. In this system, a polymer solution is fed onto a stationary wire along the spinning width using a reciprocating applicator (Fig. 2.8). The wire is linked with the high voltage source and serves as a spinning electrode. High electric field around a small diameter wire allows to spin a wide variety of polymer solutions rather easily. At the top of spinning device, a supporting planar material moves along the collector electrode in the same way as described at the roller ES device. The polymer solution is stretched between electrode wire and grounded or oppositely charged collector under the electric field and fibers are formed. Fiber diameter range is 80-700 nm [52]. It is possible to spin polymers from water as well as from organic solvents. Required width of nanofiber layer is easily adjusted by setting turning points of reciprocating solution applicator.



Fig. 2.8. Stationary wire electrode [52].

Among presented nanofiber production technologies, the meltblown technology, centrifugal technology and bicomponent fibers show high productivity. On the other hand, fiber diameter distribution and homogeneity of product are rather poor at the first two of them. Production of nanofibers via bi-component fibers requires a demanding step of dissolution the polymer matrix. These technologies will likely be used in cost sensitive applications like hygiene nonwovens, while high quality electrospun technologies will be used in products with high added value and where is the need for low amounts of the material (air and liquid filtration,biomedicine). In the case of roller electrospinning system, the use of organic solvents (in the case of some polymers) and low production rate are disadvantages. To overcome low productivity, it is necessary to understand the system better. By optimizing ES parameters, productivity and fiber quality can be improved.

2.3. PARAMETERS OF ELECTROSPINNING

The aim of this chapter is to define key parameters of the roller electrospinning process. The ES parameters are divided into two groups, namely independent and dependent ones. In the group independent parameters, primary and secondary independent parameters are distinguished, for instance: kind of polymer, its molecular weight, kind of solvent, type and amount of additives and concentration of polymer solution are primarily independent parameters, whereas viscosity, conductivity and surface tension as a result of above parameters, directly influencing the electrospinning process, are secondary independent parameters.

There are two groups of parameters described in the following chapter, namely these described and studied in the previous works and the new parameters defined by the author. The author hopes that it will be possible to understand the electrospinning process when using and studying her new defined and measured parameters which potentially yield more detailed insight into the process (Table 2.1).

Table 2.1. Dependent and independent parameters of needleless electrospinning system (described in literature)

Independent Parameters	Dependent Parameters
<ul style="list-style-type: none"> • Polymer solution properties (concentration, viscosity, composition, surface tension, conductivity, molecular weight) • Applied voltage • Distance between electrodes • Velocity of rotating roller* • Velocity of take-up fabric • Geometry of electrode • Geometry of collector • Ambient conditions (temperature, relative humidity) 	<ul style="list-style-type: none"> • Number of cones, density of jets • Life time of jets • Spinning performance, spinning performance/per jet • Total avr. current , current/jet* • Thickness of polymer solution layer on the surface of the roller* • Force acting on a jet* • Spinning area* • Distance between neighboring jets* • Jet length in stable zone • Fiber diameter and distribution • Non-fibrous area • Launching time of jets

*The parameters defined or studied by the author

Some of these parameters were studied before and all the results show and explain the relation between dependent and independent parameters [32,33,53,54,55,56,57,58,59].

2.3.1. PARAMETERS DESCRIBED IN LITERATURE

2.3.1.1. Independent Parameters

2.3.1.1.1. Concentration/Molecular Weight /Viscosity

Polymer jets must show some level of strength to create nanofibers during electrospinning. If the strength is too low, the jets break and create beads instead of fibers. Shenoy et al. [60] introduced the term “entanglement number” as a quantity responsible for the strength of jets. They also found the limiting value of entanglement number in regard to fiber production: if the value is greater than 3.5, fibers are produced, below 3.5 the production of beads starts. The entanglement number depends on the kind of polymer, namely on the content of polar groups and molecular weight, on the kind of solvent and polymer concentration in the solution. As the determination of the entanglement number is not easy, viscosity is often taken as a measure of it, as it in principle depends on the same parameters as entanglement number.

In a suitable concentration, the chain entanglements of macromolecules are adequate to electrospin a polymer into fibers under a strong electrostatic field.

Graessley [61] classified polymer solutions into five different regimes according to concentration and molecular weight; see Fig. 2.9. Polymer molecules are isolated from each other in the dilute regime. Dilute solutions of low molecular weight are nearly Newtonian.

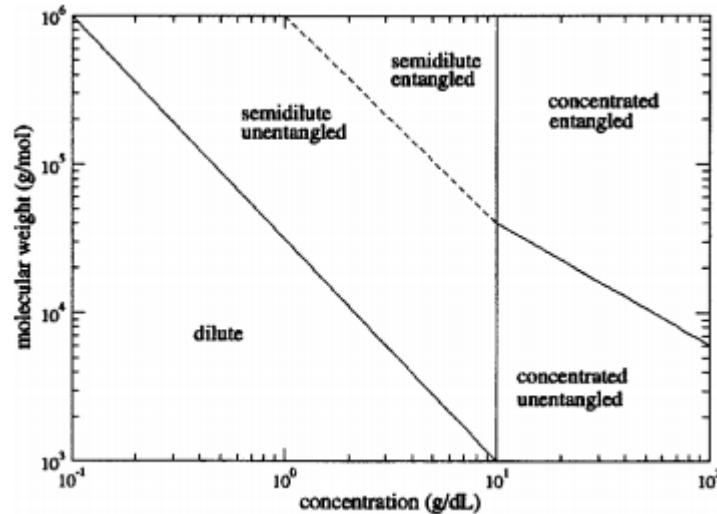


Fig. 2.9. Classification of polymer solutions in terms of concentration and molecular weight (Graessley, 1980) [61].

In the polymer solutions of a very low concentrations ($c < c^*$) the polymer chains are isolated from each other. Increasing molecular weight occurs rising elasticity on time-scale corresponding to random thermally-induced intramolecular motions of polymer molecule sections. With rising concentration, coils overlap, the solutions become semidilute. In the overlap concentration, polymer chains are overlapping and the chain entanglements are increasing which results into a decrease of chain mobility. This overlap concentration (c^*) scales with molecular weight as $c^* \sim M_w^{1-3\nu}$. This can be expressed in the alternate form $c^* \approx 0.77/[\eta]$ where the ‘intrinsic viscosity’ or ‘limiting viscosity number’ is given by the Mark-Houwink-Sakurada equation $[\eta] = KM_w^a$ with the exponent $a = 3\nu - 1$ [61].

The coils shrink with rising concentration in the semidilute regime until they depend only weakly on concentration and approach near-random coil dimensions. In the semi-diluted and concentrated regimes the macromolecules are either not-entangled or entangled.

The molecular weights of polymers are very high, ranging from about 25,000 to 1,000,000 g/mol or higher. Solution properties vary dramatically with changes in solution concentration and molecular weight. For a given polymer and its molecular weight, there is a critical concentration, c^* , below which the polymer coils do not overlap each other. When the concentration of solution is lower than critical concentration, $c < c^*$, this solution is considered as dilute. In this regime the characteristic properties of polymer solutions are significantly influenced by the interaction of the polymer with solvent. The relationship between intrinsic viscosity $[\eta]$ and molecular weight is given Eqn. 2.4. There is another concentration c^{**} above which the solvent ceases to affect the properties of solution. If $c > c^{**}$, the solution is considered as concentrated. The molecular weight of chains should be about twice a critical molecular weight (M_c) to expect entanglements. So it is possible to have a solution which is concentrated but unentangled if the molecular weight is small, even though the concentration is large. For unentangled, concentrated solutions, $\eta_0 \sim cM_w$. For the solutions in which the entanglements dominate, $\eta_0 \sim c^4M_w^{3.4}$. the zone between these two

regions is considered as semidilute, where both solvent effects and the effects of entanglement density become important [62].

DeGennes and Graessley show by scaling arguments that the critical concentration (denoted c^{**}) for crossover into the concentrated regime is independent of molecular weight (since the long range hydrodynamic interactions of the intermingled chains are all screened out) and is approximately $c^{**}/\rho \approx 0.1$. As the molecular weight of the chains increase, they become entangled by the constraints of neighboring chains and the molecular motion becomes dominated by curvilinear diffusion or reptation. In the melt, the critical molecular weight for entanglement is found to be $2M_e \leq M_c \leq 5M_e$. In concentrated solutions, the dilution of the number of entanglement interactions leads to a linear variation in the entanglement crossover; $(M_c)_{\text{soln}} = (\rho/c)(M_c)_{\text{melt}} c^{**} \leq c \leq \rho$. At intermediate values of the concentration the solution is described as semi-dilute. In this regime, hydrodynamic interactions may be important below a certain 'screening length' or 'blob' size (ξ) which is dependent on the solvent quality. For very long chains, in the semi-dilute regime entanglement constraints may also be important. Experiments with polystyrene suggest that the crossover between semi-dilute, non-entangled and semi-dilute, entangled systems can be represented by an equation of the form $(M_c)_{\text{soln}} \approx (c^{**}/c)^{1/(3v-1)}(\rho/c^{**})(M_c)_{\text{melt}}$ for $c^* < c \leq c^{**}$ [61].

The polymer solution viscosity is determined by such molecular interactions, either attractive or repulsive, and can be altered by changing the solvent type. The viscosity of polymer solutions also depends on shear rate and temperature (and in some extreme cases pressure), also depends on the molecular weight distribution and the concentration. Properties of solvents are effecting the chain entanglement. In a good solvent, the polymer swells and its volume increases. Intermolecular forces between the solvent and monomer subunits dominate over intramolecular interactions. In a bad solvent or poor solvent, intramolecular forces dominate and the chains contract. In theta-solvent, the intermolecular polymer-solvent repulsion balances exactly the intramolecular monomer-monomer attraction [63]. In aqueous systems, some polymers have charges distributed along the chains. In that case, the amount of electrolyte (salt) in the aqueous solvent will affect the overall shape of the chain. In the absence of electrolyte, the charges are unshielded and repel one another. This results in the chain being stretched out. However, when electrolyte is present, the charges are shielded and their effect is suppressed, resulting in the chain tending to shrink towards its natural random configuration. This change from a rod to a sphere obviously causes the viscosity to decrease [64].

The intrinsic viscosity $[\eta]$ (mentioned above) of many polymer solutions is given by the Mark-Houwink equation [65].

$$[\eta] = KM^\alpha \quad (2.4)$$

where M is the molecular weight and K and α are constants for particular kinds of polymer and solvent. The value of α varies from 0.5 for a random coil to 2 for a rigid rod [64].

For simple low-molecular weight liquids, viscosity η is usually independent of the shear rate. Polymer solutions generally do not fall into this category of Newtonian liquids. At moderate shear rates polymer solutions generally show reduced viscosity or undergo shear-thinning. Fig. 2.10 shows a comparison of the shear rate dependence of viscosity for a Newtonian liquid and a non-Newtonian polymer solution. At the extremelly high shear rates, however, a non-Newtonian liquid may revert to Newtonian behaviour [32].

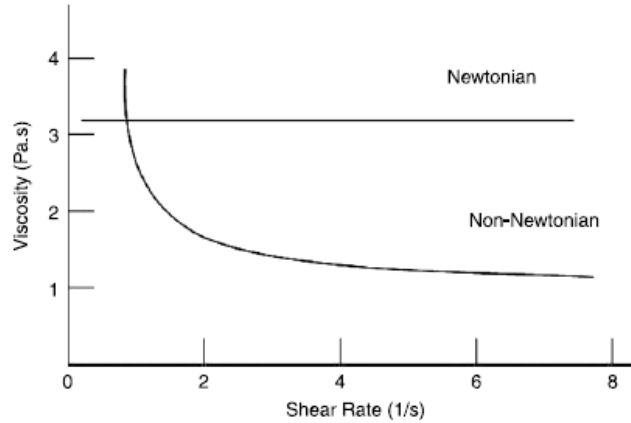


Fig. 2.10. Dependence of viscosity on the shear rate for a Newtonian liquid and a non-Newtonian pseudoplastic polymer solution [32].

The viscosity η of a polymer solution (at a concentration c) in a solvent of viscosity η_{solv} is conveniently expressed by its relative viscosity η_r and several other common measures:

Relative viscosity	Specific viscosity	Reduced viscosity	(2.5)
$\eta_r = \eta / \eta_{solv}$	$\eta_{sp} = \frac{\eta - \eta_{solv}}{\eta_{solv}}$	$\eta_{red} = \frac{1}{c} \left(\frac{\eta}{\eta_{solv}} - 1 \right)$	

Inherent viscosity	Intrinsic viscosity	(2.6)
$\eta_I = \frac{1}{c} \ln \eta_r$	$[\eta] = \lim_{c \rightarrow 0} \left(\frac{\eta_{sp}}{c} \right)$	

η_{sp} is essentially the incremental increase in η due to dissolved solute (polymer). Both η_{sp} and η_I are concentration dependent, and extrapolating the linear plots of either of these versus the concentration to zero concentration yields the intrinsic viscosity $[\eta]$, which I related to the dimensions of an isolated polymer chain in solution [32].

The zero-shear rate viscosity of the solution measured in steady simple shearing flow is plotted against the dimensionless ratio, c/c^* (corresponding to the degree of overlap between the polymer molecules) for solutions. At higher concentrations, the viscosity of the test fluids are dominated by the entanglements of the high molecular weight chains and filament stretching rheometry is now being used to test ideas from reptation theory. Far above the overlap concentration, reptation gives the following result [63]:

$$\eta_0 \approx \frac{\pi^2}{4} G_N^0 \tau_e (c/\rho)^4 (M_w/M_{e,melt})^3 \quad (2.7)$$

where G_N^0 is the plateau modulus of the melt and τ_e is the Rouse time for a single entangled segment. The zero-shear-rate viscosity thus depends strongly on the concentration and molecular weight.

With increasing the concentration of polymer solutions prepared using polymers with different molecular weight, the viscosity of polymer solutions was found to increase due to the densely entangled polymer chains [66].

A certain amount of chain entanglement is needed to keep the solution jet coherent during the electrospinning. At higher concentrations or higher viscosities, the charged jet did not break up into small droplets, a direct result of the increased chain entanglements (and hence an increase in the viscoelastic force) which were sufficient to prevent the break-up of the charged jet and to allow the Coulombic stress to further elongate the charged jet during its flight to the grounded target, which ultimately thinned down the diameter of the charged jet [67]. With any further increase in the concentration (or viscosity) of the solution, the number of beads along the fibers was found to decrease and their shape appeared to be more elongated [68].

Demir et. al. investigated that fiber morphology of polyurethaneurea fibers varies with the concentration of solution subjected to electrospinning. Different fiber morphologies occur at different concentrations and have significant effects on surface area to volume ratio of the fibers. At high concentrations, fibers exhibit curly, wavy, and straight structures. On the other hand, fibers obtained from low concentration (5.2 wt %) solutions exhibit 'beads on string' morphology. The average bead length was 700 nm. Lower viscosity solution favors the formation of beads and also favors the formation of thinner fibers [69].

Cengiz et. al. [57] studied the effect of polymer molecular weight and some solution properties such as conductivity, surface tension and rheological behavior on the roller electrospinning of poly(vinyl alcohol) concerning spinnability, process performance, fiber diameters, diameter distribution and nonfibrous particles. It was found that electric conductivity and surface tension of the solutions did not influence both throughput and fiber diameter significantly, whereas molecular weight has an important effect on the spinnability. On the contrary, concentration influences the process throughput considerably and properties of nanofibers and nanofiber layers to some extent.

Bhattercharjee et al. [70] indicated that further increasing the number of entanglements per polymer chain (e.g. by increasing the concentration of the solution while holding the polymer molecular weight constant) results eventually in an increased degree of extensional thinning and less stabilization of the jet as the strain rate increases due to the dramatic stretching of the jet. According to Shenoy et. al., for a concentrated solution, the stabilization of the jet requires at least one entanglement per chain in order to achieve a sufficiently high elasticity and subsequently extensional viscosity [60].

Bhardwaj found that a low molecular weight polymer solutions tend to forming beads instead of fibers and a high molecular weight solutions tend to form fibers with larger average diameter [71].

If we generalize the relation between molecular weight, viscosity and concentration, the number of entanglements per chain increases with molecular weight while entanglement per unit volume increases with concentration.

In the previous works it was found that increasing concentration increases viscosity and as a result more polymer solution is transferred per one jet. Therefore fabric throughput and fiber diameter increases [32,53].

2.3.1.1.2. Surface Tension

Surface tension tends to decrease the surface area per unit mass (and the surface energy) of a fluid. If the electrostatic force overcomes the surface tension, a charged jet of a polymer solution is ejected. So, for a higher surface tension, a stronger electric field is required. Surface tension is related to the interaction between the molecules of polymer and solvent in solutions.

If there is a high concentration of free solvent molecules, there is a greater tendency for the solvent molecules to congregate and adopt a spherical shape due to surface tension. A higher viscosity means that there is greater interaction between the solvent and polymer molecules thus when the solution is stretched under the influence of the charges, the solvent molecules will tend to spread over the entangled polymer molecules thus reducing the tendency for the solvent molecules to come together under the influence of surface tension as shown in Fig. 2.11[72].

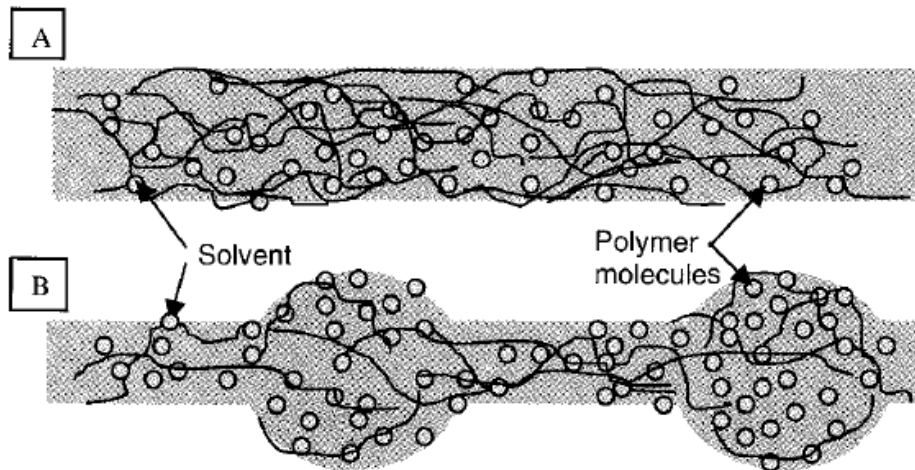


Fig. 2.11. (A) At high viscosity, the solvent molecules are distributed over the entangled polymer molecules. (B) With a lower viscosity, the solvent molecules tend to congregate under the action of surface tension.

Fong et al found that the number of beads decreased with increasing viscosity and net charge density and it also decreased with decreasing surface tension coefficient of the solutions [73].

2.3.1.1.3. Conductivity and permittivity

Electrospinning process operates due to external electric field, viscoelastic force due to the viscosity of the solution, surface tension force, conductivity, etc. Electric field between electrode and collector causes the solution to stretch. If the electrostatic field overcomes the surface tension, the nanofibers are formed. The stretching of the electrospun jet and the bending instability are mainly controlled by the Coulombic force between charges and the electric field. These forces arise due to the surface charge on the jet which can be varied by changing the conductivity of the solution. The increased charge carried causes the jet to elongate and can produce uniform fibers with a smaller diameter. A higher net charge density of the polymer solution could, therefore, yield thinner fibers with no beads. Filatov et. al. found that acceptable range of conductivity in electrospinning is rather wide from 10^{-6} to 10^{-2} $(\Omega.m)^{-1}$, where the upper limit is governed by the threshold of initiation of the gas discharge from the jet that destabilizes it. It was also discussed that the conductivity is associated with relative dielectric permittivity which usually varies little from its value of the solvent that is used. The lower permittivity, the

lesser the attenuation of the electric field inside the nascent liquid jet and the higher the rate of electric charge transfer in the solution. However, decreasing of the polarity of solvent molecule reduces the extent of dissociation in it of ionogenic substances with concurrent reduction in electrical conductivity. For the electrospinning, the best values of relative permittivity were found to be between 5 and 30, with a limit not exceeding 100 [74]. In our experiments, we were able to spin the solutions in the range of conductivity from 10^{-5} to 10^{-1} ($\Omega.m$)⁻¹.

The dielectric constant (ϵ) is defined as the ratio of the permittivity of a substance to the permittivity of free space (ϵ_0) which means a material concentrates electric flux, and is the electrical equivalent of relative magnetic permeability. The dielectric constant is always higher than or equal to 1. High dielectric constant means that more charge can be stored. For the most of polymers, the dielectric constants are usually in the range of 2 to 10. It was found that even low dielectric constant materials can be spun in electrospinning system [75].

Conductivity of solution is the factor that determines the current and fiber diameter. Solution with a high conductivity is able to carry more charge on the jet. Kim et. al. found that nanofibers with the smallest fiber diameter can be obtained from the solution with the highest conductivity [76]. On the other side, Heikkilä et. al. found that at the same viscosity, PAN/Salt solution produced slightly larger fibres because increased conductivity enhanced the mass flow. The higher conductivity of the PAN/Salt solution increased the instabilities in the electrospinning process [77].

For a conductive fluid there is a layer of charge carriers which is described by Poisson–Boltzman equation on the surface, of thickness on the order of the Debye length that is in a perfect equilibrium state. This equilibrium state on the surface is disturbed when the liquid starts to move and some of the charges are swept away by flow. On the other side, the surface layer is maintained if the charges are replenished faster than the rate at which they are removed. The ‘quasi-electrostatic’ (in which the charge distribution on the surface is unaffected by translocation or alteration of the shape of the interface) condition is valid in this limit. It is realized when characteristic times of fluid flow (t_f) \gg charge relaxation (t_e). The latter is given by $t_e = \epsilon\epsilon'/4\pi K$, where ϵ is the dielectric constant of the fluid, ϵ' is the dielectric permittivity of vacuum, and K is the conductivity of the solution. For momentum transfer to a viscous fluid, for instance, the hydrodynamic time (t_f) = $\rho h_0^2/\eta$ can be considered [62].

It is common to use a salt in polymer solutions to increase their conductivity. According to previous work, adding a salt to polymer solution such as PU and PVB increases the number of jets on the roller surface and as a result the productivity increases [53,54]. On the contrary, in the case of some other polymers such as PEO and PVA, addition of a salt decreases the spinning performance [55,78]. This case can be explained by the leaky dielectric model which was first proposed by Melcher and Taylor [79]. Bhattacharjee et al. [62] explained that “a leaky dielectric differs from a perfect conductor or a dielectric material in that free charges accumulate on the surface of the material in the presence of an external electric field and modify the local field. Under these conditions, two components of the electrical field develop, one tangential to the interface and another normal to it. The presence of a tangential component on the surface prevents the interface from being in an equilibrium condition and provokes it to deform. In contrast, the electrical stress in perfect dielectrics and conductors is always perpendicular to the interface. Electromechanical coupling occurs at the fluid-fluid interface alone; forces resulting from charges in the bulk are negligibly small. As the fluid accelerates, the tangential component of the electrical stress is largely balanced by the viscous, or viscoelastic, response of the fluid.

Thus, both the constitutive behavior and the electrical properties of the fluid determine the condition of the process. It is important to bear in mind that if the changes in conductivity resulting from salt additions are large enough to alter the behavior of the fluid from that of a leaky dielectric to that resembling a conductor, then the tangential component of the electrical stress that accelerates the fluid is likely to diminish and the flow process be stopped. In this limit the electrical stress will be balanced by the alteration of the shape of the interface and surface tension only” [62].

In general, the permittivity depends strongly on frequency, humidity absorption, sample thickness, temperature, bias field, and dopant concentration. Permittivity of a solution also depends on permittivity of solvent, polymer and additives. In this work, salts were used as additives. Additional salt creates direct and indirect link to polymer solution which increase the permittivity of solution. This link can be explained as the link between polymer and solvent and solvent to salt (indirect link).

The relative permittivity of water is around 80 while 38 for dimethylformamide. So, the permittivity of PEO-water solution is quite high around 78.5 [80]. Permittivity of PU is around 3.4-6.3 [81,82].

On the other hand, there is still not enough knowledge about the effect of polymer permittivity on electrospinning process.

2.3.1.1.4. Applied voltage

It was investigated that a drop of liquid having surface tension γ , held at the end of a capillary tube of radius r_0 , and raised to a potential difference of V disintegrates into a spray and at the point of disintegration the ratio $V^2/r_0\gamma$ remained approximately constant [83]. Then Taylor [30] found that the critical angle of meniscus which is called as ‘Taylor’s cone’ closed to disintegration is 49.3° . On the other hand Yarin et al showed that Taylor’s cone represents a specific self-similar solution, while non-self-similar solutions that do not tend to the semivertical angle. The shape of the meniscus changes as the concentration of the polymer in solution and the solution viscosity increases [84]. Another work showed that conductivity of solution changes the shape of meniscus.

Various voltages have significant effects on droplet size, fiber diameter and current transport. It has been verified experimentally that the shape of the initiating drop changes with applied voltage [85].

It has been demonstrated that above a critical voltage there are significant changes in the shape of the originating surface and the voltage dependence of the electrospinning current, and that these changes correspond to an increase in the number of bead defects observed in the electrospun fiber mats [86].

The self-organisation of liquid jet was analyzed by Lukas et. al. [35]. In this analysis, it is supposed that electrohydrodynamics of a liquid surface can be analyzed with the capillary waves running on an one dimensional approximation of the liquid surface, oriented along the horizontal axis, like x-axis, of Cartesian system of coordinates. The critical electric strength E_c for unstable waves which starts to form cone was formulated as:

$$E_c = \sqrt[4]{\frac{4\gamma\rho g}{\epsilon^2}} \quad (2.8)$$

Where γ is linear force of surface tension, ρ is mass density of liquid, g is gravitational acceleration, ϵ is permittivity. The assumption above that the critical electrical field strength, E_c , allows the creation of surface wave for initiating of jets.

The dimensionless electrospinning number Γ as

$$\Gamma = \frac{\alpha \epsilon E_0^2}{2\gamma} \quad (2.9)$$

Where α is capillary length and $\alpha = \sqrt{\frac{\gamma}{\rho g}}$. Using this definition, electrospinning is initiated only if the electrospinning number, Γ , is greater than one ($\Gamma_c=1$, critical electrospinning number).

The average inter-jet distance is described in terms of wavelength (λ) was calculated as

$$\lambda = 2\pi/k \quad (2.10)$$

where k is wave number and

$$k = (2\epsilon E_0^2 \pm \sqrt{(2\epsilon E_0^2)^2 - 12\gamma\rho g})/6\gamma \quad (2.11)$$

From previous work [78] it was found that raising applied voltage increased number of cones on the surface, as a result fabric throughput increased.

All these assumptions above are for needleless electrospinning. The minimum electric field depends on the surface tension and density of solution, relative permittivity of the surrounding gas and gravitational acceleration. If the electric field increases and exceeds the critical electric field a charged jet ejects from the apex of the cone and deposits on the collector.

Increasing the voltage has been shown to increase jet diameter, as a result fiber diameter increased [69]. In other investigations, increasing the voltage was shown to decrease the jet diameter, decrease the fiber diameter [67,73,87,88].

2.3.1.1.5. Distance between electrodes

The distance between electrodes is another phenomenon that controls the final fiber diameter and morphology. Sufficient time to dry out the solvent from polymer solution is necessary. If the distance between electrodes is too small, there is not enough time for drying, beaded and sticky fiber structures can be observed. On the contrary, if the distance is too big, the electric field between electrodes decrease and forming of fiber is difficult.

X. Yuan et. al. found that there were no obvious differences between the morphologies of the electrospun polysulfone (PSF) fibers at 10 cm and 15 cm electrode to electrode distance. Increasing the collection distance could give more time for the solvent to evaporate and for the charged fluids to split more times [89]. The effect of the tip to collector distance on the fiber morphology is not as significant as that of other parameters and this has been observed by many investigators [90,91,92].

2.3.1.1.6. Ambient conditions

Electrospinning is affected by electric field. It means that any changes in the electrospinning environment will affect the electrospinning process. Many works showed that ambient conditions (relative humidity, temperature) influence fiber diameter, morphology and spinning performance [59,69,93,94]. If the humidity is too high, the surface of the electrospun fibers tends to form pores. The temperature of the solution and of the surrounding air affects the viscosity of the polymer solution as well as the solvent evaporation rate. An increase in temperature leads to the decrease in viscosity and to the increase of mobility of polymer molecules. This allows higher degree of deformation of jets by Columbic force and results in fibers of smaller diameter.

When humidity is high, it is likely that water condenses on the surface of the fiber. At a very low humidity, a volatile solvent may dry out very rapidly. The evaporation of the solvent may be very fast. As a result, the electrospinning process may only be carried out for a few minutes before the needle tip is clogged [72]. Cengiz et. al. found that ambient humidity has an important effect on the spinning performance, fiber diameter and surface properties of polyurethane polymer. The spinning performance as well as the fiber diameter increased with increasing humidity. On the other hand, very high humidity restricts the spinnability of solution in time due to increasing viscosity of solution on the roller surface. This is caused by absorption of water vapour by the hygroscopic solvent (dimethylformamide in this case) and leads to continuous changes of solution viscosity, spinning performance and fiber quality in running time of electrospinning process. The highest fiber diameter was achieved in higher relative humidity [59]. Generally, every specific polymer solution requires optimized values ambient temperature and humidity. In this work, the optimized values of temperature and humidity were set for used polymers.

2.3.1.1.7. Velocity of take-up fabric

During the roller electrospinning process, a supporting material (often a nonwoven fabric) is passing along the collector electrode to collect the fibers in the form of a more or less regular nanofiber layer on its surface. The speed of this fabric (in meters per minute) influences the area weight of nanofiber layer and also affects the quality of nanofibers membrane, namely its regularity and non-fibrous area. The area weight of resulting nanofiber layer can be easily calculated from the spinning performance and the velocity of supporting material. Typical values of the velocity amount from 0.1 up to 10 meters per minute.

2.3.1.1.8. Geometry of electrodes

In the needleless ES, many jets are formed simultaneously on the surface of the spinning electrode. Jets are generated on the free liquid surface by a self-organizing process. Because of this it is more difficult to control the spinning process when compared with the needle electrospinning process. The spinnerets in the needle electrospinning play essential role in determining the product quality and productivity. Despite of the success in needleless electrospinning, a design of a principle for better needleless electrospinning process is still in progress. That is why the effort of scientists was focused on the shape of spinning electrodes.

Niu et. al. [95] studied the influences of spinner shape on electrospinning process using three rotating fiber generators, cylinder, disc and coil (Fig. 2.12). The electric field generated in the vicinity of these spinners was analyzed by a finite element method and the calculations indicated that electric field intensities on these spinnerets are distributed differently as shown in Fig. 2.12.

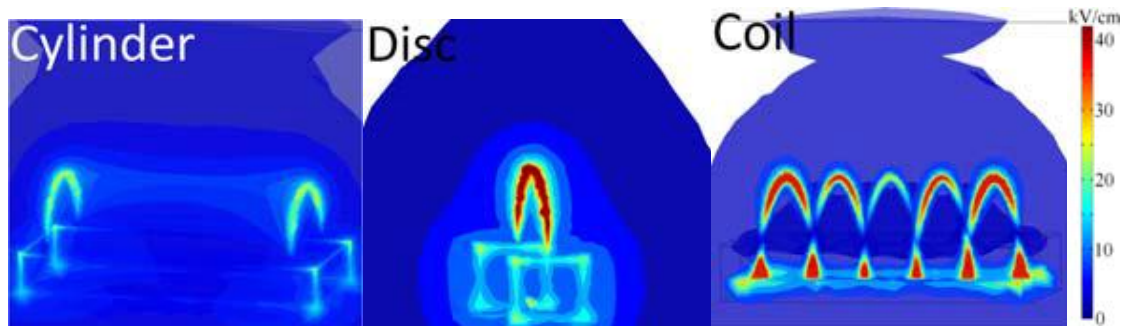


Fig. 2.12. Electric field intensity profiles of cylinder, disc, and spiral coil spinnerets [95]

The electric field analysis indicated that high electric field intensity was formed by disc and coil spinnerets, which distributed narrowly on the surface of disc circumferential edge and coil wire, respectively. The cylinder spinneret formed unevenly distributed electric field at the end and middle area with lower strength. The intensity peak was formed only on the coil surface. Finer nanofibers with narrower diameter distribution were produced by disc and coil spinnerets, compared to needle and cylinder electrospinning. The fiber production rate in coil electrospinning was as high as 23 g/hr, which was much higher than those in cylinder, disc, and needle electrospinning [95]. In another work, a rotating cylinder, ball, and disc spinnerets have been compared. These spinnerets had much higher productivities (cylinder 8.6 g/hr, disc 6.2 g/hr, and ball 3.1 g/hr) in comparison with the needle electrospinning. Under the same working conditions, the disc produced finer nanofibers (257 ± 77 nm) with a narrower diameter distribution compared to the ball (344 ± 105 nm) and the cylinder (357 ± 127 nm) spinners. Electric field was analyzed by a finite element method, and high electric field was found to be narrowly distributed on the disc top, which led to a high stretching rate to the solution jets. The cylinder spinneret had a large surface area, but the electric field distributed unevenly on the fiber-generating surface. The ball formed an electric field with a low intensity, thus generating fewer jets when compared to the disc and the cylinder spinnerets [96]. Fig. 2.13 Rotating spinners that have been reported for needleless electrospinning [97].

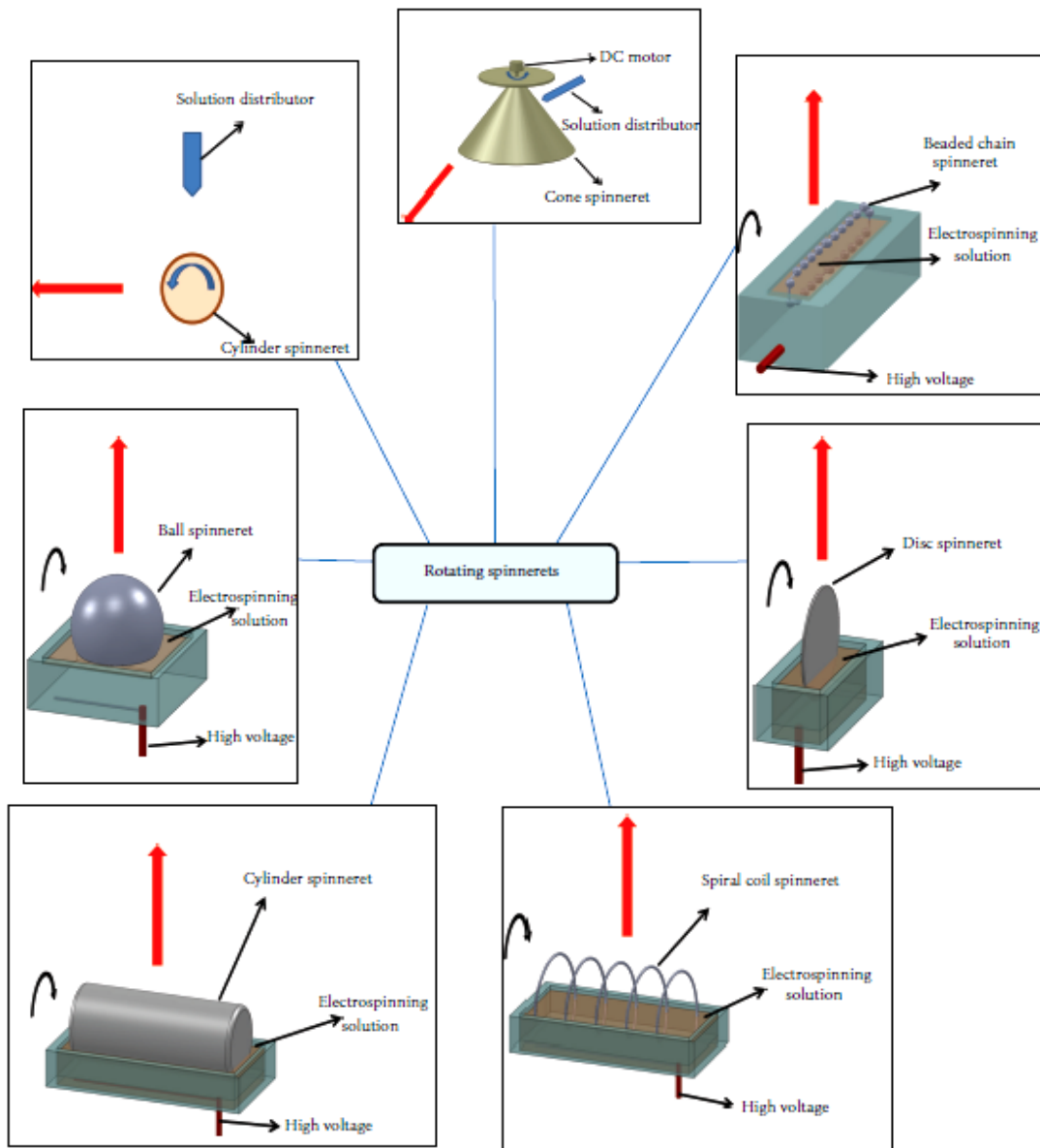


Fig. 2.13. Schematic summary of needleless rotating spinnerets (electrospinning direction along the red arrow).

In this study, only a rotating cylinder was used. Investigation of the other parameters affecting the spinning results such as the fiber diameter, morphology and productivity seems to be more important than the effects of spinning electrode. Therefore, this work is focused on the relations between selected dependent and independent parameters of needleless electrospinning process.

2.3.1.1.9. Geometry and conductivity of collector electrode

The collector electrode in electrospinning is generally a conductive material. Collector can be directly connected to a high voltage supplier which gives the opposite charge than the spinning electrode has or it can be grounded. Fibers that are collected on the non-conducting material

usually have a lower packing density compared to those collected on a conductive surface [98]. Beside this, a non-conductive collector or even a non-conductive take-up fabric reduce the spinning performance considerably. Collectors of various shapes were described in the literature, mainly designed to influence the structure and/or anisotropy of produced nanofiber layers [99,100,101].

During all the experiments performed in the framework of this thesis, a conductive, flat and grounded collector was used.

2.3.1.2. Dependent parameters

2.3.1.2.1. Number of cones

A number of Taylor's cones are simultaneously present on the spinning surface of the spinning roller electrode. Number of cones (N_c) depends strongly on independent electrospinning parameters as the experience shows. This phenomenon affects directly the spinning performance. Cones are counted using a camera record as shown in Fig. 2.14 and their number is related to the spinning area determined from the same record.



Fig. 2.14. Number of cones on the roller surface

To calculate the density of cones, the spinning process is recorded by a camera. The average number of cones (N_c) was counted from these pictures as shown in Fig. 2.14. The density of cones (D) can be calculated as the ratio of number of cones (N) to the spinning area (A).

$$D = \frac{N_c}{A} (1/m^2) \quad (2.12)$$

2.3.1.2.2. Jet length

Length of the jet of polymer solution was described and studied by Dao [32]. The distance between the tip of a Taylor cone and the splitting point of a jet is called length of jet. The long range repulsive electrostatic forces between ions of the same sign cause the disintegration of charged jet body. If electric forces are stronger than the capillary forces, the jet will split or will be formed by the whipping instability. The process of concentration of ions at the surface of a jet preceding the onset of splitting or whipping instability is shown in Fig. 2.15. The condition of

the process, such as solution viscosity, amount of ions per volume unit etc. predetermine the length of a jet.

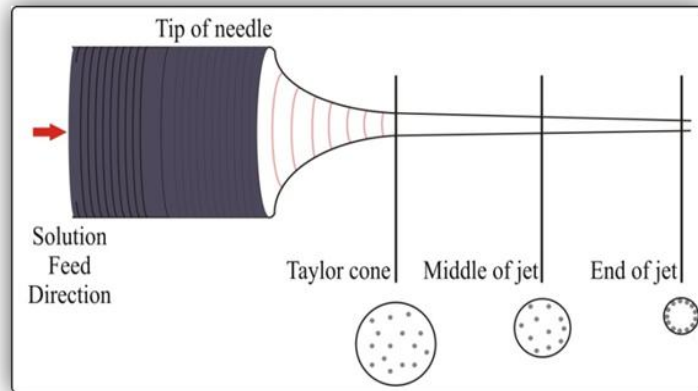


Fig. 2.15. Radial movement of ions in a jet.

In the polymer solution entering the electrospinning process, the ions are more or less regularly distributed in the volume. When the stretching of a jet starts, the ions move towards the surface of the jet due to repulsive forces. As soon as the concentration of ions at the surface and the corresponding repulsion forces are big enough, the disintegration process starts. The viscosity and conductivity of solution are the key parameters influencing the time necessary for the start of disintegration. If viscosity is high, movement of ions towards the surface takes more time and the length of jet will be greater [32]. Adding salt increases conductivity of solution as well as number of ions in the solution. If number of ions is high, the time for ions to reach critical concentration will be shorter. Consequently, the jet will be shorter [32]. In the experimental part, the rod electrospinning technique was used to measure the length of jets because the length of jet and average current in the rod and roller system are similar and the experiments in the rod electrospinning are easier.

2.3.1.2.3. Spinning performance and spinning performance per jet

Spinning performance (SP) is one of the most important characteristics of nanofiber production process, influencing the production costs. The spinning performance of needle electrospinning is quite low while rather a high performance can be achieved by needleless system. Spinning performance strongly depends on all the independent parameters and influences the quality of nanofibers as well as that of nanofiber layers.

SP can be determined from the mass of nanofibers produced in a one meter long roller spinning electrode in one minute. Spinning performance is calculated from area weight of produced nanofiber layer as follows:

$$SP = \frac{G * v * Lf}{Lr} \quad [\text{g/min/m}] \quad (2.13)$$

Where,

G is area weight of nanofibers membrane per area in g/m².

v is velocity of running collected fabric, in m/min.

Lf is the width of nanofibers membrane on collected fabric, in m.

Lr is the length of spinning roller, in m.

Spinning performance per one Taylor's cone (SPC) can be calculated from the known values of SP and an average total number of Taylor's cones on the spinning electrode N_c using the Formula (2.14). SPC is an amount of polymer solution that is transported through one Taylor's cone (or a jet).

$$SPC = \frac{SP * Lr * 60}{Nc} \quad [g/h] \quad (2.14)$$

SPC is one of parameters which will be measured during following experiments to see whether SP is realized through SPC or rather through N_c .

2.3.1.2.4. Fiber diameter and fiber diameter distribution

The fiber diameters are easily measured on the SEM microphotographs using the Lucia software. Fiber diameters distribution can be expressed using a standard deviation value according the Eqn. 2.15 [28].

$$\sigma = \sqrt{\frac{1}{N} \sum_{i=1}^N (x_i - \mu)^2}, \quad \mu = \frac{1}{N} \sum_{i=1}^N x_i \quad (2.15)$$

σ is standard deviation.

N is the number of elements (measured nanofiber diameters)

x_i is nanofiber diameter

μ is average nanofiber diameter

2.3.1.2.5. Non-fibrous area

The term non-fibrous area (NFA) was created as a measure of nanofiber layer quality. This is a percentage of the area of a SEM microphotograph of nanofiber layer occupied by non-fibrous formations such as beads, foils etc. A typical example of such microphotograph is shown in Fig. 14. A SEM image of a nanofibrous layer is taken in low magnification (x500 or x1000). The aim of using a low magnification is to measure a larger area. Using a Lucia software, the total sample area and the non-fibrous area can be measured. NFA (Fig. 2.16) is then expressed according to the formula

$$NFA = \frac{\text{Total Non - Fibrous area}}{\text{Total Membrane Area}} * 100, [\%] \quad (2.16)$$

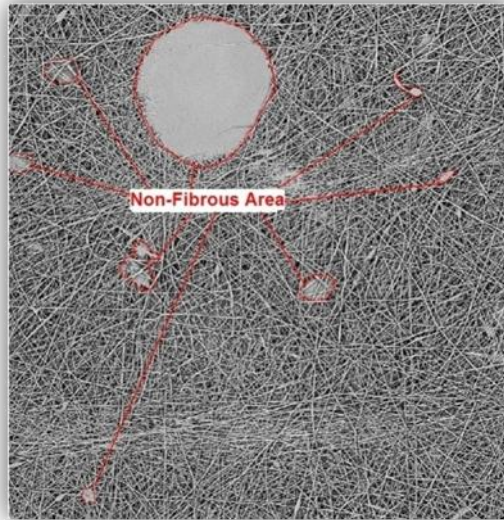


Fig. 2.16. Non-fibrous area of a nanofiber layer

2.3.1.2.6. Life time of a jet

Life time of a jet can be defined as the period of time from the point that the jet appears on the spinning electrode to the point that the jet disappears. The solution properties, roller speed, electric field strength, number of cones and the thickness of layer on the roller surface are the main parameters that affect the life time of jet. Because of rotating roller movement, the jet life is limited.

The life time of a jet can be measured using a camera record of the spinning area during electrospinning. The measurement procedure consists in tracing a specific Taylor's cone during step-by-step playing the record.

2.3.1.2.7. Measurement of current

Measuring the jet current is a useful method of studying the mechanism of electrospinning [76,86,102,103,104,105,106,107,108,109,110,111,112,113,114]. Most of the papers describing measurement of the jet current deal with needle electrospinning [76,86,102,103,104,105,106,107,108,109,110,111,112,113]. Another article is based on the rod electrospinning [114]. The aim of this paper is to study the current during the roller electrospinning. To show the relations between the currents in the needle, rod, and roller electrospinning, the current was measured in all three electrospinning techniques.

The current is usually measured as the voltage drop across a resistor placed in series between the collector electrode and ground [86,102]. Some authors use a microammeter [76] placed in the same position.

The dependence of the jet current on independent process parameters, such as solution concentration and conductivity, feed rate, voltage, and so on, has been studied

[103,104,106,109,112]. Bhattacharjee et al. [112] found the dependence of the jet current on the voltage, feed rate, and solution conductivity, expressed as

$$I_{\text{total}} \sim E Q^{0.5} K^{0.4} \quad (2.17)$$

where E is voltage, Q is the feed rate, and K is the solution conductivity.

Eqn. (2.17) is valid for various polymer solutions and other process and material parameters.

In the study of jet current, Kim et al. [76] and Bhattacharjee et al. [112] identified two distinct components of the total measured current, one linked with the transport of mass and its conductivity, the other with secondary electro spray emanating from the surface of the jet.

Fallahi et al. [111] calculated the volume and surface jet charge density from a measured jet current.

Lee et al. [105] and Munir et al. [110] studied the relation between jet current and nanofiber quality and uniformity. Munir suggested a constant-current electrospinning system to control the spinning process and product uniformity.

Samatham and Kim [106] used real-time electric current measurement during the needle electrospinning process. Based on the variations of current in time, they identified four different jet regimes:

1. Fluctuating jet: typical for a high ratio of voltage/feed rate. The jet flow rate exceeds the feed rate, and therefore the jet must be interrupted repeatedly and the current is fluctuating.
2. Stable jet: typical for medium ratio of voltage/feed rate. The jet flow rate is close to the feed rate. The jet and current are stable.
3. Stable jet with polymer drops: typical for a low ratio of voltage/feed rate. The jet flow rate is smaller than the feed rate. The droplet at the tip of the needle grows and drops down repeatedly.
4. Multiple jets are observed in some cases. More than one jet occurs from the droplet of polymer solution. The current increases in correspondence with the number of jets.

Jet current was measured in the rod electrospinning process by Pokorny et al. [114]. In rod electrospinning, a droplet of polymer solution is placed on the upper surface of a vertically positioned metal rod. The rod is linked with the DC voltage and serves as a spinning electrode. The spinning process is limited in time because of the small volume of the solution droplet; nevertheless it serves as a model of needleless (or surface) electrospinning.

In [114], a high-speed camera and a memory oscilloscope were used to simultaneously measure Taylor's cone formation and the development of the jet current. The mechanism of Taylor's cone formation was recorded and discussed.

The measurement of electric current has been studied in the previous work in the roller electrospinning [33]. Details will be explained in sub chapter 3.1.

2.3.1.2.8. *Launching time of jet*

Highly concentrated solutions have an intensive entanglement of polymer chains, therefore coulombic repulsion force will not be sufficient to start jetting. However, the surface area has to be increased to accommodate the charge build-up on the jet surface which occurs through the formation of fibers. Deitzel et al. [115] suggested mobility of particles in electrospinning jet initiation to occur from the surface layers of the cone. This is partly due to surface shear forces generated by the potential difference between the electrodes.

Recently, the time needed for Taylor cone formation (characteristic hydrodynamic time) was experimentally determined from voltage–time oscilloscope records of the electrospinning onset event that were accompanied by video-records [116]. It was hypothesized that the characteristic hydrodynamic time is of the same order as the theoretically derived reciprocal value of the wave growth rate that is denoted here as ‘relaxation time’. The derivation was based on the linear stability analysis. It was found that these times are of dynamic nature and hence they are viscosity dependent. The theoretical derivation of relaxation time for conductive viscous liquids was introduced and related to experimental measurements of characteristic hydrodynamic times. It was assumed that relaxation time T is the reciprocal quantity to the growth factor A , $A = 1/T$.

$$A = -O_h K^2 + \sqrt{O_h^2 K^4 - \Omega_0^2} \quad (2.18)$$

Where Ω_0^2 is a dimensionless square of the angular frequency of a non-viscous liquid, A is a dimensionless growth factor of a viscous liquid; K is the dimensionless wavenumber and O_h Ohnesorge number.

2.3.2. THE NEW PARAMETERS INTRODUCED BY AUTHOR

Until now many researchers have tried to explain mechanism and parameters of electrospinning process. Many of them concentrate on the needle electrospinning while only a few on the roller system. The aim of this work is to contribute to understanding the roller electrospinning mechanism using new measurable independent and dependent process parameters which were not yet investigated and which have the potential, when studied, to bring new information. Previous parameters are not sufficient to explain experimental results. We found that suggested parameters affect our spinning performance and fiber morphology excessively. For instance, the roller rotation speed affects spinning area and spinning performance as well as the fiber and nanoweb quality.

2.3.2.1. Independent parameters

2.3.2.1.1. *Velocity of rotating roller and related quantities (Secondary independent parameters)*

Spinning roller electrode is one of the most important parts of the roller electrospinning device. The first description of the roller spinning electrode, its design, function and variants, was presented in [13]. The main function of the roller consists in feeding the polymer solution from a tank in the form of solution layer on the roller surface into the electrospinning process between the spinning and collector electrode. The main primary parameters of the roller electrode are:

- Geometry (shape and diameter)

- Velocity (rpm) of roller rotation on its axis.

Above mentioned roller parameters influence, together with other ES parameters, a number of secondary independent ES parameters, ruling the spinning process, namely:

- Thickness of polymer solution layer on the surface of roller
- Feeding rate of polymer solution
- The time available for formation Taylor's cones and the spinning process from these cones.

In spite of obvious and known importance of above mentioned secondary ES parameters, no works dealing with systematically with them are known. In the roller ES process, rollers of cylindrical shape are mostly used with diameters close to 20 mm. Roller velocities are set mostly by experience and intuition.

Therefore, the relations between the roller velocity and secondary ES parameters will be analysed in following text and the roller velocity will be incorporated into the plan of experiments as one of basic primary parameters. On the other hand, the work will deal with cylindrical spinning roller of 20 mm diameter only.

2.3.2.1.1.1. Thickness of layer on the surface of roller

The main mechanism of roller electrospinning system is based on a roller which is immersed in a polymer solution tank. The role of roller is feeding polymer solution to surface of roller by rotational movement. The fibers are formed on the surface of the solution. It is necessary to examine the movement of roller since it determines feeding of polymer solution, thickness of solution layer on the roller, number of Taylor's cones on the surface and spinning performance of fibers. When velocity of roller (rpm) falls below certain limit, there is not enough solution on the roller surface to feed and form cones. As a result spinning does not start.

Roller rpm was never optimized and understood. It is one of the aims of experiment to clarify the role of roller rpm.

The effect of roller rotation on the thickness of polymer solution layer has been examined in several papers [117,118,119].

The stability of fluid flowing down a vertical or inclined wall has been studied by many researchers [120,121,122,123,124,125]. The time evolution of thickness of a viscous liquid film spreading over a solid surface under the action of the gravity and surface tension can be described by lubrication models [126,127,128,129,130]. These models approximate the full Navier-Stokes system that describes the motion of the liquid flow.

There have been several recent theoretical and experimental advances. Frenkel et. al. investigated the nonlinear stability of a film flowing down a cylinder using the strong surface tension approximation and showed that wall curvature has an important influence on the transverse disturbance of the film, suppressing harmonics of high angular frequency [118].

Chugunavo et. al. studied the dynamics of a viscous incompressible thin fluid film on the outer surface of a horizontal circular cylinder that is rotating around its axis in the presence of a

gravitational field. The motion of the liquid film is governed by four physical effects: viscosity, gravity, surface tension, and centrifugal forces. These are reflected in the parameters: R : the radius of the cylinder, ω : its rate of rotation assumed constant, g : the acceleration due to gravity, ν : the kinematic viscosity, ρ : the fluid's density, and σ : the surface tension [131].

Campanella and Cerro [119] consider a related flow exterior to a rotating cylinder for the case when the cylinder is partially submerged. Theoretical and experimental results showed that thickness of the liquid film depends on density ρ , viscosity μ , surface tension σ (or γ) of the fluid and immersion angle θ_0 , which described the flooding of the cylinder. Fig. 2.17 below shows the geometry of the system. A cylinder of radius R and infinite length was partially submerged in a pool of viscous fluid. The cylinder was rotating around its own axis at an angular speed ω . They found that theoretical and experimental results are comparable.

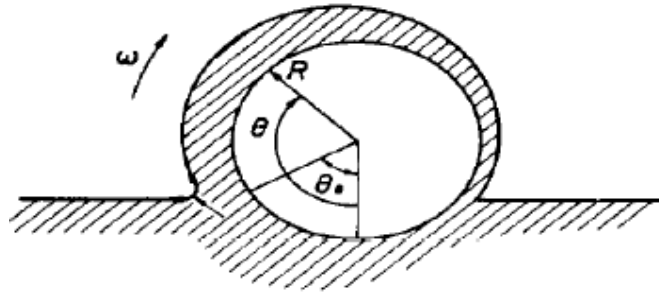


Fig. 2.17. Overall system geometry [119].

Campella and Cerro used the rapid flow approximation done by Cerro and Scriven [132] to simplify the equation of motion in order to a relationship between film thickness and operating parameters.

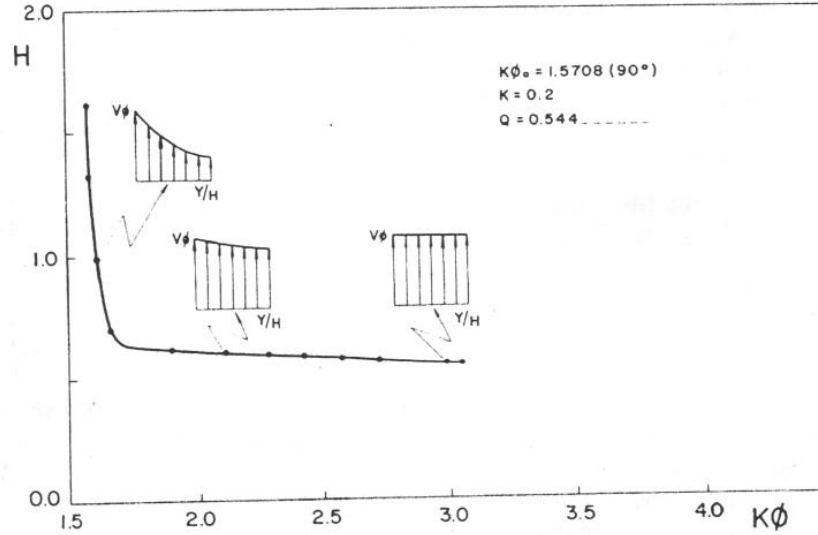


Fig. 2.18. Graph of dimensionless thickness (H) as a function of immersion angle ϕ [119].

Keeping in mind the fact that gravity force in the longitudinal direction of flow (i.e. azimuthally) are minimal at the lower part of the cylinder and grow to a maximum for $\theta_0 = 90^\circ$. Depending on the angle of immersion, the flow will be subject to a growing ($K\phi_0 < 90^\circ$) or diminishing ($K\phi_0 > 90^\circ$) force of gravity. For small immersion angles gravity increases as the film moves upwards causing a maximum film thickness as shown in Fig. 2.17. After the predicted maximum, viscous forces take over and the film is continuously accelerated, hence, the solution layer becomes thinner.

Fig. 2.18 shows the decrease in dimensionless thickness $H [-]$ as the product $K\phi$ increases, while H , K and ϕ are defined as follows:

$$H(\phi) = \frac{h}{h^*}, \quad h^* = \sqrt{\frac{\mu\mu^*}{\rho g}} \quad (2.19)$$

$$\theta = K\phi, \quad K = \frac{\mu^*}{Rg} \quad (2.20)$$

Eqn. 2.19 shows that the increase in speed rotation of the roller and viscosity of the fluid lead to higher thickness of the fluid of on the surface of the roller. And Eqn. 2.20 in simplicity state that the deeper is the roller on the fluid the thicker is the layer on the surface.

The asymptotic evolution equation for the thickness of the fluid film with the surface tension effect was derived by Pukhnachev in 1977 [117,133] Eqn 2.21.

$$\frac{\partial h}{\partial t} + \frac{\partial}{\partial \theta} \left[\omega h - \frac{1}{3} \frac{g}{\nu R} h^3 \cos \theta + \frac{1}{3} \frac{\sigma}{\rho R^4 \nu} h^3 \left(\frac{\partial h}{\partial \theta} + \frac{\partial^3 h}{\partial \theta^3} \right) \right] = 0 \quad (2.21)$$

It is valid under the assumptions that the fluid film is thin $h \ll R$ and its slope is small $(1/R)(h/\partial\theta) \ll 1$.

The iterative boundary-integral technique of Hansen et. al. provides both two dimensional Stokes-flow solution and estimates for the Maximum-Supportable Loads (MSLs) well beyond the thin film regime, specially for film thickness of the order of the cylinder radius. However, they demonstrated that the free surface profiles are very weakly depending upon the surface tension [134].

Kelmanson [135] analyzed (Eqn. 2.22), asymptotically and numerically, diverse effects of inertia in both small- and large-surface-tension limits and presented a more general model by taking into account inertial effects:

$$\frac{\partial h}{\partial t} + \frac{\partial}{\partial \theta} \left[\omega h - \frac{1}{3} \frac{g}{\nu R} h^3 \cos \theta + \frac{1}{3} \frac{\sigma}{\rho R^4 \nu} h^3 \left(\frac{\partial h}{\partial \theta} + \frac{\partial^3 h}{\partial \theta^3} \right) + \frac{1}{3} \frac{\omega^2 \rho}{\nu R} h^3 \frac{\partial h}{\partial \theta} \right] = 0. \quad (2.22)$$

Benjamin [136] in his work in (1995) also concluded that the amount of raised fluid by roller is a function of roller speed, immersion depth and rheological and interfacial properties of fluid. If the roller is deepened into the feeding pan, and then the thickness of the film onto the roller can be estimated with the result from deep coating theory as follows:

$$h = 0.994 \left[\frac{\mu V}{\sigma} \right]^{\frac{1}{5}} \left[\frac{\mu V}{\rho g (1 - \sin \theta)} \right]^{\frac{1}{2}} \quad (2.23)$$

provided that $\mu V/\sigma < 10^{-2}$. The film thickness is a function of the absolute speed of roller, V , gravity, g , the angle of inclination of the roller as it leaves the liquid, θ , and the physical properties of the liquid: σ is the surface tension, μ is the viscosity, ρ is the density.

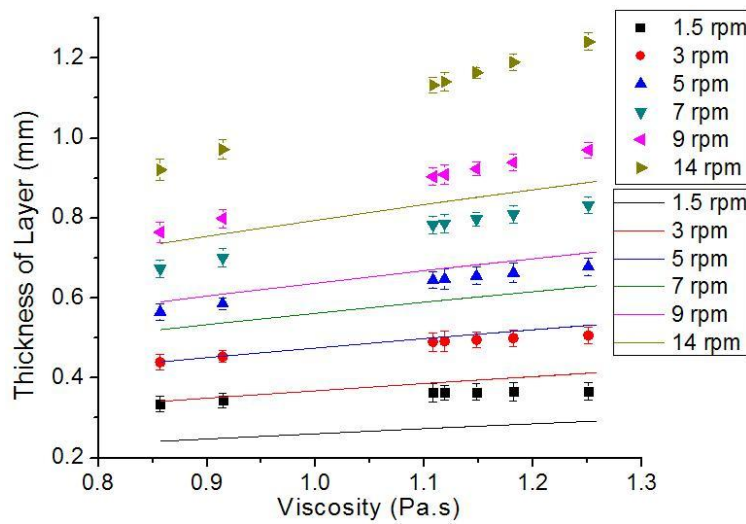
In one of our previous works (the author was a consultant of this diploma thesis) [93], the thickness of a polymer solution layer on the roller was measured as a function of roller velocity and solution viscosity. An alumina roller of 20 mm diameter and polyvinyl alcohol-water solutions of various concentrations were used in the experiment. The thickness of solution was measured using an especially designed apparatus on the top of the roller. The experimental results were processed using a multi regression method:

The function $z=f(x,y)$ was calculated, where x is solution viscosity (Pa.s), y is the roller velocity (rpm) and z is the thickness of polymer layer (mm) with the following result:

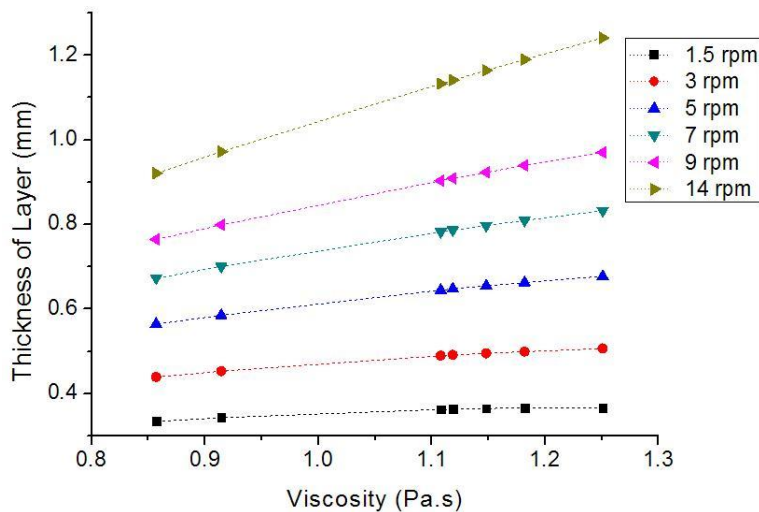
$$z = a + b \cdot x + c \cdot y + d \cdot x \cdot y + e \cdot x^2 + f \cdot y^2 + ee \quad (2.24)$$

where ee is the random error. Quality of the fit is relatively good, about evidenced by the high value of the coefficient of determination 0.9648.

The results of the measurement for the polymer solutions of polyurethane and polyethylene oxide used in the experimental part of this thesis are shown in Fig. 2.19 and Fig. 2.20. Experimental results are with error bars at 95% confidence intervals.

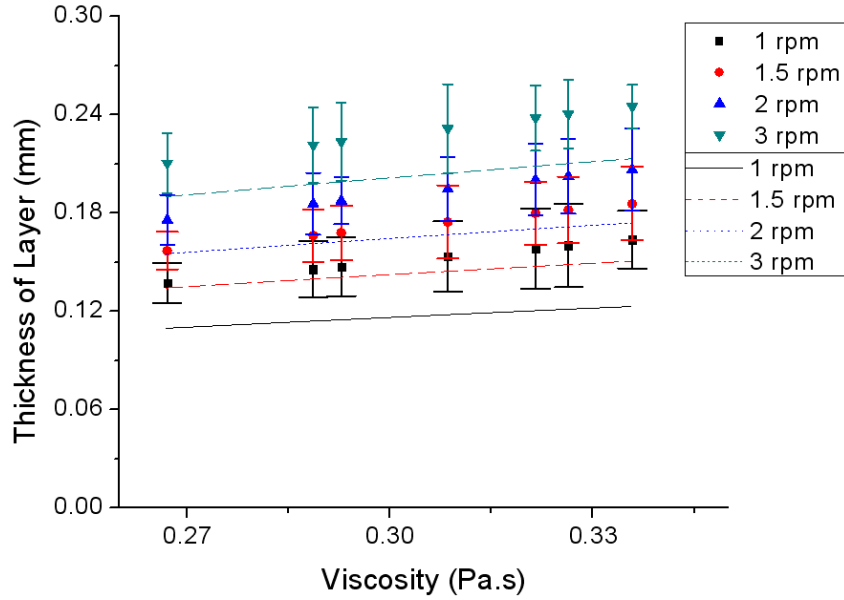


(a)

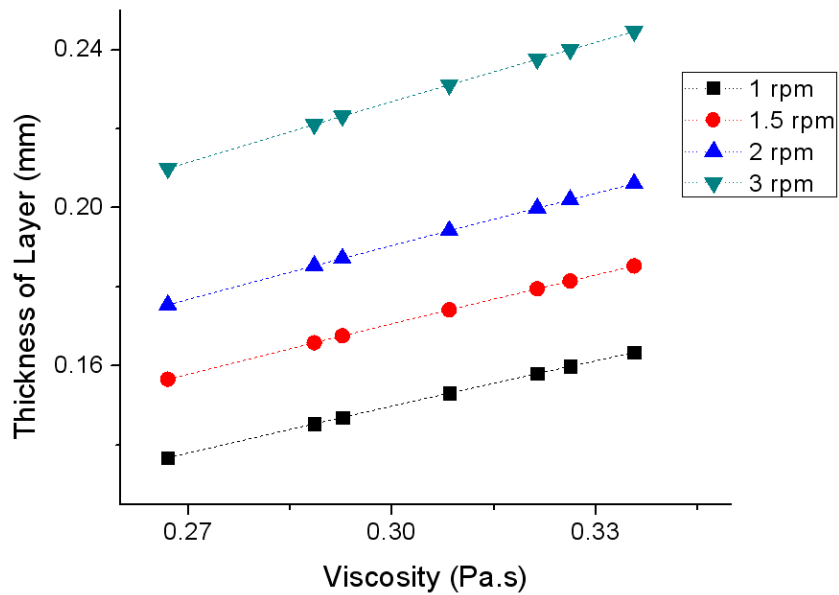


(b)

Fig. 2.19. Thickness of PU solutions layer as a function of roller rpm and viscosity; (a) comparison of measurement results (points) and theoretical (lines) calculation, (b) measurement result of thickness (dot lines represent connection of points).



(a)



(b)

Fig. 2.20. Thickness of PEO solutions layer as a function of roller rpm and viscosity; (a) comparison of measurement results (points) and theoretical (lines) calculation, (b) measurement result of thickness (dot lines represent connection of points).

2.3.2.1.1.2. Feeding rate of polymer solution

Feeding rate is another secondary independent parameter depending on the roller velocity. It is well known from the needle electrospinning that the feed rate, here directly set on the syringe pump, influences the spinning mechanism and product quality considerably. The same can be

expected in the roller electrospinning. The feed rate depends on the roller velocity in following way:

Let be: h – the thickness of solution layer (m)

ω - angular speed of roller (rpm)

d - roller diameter (m)

ℓ - roller length (m)

Then the linear velocity of the roller surface v is equal to

$$v = \omega \cdot \pi \cdot d / 60 \quad (\text{m/s}) \quad (2.25)$$

and the voluminous feed rate \dot{v}

$$\dot{v} = h \cdot v \cdot \ell = h \cdot \omega \cdot \pi \cdot d \cdot \ell / 60 \quad (\text{m}^3/\text{s}) \quad (2.26)$$

The voluminous feed rate of polymer solution per 1 meter length of roller \dot{v} / ℓ is equal to

$$\dot{v} / \ell = h \cdot \omega \cdot \pi \cdot d / 60 \quad (\text{m}^3/\text{s}/\text{m}) \quad (2.27)$$

The voluminous feed rates of the solutions used in the experimental part of this thesis calculated according to Eqn. 2.27, are illustrated in Fig. 2.21 and Fig. 2.22.

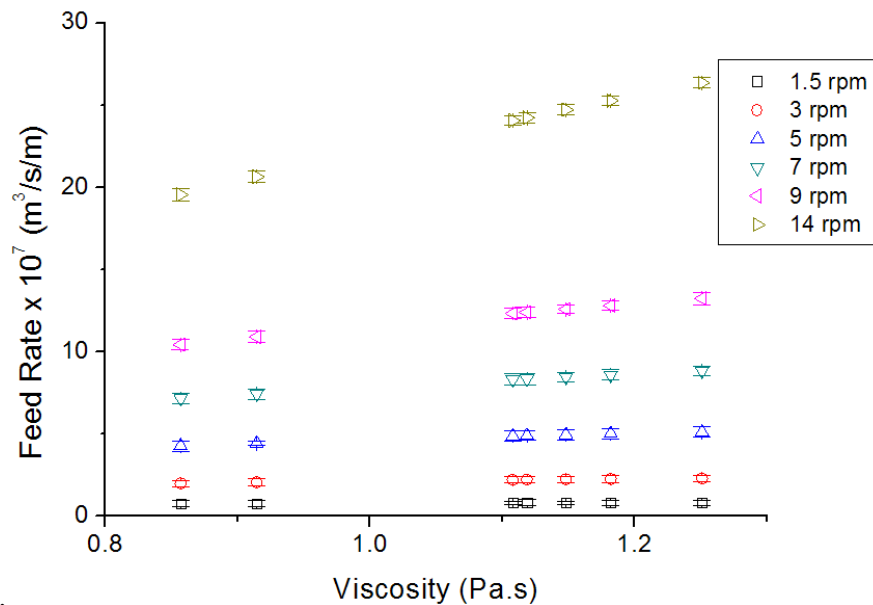


Fig. 2.21. Feed rate of PU solution.

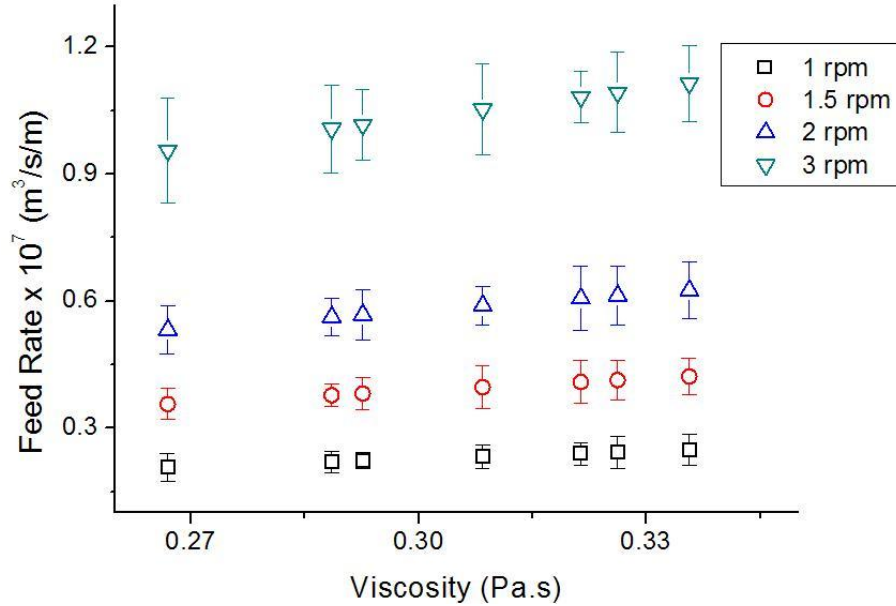


Fig. 2.22. Feed rate of PEO solution with standart deviation.

2.3.2.2. Dependent Parameters

2.3.2.2.1. Average current and current per jet

Under an electrostatic field, the polymer solution droplet becomes distorted by the induced electrical charge on the liquid surface, and a stable jet of polymer solution is then ejected from the cone. The break-up of the jet depends on the magnitude of the applied electric current. Reneker and Chun characterized the bending instability in a charged jet during electrospinning [137].

Many investigators on electrospaying have focused on the understanding of a current–voltage relationship. Previous attempts to correlate current with electric field and flow rate suggested nonunique linear [102] or power law [103] dependencies. Using the power law, Fallahi [107] showed that the relationship between current and voltage as $\text{current} \sim (\text{voltage})^{2.53}$.

Demir et al. [69] reported a power law relationship between the solution flow rate (Q) and the applied voltage (V) with an exponent value of three in the experiments where Q was not controlled. Bhattacharjee et al. [112] showed that current is not only depends on applied voltage but also conductivity and feed rate of polymer solution. The relationship between current and other parameters were indicated that $I \sim E * Q^{0.5} * K^{0.4}$. Theron et al. [103] reported that the average electric current increased with the increase in the feed rate and voltage. It was also found that increasing the applied voltage and solution conductivity, both the jet current and fiber diameter were increased [107]. Because increasing the electric field increases the electrostatic stresses, which in turn, draw more material towards to collector. Kim et al. found that there is an optimum average electric current for the electrospinning process that depends on the solution properties [138]. In this work, average current was measured using a multimeter. Current per one jet was calculated according to Eqn 2.28 which was suggested in [33]:

$$\text{CPJ} = \frac{TAC}{N} \quad (2.28)$$

CPJ implies current per one jet, TAC means total average current and N is total number of jets. Cengiz et. al. investigate a strong connection between the current of polymer solution jet and spinnability as well as spinning performance. Measurements were done on rod electrospinning system. They found that electric current of the solution jet increases with PU and TEAB concentrations increase and current indicates the spinning performance [56].

In the previous works, the current was measured using various methods. All the measurements were performed in the needle electrospinning. It is the aim of this work to apply the current measurement in the roller electrospinning. To interpret the results correctly, the relations between currents in the needle- rod- and roller electrospinning will be studied in the first group of experiments.

2.3.2.2.2. Parameters measured using camera records

In the experimental part, for the measuring of number of jets, spinning area, jet life, positions of jets and distance between jets were measured using camera records

Spinning area and positions of jets

Spinning area on the roller can be defined as the part of roller surface where the Taylor's cones occur. It was assumed in the literature [33] that the spinning area covers approximately one third of the roller surface. Our experiments showed that spinning area depends on a number of parameters. Movement of roller and life time of jets are the main parameters influencing the size and position of spinning area. Other parameters such as polymer solution properties, additives in the solution, electric field strength, number of jets, etc. also affect the spinning area. Spinning area will be determined by camera record. From this record a number photos will be used as shown in Fig. 2.23. For this purpose, a special roller was designed with a grid on its surface. The grid consists of oblongs 5.3 x 5 mm (Fig. 2.24) and helps to quantify the size and position of spinning area.



Fig. 2.23. Spinning area on the roller surface

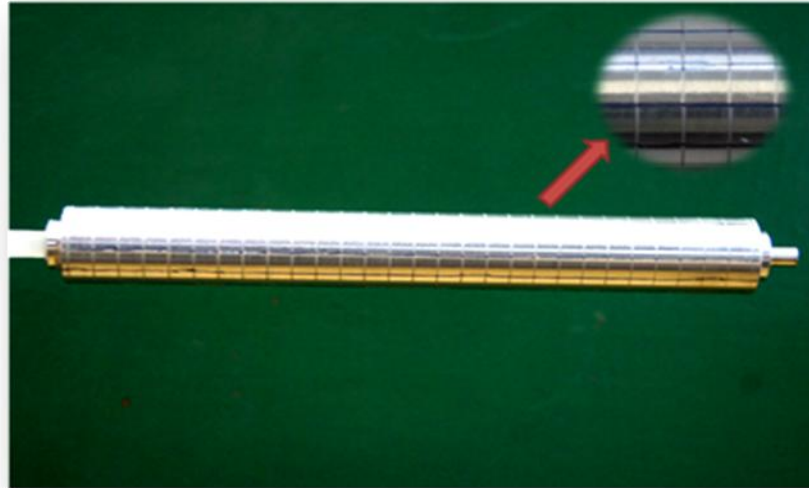


Fig. 2.24. Surface of roller

Spinning area strongly depends on the roller velocity. The position of jets vs. velocity of roller is illustrated in Fig. 2.25.

Thickness of polymer solution layer on the roller influences solution flow into Taylor cones. Thickness of layer depends on velocity of roller and viscosity of solution as shown in one of previous chapters. Simultaneously, polymer solution, when moving out of tank, needs certain time to create Taylor's cones. Subsequently, solution from the vicinity of Taylor's cones is dragged into the cones and following jets, being consumed gradually. If the velocity of roller is small, there is only a small amount of solution brought to the surface and the solution is spun away before it reaches tank again. Thus, only a part of potential spinning area is utilized. On the other hand, if roller velocity is too high, there is not enough time for solution to create Taylor's cones and spinning area is small again (Fig. 2.25).

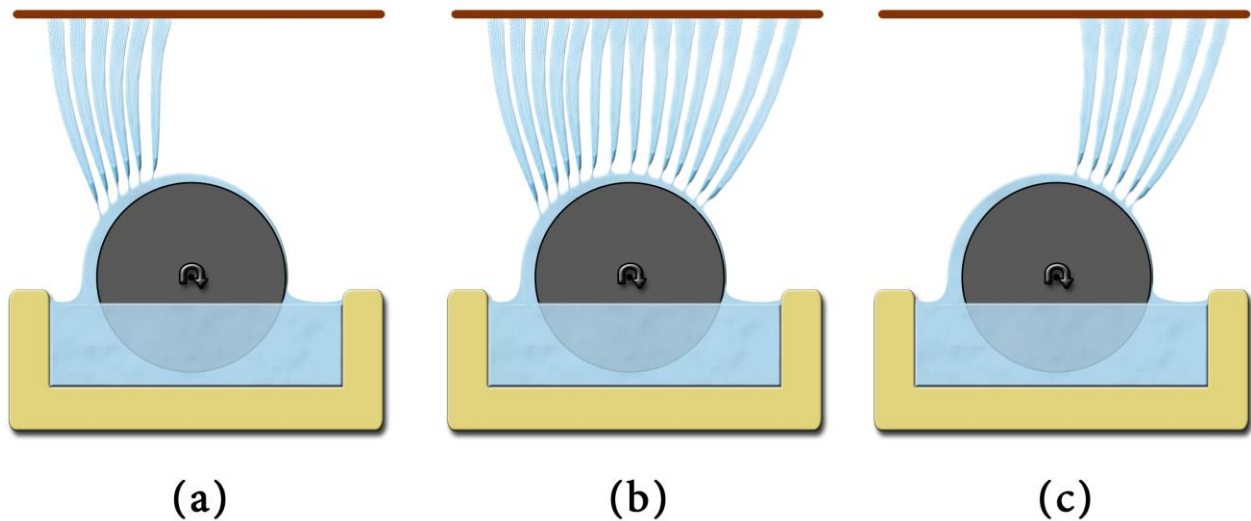


Fig. 2.25. Spinning of low (a), optimum (b) and high (c) roller rpm.

Number of Taylor's cones per spinning area/Distance between neighbouring jets

The average inter-jet distance is described in terms of wavelength (λ) as it was calculated by Lukas et. al. (In section 2.3.1.1.4, Eqn 2.10). According to this formula, electric field strength, surface tension and density of solution, relative permittivity of the surrounding gas and gravitational acceleration are the main parameters which affect the inter-jet distance. In this work, the distance between neighbouring jets will be calculated using the number of jets (n) and spinning area (A). The spinning area A is supposed to be composed of n identical squares belonging to Taylor's cones.

$$A = n \cdot x^2 \quad (2.29)$$

x (m) is the length of the square side (and simultaneously the distance between Taylor cones). Then the average distance x between adjoining Taylor cones is

$$x = \sqrt{\frac{A}{n}} \quad (\text{m}) \quad (2.30)$$

2.3.2.3. Theoretical considerations concerning the new parameters

2.3.2.3.1. Throughput per Taylor's Cone

Relationships between thickness of polymer layer, viscosity of polymer solution, Coulombian force and throughput per one Taylor's cone [139]

It is the aim of this chapter to perform an analysis and calculation of the force acting on a jet versus flow of polymer solution into this jet during spinning process. Navier-Stoke equation has been proposed to describe the force. Relations between the force acting on a jet and the volume flow rate \dot{V} , dynamic viscosity μ and thickness of the fluid layer h were calculated.

It seems to be very difficult to calculate the force acting on the on the jet based on the Coulomb's law as the electric field between the electrodes in electrospinning device is certainly not static. Therefore, we calculated the force from the volume flow rate, thickness of polymer solution layer on the roller spinning electrode and the diameter of the base of Taylor's cone.

The calculation is based on the idea that the polymer solution flows from the layer on the spinning roller into the jet through the cylindrical area of radius R and the height h as it is shown in Fig. 2.26. The flow is described using the Navier-Stokes equation as follows:

Steady Laminar Stokes Flow over a Plate

Full formulation of the momentum equations of the Navier-Stokes equation is:

$$\frac{\partial \mathbf{u}}{\partial t} + \frac{\partial(\mathbf{u}\mathbf{u})}{\partial x} = \frac{\partial p}{\partial x} + \mu \frac{\partial^2 \mathbf{u}}{\partial x^2} + \mathbf{f} \quad (2.31)$$

The previous Eqn. (2.31) is rewritten in the form only for relevant direction x and the first unsteady term is zero, the second term depicts nonlinear flow behavior and it is zero, pressure gradient is zero, the viscous term is partially neglected, external force remains and so the simplified equation after revision is as follows:

$$\mu \frac{\partial^2 u}{\partial y^2} = -f_y = -f \quad (2.32)$$

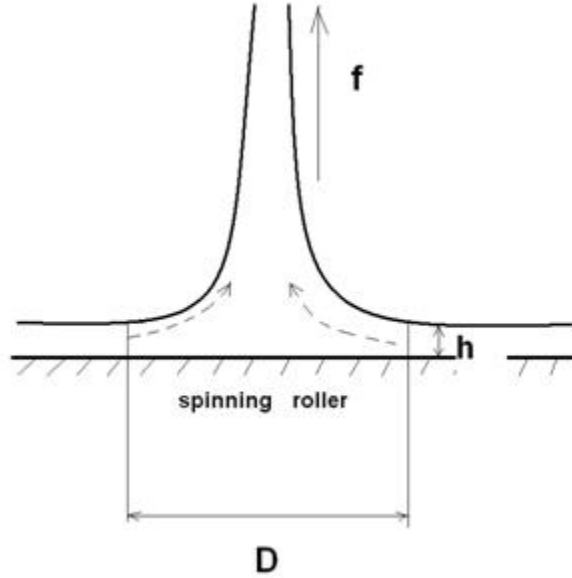


Fig. 2.26. Schematic diagram of Taylor's cone. f – electric force, h – thickness of fluid layer, D – diameter of the base of Taylor's cone

The next step is to find the velocity as a function of the y -coordinate, so the previous Eqn. (2.32) must be integrated and coefficients will be determined from the boundary conditions (b.c.) as follows:

$$\frac{\partial^2 u}{\partial y^2} = -\frac{f}{\mu} \quad (2.33)$$

$$\frac{\partial}{\partial y} \left(\frac{\partial u}{\partial y} \right) = -\frac{f}{\mu} \quad (2.34)$$

$$\left(\frac{\partial u}{\partial y} \right) = -\frac{f}{\mu} y + C_1 \quad \dots \quad b.c.: \quad y = h, \tau = \mu \frac{\partial u}{\partial y} = 0, \quad \dots \quad \frac{\partial u}{\partial y} = 0 \quad C_1 = \frac{f}{\mu} h \quad (2.35)$$

Note: The previous condition took account the Newton fluid behavior. This place should be revised in case of the non-Newtonian fluid. However, if non-Newtonian fluid will be still based on the velocity gradient, then this relation will be valid for non-Newton fluids as well.

$$\left(\frac{\partial u}{\partial y} \right) = -\frac{f}{\mu} y + \frac{f}{\mu} h \quad (2.36)$$

$$u(y) = -\frac{1}{2} \frac{f}{\mu} y^2 + \frac{f}{\mu} h y + C_2 \quad (2.37)$$

$$b.c.: \quad y = 0, \quad u = 0, \dots \quad C_2 = 0 \quad (2.38)$$

The velocity depends on the y -coordinate:
$$u(y) = -\frac{1}{2} \frac{f}{\mu} y^2 + \frac{f}{\mu} h y \quad (2.39)$$

After formal rewritten:
$$u(y) = \frac{1}{2} \frac{f}{\mu} [2hy - y^2] \quad (2.40)$$

The Eqn. 2.40 describes the velocity distribution on the y-coordinate so called the velocity profile.

Mass flow rate:

$$\begin{aligned} \dot{Q} &= \int_S u(y) \rho dS = \frac{1}{2} \pi D \rho \int_0^h \frac{f}{\mu} [2hy - y^2] dy \\ &= \frac{\pi D f}{2\vartheta} \left[hy^2 - \frac{1}{3} y^3 \right]_0^h = \frac{\pi D f h^3}{3\vartheta} \end{aligned} \quad (2.41)$$

where ϑ represents a kinematic viscosity in units m^2/s .

External local force per volume of the fluid is calculated from Eqn. 2.42 and takes a form as follows,

$$f = \frac{3\dot{Q}\vartheta}{\pi D h^3} = \frac{3V\rho\mu}{\pi D h^3 \rho} = \frac{3V\mu}{\pi D h^3} \quad (2.42)$$

where \dot{Q} is the mass flow rate (kg/s), \dot{V} is the volume flow rate (m^3/s), ϑ is kinematic viscosity and μ is dynamic viscosity, respectively.

The total force for the whole volume of the fluid in a Taylor cone is:

$$F = \int_V f dV = \int_0^{2\pi} \int_0^h \int_0^R f r d\varphi dy dr = \frac{3V\mu}{2\pi h^3} \int_0^{2\pi} \int_0^h \int_0^R \frac{1}{r} r d\varphi dy dr = \frac{3V\mu R}{h^2} \quad (2.43)$$

$$\left[\frac{kg \cdot m}{s^2} \right]$$

In fact, the force F depends on electrical characteristics of the space between electrodes and on applied voltage. The quantities on the right side of Eqn. 2.43 influence each other in such a manner that the Eqn. 2.43 remains true when any of these quantities is changed.

For instance, the increase in the thickness h causes corresponding increase of V and/or R.

The influence of the fluid viscosity seems to be out of validity of Eqn. 2.43. Growth of the solution viscosity depending on both polymer concentration and its molecular weight is linked with greater degree of macromolecules entanglement and with the strength of jets. This generally increases the volume flow rate. Above mentioned relations make it rather difficult to study influences of specific parameters separately.

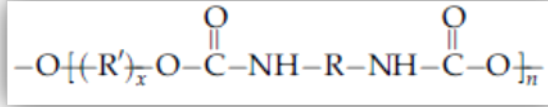
The results are a theoretical base for future experimental investigations. Nevertheless, some specific influences must be taken into account in planning and evaluation of the experiments which are discussed above.

Eventually we hope that it will be possible to use ideas similar to those developed here to calculate accurate force by counting all specific influences. It would help to understand roller electrospinning system more deeply [139].

2.4. PROPERTIES OF POLYURETHANE AND POLYETHYLENE OXIDE AND THEIR ELECTROSPINNING

2.4.1. Polyurethane

Polyurethanes were discovered by Bayer in 1937 [140] These are produced by the addition of diols or polyols to diisocyanates.



R= diisocyanate unit

R'= polyol segment

The most of urethane polymers are thermosets. They are mainly used in the production of foams, taking advantage of the reaction of water and of the precipitation of insoluble ureas, which stabilize the foam even before the system gels chemically. Linear polyurethanes are thermoplastic and soluble in various organic solvents. Linear polyurethanes can be processed into nanofibers by electrospinning.

Many polyurethanes are block polymers prepared with a diisocyanate, a short diol such as 1,4-butanediol or 1,6-hexanediol, or a diamine (the chain extender), and a diol with molecular weight between 500 and 4000, based on a polyether, polyester or polycarbonate. Most often, the preparation is performed in two steps: firstly, reaction of the longer polyol with the isocyanate, then with the chain extender in the second stage [141].

An important and desirable feature of polyurethanes and polyureas is the phase separation of the small isocyanate/chain extender blocks. These 'hard' blocks act as physical crosslinks at a temperature lower than their melting point, and thermoplastic elastomers (including elastic fibers) can therefore be obtained [142].

General application area is; polyurethane flexible foams and applications in protective packaging, gaskets, textile laminates, protective cushioning in automobiles, and two component injection-grouting resins. Rigid polyurethane foams are used as thermal insulating materials in refrigerators, freezers, and water heaters. It is also used as a roof proofing material. PU has excellent damping properties, good mechanical and physical properties even at low temperatures, high combustion resistance, and a low thermal conductivity [142].

Due to easy care, resistance to microorganism, easy spinnability and excellent hydrolytic stability PU has received considerable attention in electrospinning process. Many researchers focus on PU nanofibers [69,143,144].

In the experimental part of this thesis polyurethane was studied in the roller electrospinning process. There are two reasons for choosing PU in this work. First, the used sort of PU is pure, industrially produced and used. Second, a plenty of information on this polymer is available from the previous work including more or less optimum spinning conditions. This polymer shows a good spinnability if a salt are added. Two kinds of salts (TEAB, LiCl) will be used as additives; both of them increase the conductivity as well as viscosity of solutions. Cengiz et. al. [53] observed that TEAB increases viscosity of polyurethane solutions. They explained that it can be

caused by better solubility of polyurethane in the presence of TEAB which leads to more extensive entanglement of macromolecules. Polymer network is then more solid. They found that adding salt improve the performance of fabric [58]. In case of PU and LiCl salt, there are secondary bonds similar to H-bridges between PU and LiCl ions (Fig. 2.27). Intermolecular interactions are positively influenced by polar groups, so LiCl makes the functional groups of PU more polar.

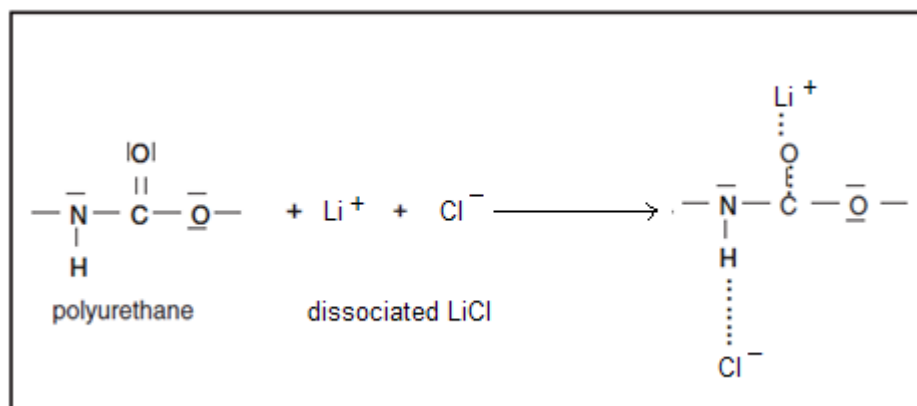


Fig. 2.27. Chemical interaction between polyurethane (PU) and Lithium chloride (LiCl).

Interactions between the polar organic solvents and salts were studied by Fry [145]. Electrostatic interaction between the dipolar solvent and the individual ions of the salt is greater than the attraction of the ions of the salt for each other in the lattice, salts dissolve in polar solvents. This phenomenon is called as ‘general solvation’. Fry [145] explained that, in addition to general solvation, small or highly charged metal cations, such as Li^+ or Mg^{+2} , in water or other electron pair donor solvents may also attract a shell of tightly bound solvent molecules.

This phenomenon, known as “inner-sphere” or “specific” solvation, provides an additional stabilization of the positive charge on the cation by association of it with the negative end of the solvent dipoles. General solvation depends primarily on the dielectric constant (ϵ) of the solvent, irrespective of its chemical structure. On the other hand, specific solvation depends upon the chemical structures of both the solute and solvent. Fry reported a computational study demonstrating that smaller tetraalkylammonium ions (Me_4N^+ and Et_4N^+) are surrounded by a strong solvation shell in the strong donor solvents N,N-dimethylformamide (DMF). The four solvent molecules are distributed symmetrically around the tetrahedral cation and, sterically, there is no remaining space for a fifth solvent molecule. The tetrahedral arrangement of solvent molecules is exactly the same as the structure found for $\text{Et}_4\text{N}^+(\text{H}_2\text{O})_4$ by molecular dynamics and is closely akin to that of the $\text{Li}(\text{THF})_4^+$ ion, established by X-ray crystallography [145].

Rastogi [146] studied ion-dipole interaction energy of alkali metal cations such as Li^+ , anions e.g. Cl^- and symmetrical tetraalkylammonium ions in DMF and other solvents. He showed that ion-dipole interaction energy decreases in increasing order $\text{Li}^+ > \text{Cl}^- > \text{Et}_4\text{N}^+$ in DMF solvent. Beside this, the ion-dipole interaction energy of ions is generally higher than dipolar interaction energy of solvents which cause secondary solvation in larger ions (Cl^- , Br^-) and long-range polarization in small ions (Li^+).

The values of solution conductivities of LiCl and TEAB salts in the same molar concentration in DMF are illustrated in Fig. 2.28. Dash lines indicate the connection points. The standart deviations of measurements are less than 1%.

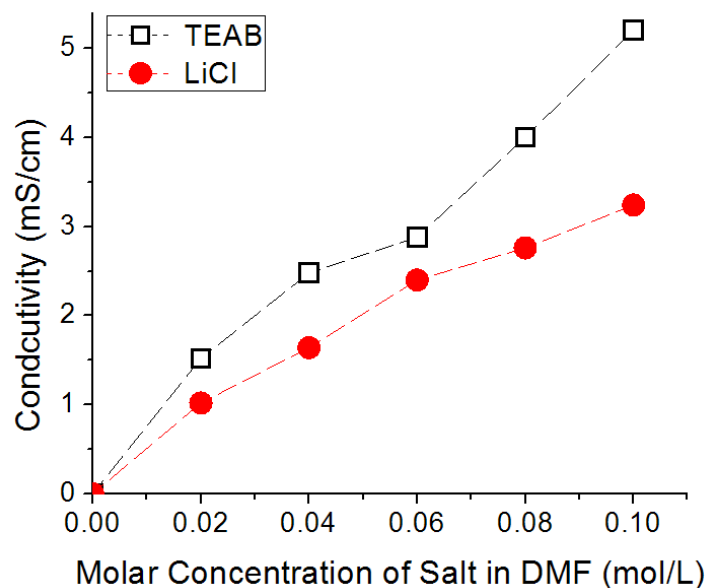


Fig. 2.28. Conductivity of TEAB and LiCl solutions in DMF. Dash lines indicate connection of points.

Addition of LiCl to PU solution increases the viscosity. Erokhina et. al. explained that this is probably due to the same coordination bonds of lithium cation in the solution with the DMF molecules and they concluded that partial recoordination of the lithium cation from the DMF carbonyl groups to the polyurethane carbonyl groups in the ternary system probably caused unfolding of macromolecular coils in PU with formation of intermolecular crosslinks [147].

Cengiz et. al. investigated the effect of ambient condition on dependent parameters. According to the obtained results, ambient humidity has an important effect on the spinning performance, fiber diameter and nano surface properties. The best spinning performance, fiber diameter, diameter uniformity and surface morphology were obtained from 27 % ambient humidity, given the ideal polyurethane nano web structure [59]. They also examined the TEAB salt effect on PU nanofibers. It was found that spinnability increases and non-fibrous area decreases as the PU polymer concentration increases. Also it was observed that fiber diameter increases and number of beads on nanofibrous structure decreases prominently with PU and TEAB concentration. On the other hand it was found that there was no relationship between the fiber diameter uniformity coefficient and PU and TEAB concentrations [148]. Yalcinkaya et. al. had the same results with electrospun PU fibers [149]. In another work it was found that independent and dependent parameters were affected by varying the concentrations of polyurethane and tetraethylammonium bromide salt. In particular, the spinning performance of the polyurethane solution, which is the most important factor for the roller electrospinning method, significantly increased with the TEAB concentration [58].

Application areas of PU nanofibers

Polyurethane is a thermoplastic, water insoluble polymers. It has great mechanical properties and it can be used as biomaterial. Sheikh et al. produced electrospun PU nanofibers containing silver (Ag) nanoparticles (NPs) polymeric matrix. The results showed that the prepared silver NPs/PU nanofibrous matrix could be properly employed as recommended candidate for many biological applications such as prolonged antimicrobial wound dressing agents and water and air filters

[150]. It was also reported PU nanofibers are good candidate for bio-sensor [12], protective clothes [115] and wound healing [151] applications. Kimmer et al found that filter prepared from PU shows good filtrating properties [152].

2.4.2. Polyethylene Oxide

PEO is water soluble and non-ionic polymer. One of the aims of this study is to determine different spinning behavior of both water-soluble and -insoluble polymers. It is possible to use polyvinyl(alcohol) which is mostly used in electrospinning. Although the PVA has been studied by many researchers, PEO was chosen in this work for its more stable quality and better purity.

Polymers of ethylene oxide were also frequently studied in electrospinning. They are available in a very large range of molecular weights. They found many application areas such as textile applications, cosmetics, antifoaming agents, food industry, etc. Polyethylene oxides are produced by the polymerization of ethylene oxide and have a structural polyether unit $-\text{CH}_2-\text{CH}_2-\text{O}-$. PEO is a good candidate for electrospinning system for its high spinnability and water solubility. Ferry [153] implied that the entanglement molecular weight of PEO is about 4,400 g/mol and can be used to determine the entanglement transition in the concentrated regime. In this work PEO was used with both the salts TEAB and LiCl.

Karmakar et. al. explained that in PEO-lithium salt based solid polymer the macromolecule coils around Li^+ ions and the O-atom in PEO chain provides a coordination site for Li^+ ions through Lewis acide-base interaction and Li^+ ions jump from one coordination site to another within the amorphous phase. Also the chain mobility of the polymer host, which plays an important role in ion transport, makes the ion transport mechanism in polymer electrolytes very much complex. [154].

In the case of PEO water solutions, addition of salts only affects the conductivity and most probably the permittivity. Viscosity of solutions does not change when salts are added. It seems that there is no significant interaction between salt and polymer macromolecules. PEO solution without any salt is intensely transported from the spinning electrode to the collector in the electrospinning device but no fibers are formed; only polymer solution moves towards to collector. Hundreds of jets can be observed. Additions of a salt to the solution decrease its spinning performance and the nanofibers are formed. This phenomenon is explained in by the 'leaky dielectric model' in the section 2.3.1.1.3. The conductivity of LiCl and TEAB in the same molar concentration in water is illustrated in Fig. 2.29. Dot lines indicate the connection points. The standart deviations of measurements are less than 1%.

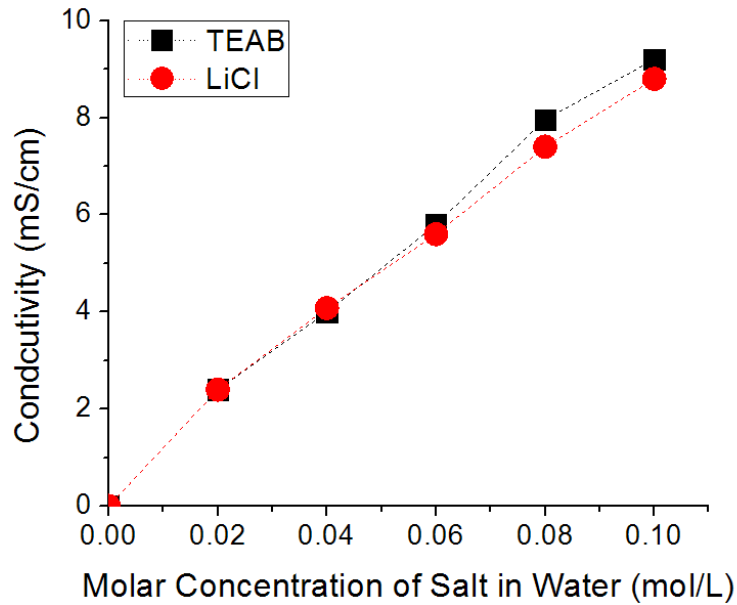
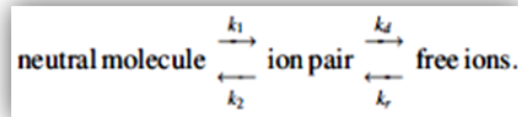


Fig. 2.29. Dependence of water solution conductivity on the concentration of LiCl and TEAB. Dash lines indicate connection of points.

Collins et. al. [155] showed that in the absence of an electric field, charged structures capable of supporting current can be produced by the general equilibrium depicted below:



They explained that the neutral molecule and the ion pair are not capable of supporting current and the rate constants, k_1 and k_2 are generally not known and are not important to the treatment of the problem of conduction in liquids. On the other hand, the step of this process that produces free ions from ion pairs is critical to understanding the development of conduction in liquids. The rate constant k_d is related to the dissociation of the ion pair into the charged ions, while the rate constant k_r relates to the removal of free ions by the recombination into ion pairs. Moreover, with the application of a voltage with a positive polarity on the electrode that supports the solution, the mechanism of charge carrier generation is ‘field enhanced dissociation’. Negative charges are immobilized at the electrode, leaving mobile positive charges to respond to the electrostatic stresses imposed by the electric field. The unconstrained surface of the fluid allows multiple spinning sites to develop as shown in Fig. 2.30 [155].

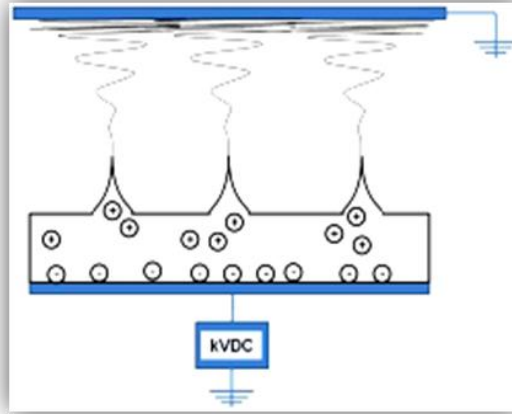


Fig. 2.30. Multiple fluid jets using plane-plane electrode configuration without capillaries.

In the case of PEO in water solution, dissociation of the ion pair into the charged ions of water molecules under electric field is depicted below:



It creates a high number of ions. Negatively charged ions are immobilized at the positively charged spinning electrode, whereas positive charges move toward collector electrode. Adding salts increases conductivity of solution over the value required for the leaky dielectric model and leads to decreasing number of Taylor's cones.

In the case of PU solution, the molecules of DMF solvent do not dissociate. Therefore, the field enhanced dissociation is also not present.

Mazari et al. studied PEO electrospinning. In his work, PEO samples of various molecular weight, solution concentration and salt content were used. It was found that the PEO molecular weight does not influence the fiber forming ability except of very low values, when the jets are not strong enough. Addition of salt was necessary for forming fibers in nano-dimensions. According to his results, the six per cent water solution of PEO with molecular weight of 400 kDa containing 0.2 – 1.0 per cent of NaCl shows the optimum spinning performance and produce good quality nanofibers [156].

Water solutions of PEO show extremely high spinning performance due to their high polarity and hygroscopicity. Because of these properties, the PEO chains are used as a hygroscopic part of detergents,. Their high polarity, especially in water solutions is characterized by the high value of dielectric constant, $\epsilon = 39$ [157,158]

Herein we can conclude that:

- PEO without any salt is spinning intensely but fibers are not formed. Only polymer solution is transported.
- Adding salt decreases number of cones, however, fibers are formed. The reason can be seen in the strong increase of conductivity. High conductivity (as it explained in leaky dielectric model) is large enough to alter the behavior of the fluid from that of a leaky dielectric to that resembling a conductor. Then the tangential component of the electrical stress that accelerates the fluid is likely to diminish.

Application areas of PEO nanofibers

PEO is a water soluble, non-ionic, low glass transition temperature and low melting point, low toxicity, biocompatibility, good binding and film forming and good lubricant polymer [159,160,161]. This is a good candidate for batteries, display devices, sensors and host for drugs to be delivered iontophoretically. In electrospinning, PEO can be added to other polymers to enhance their poor spinnability. The CMCTS (carboxymethyl chitosan)-AgNPs (silver nanoparticles)/PEO nanofibers were recommended for many biological applications such as wound dressing materials for their good antimicrobial activity [162].

2.5. SUMMARY OF THEORETICAL PART AND OBJECTIVE SETTINGS

Previous results of the studies of electrospinning mechanism were described in chapters 2.1. and 2.3. These were mainly achieved by examination of the relations between independent and dependent process parameters. The defined and studied parameters are described in the chapter 2.3.

Despite the great research effort, the present knowledge of electrospinning mechanism, especially in the field of needleless electrospinning, is rather limited and insufficient from the point of view of the full process and product control. One of the reasons of present state is undoubtedly the fact that not all of relevant needleless (roller) parameters were defined, measured and studied. Therefore, it is the first aim of present work to identify and define additional relevant roller electrospinning parameters as well as to develop the methods of their measurement. The results of this part of work are described in the chapter 2.3.2.

It is the second aim of this work to study and explain the relations between selected independent and dependent roller electrospinning parameters. The results will contribute to the knowledge of the mechanism of the roller electrospinning process.

The influence of following independent parameters on the roller electrospinning process will be studied in the Experimental part:

Parameter 1: Velocity of the roller spinning electrode (roller rpm).

The influence of this parameter was not yet studied and explained in detail. It mainly influences (together with the other parameters, such as solution viscosity) some “secondary” independent parameters, such as:

- Thickness of the polymer solution layer on the roller surface (chapter 2.3.2.1.1.1.)
- Feed rate of polymer solution (chapter 2.3.2.1.1.2.).

Parameter 2: Content of salts in the polymer solutions.

It is known from the previous studies [32,53,56,57,58,59,149] that the content of salts influences some “secondary” independent solution parameters, such as electric conductivity

and, in some cases, their viscosity. It is also known [32,53,149] that an increasing salt concentration increases significantly the spinning performance of some solutions (PU – DMF for instance) whereas, on the contrary, it decreases the spinning performance of other solutions (PEO–water or PVA-water), also significantly.

Therefore, two polymer solutions showing opposite dependencies of spinning performance on the salt concentration were selected for the experiments. It is the challenge for the author to explain the opposite dependencies. Two different salts soluble in both the solvents will be applied to the solutions in a series of concentrations. The other solution properties, namely the polymer concentration, will be kept constant. The optimum values of the constant parameters were chosen based on the results of previous research results [33,53,149] and on the preliminary experiments (chapter 3.2.).

The dependent parameters described in the chapter 2.3. will be measured in the experiments, the electric current among others.

It is the third aim of the work to clarify the relations between the currents measured in the needle- and needleless electrospinning. The measurement of current during the needle electrospinning was described in [33]. Simultaneously, the dependence of current on various spinning parameters was studied. No information on the current in the roller electrospinning process was found in the literature. Therefore, the relations between the current in both the processes will be investigated first in the Experimental part, chapter 3.1.

3. EXPERIMENTAL PART AND RESULTS

Survey of experiments

In the sub-chapter 3.1, the relations between the current measurement in the needle-, rod- and roller electrospinning are studied. As described in the chapter 2.3.2.2.1., there is a number of studies in literature dealing with the needle ES (electrospinning) whereas no studies were published on the current in needleless ES. It is the aim of this chapter to clarify whether the dependencies of current on the parameters in needle ES can be applied on needleless process.

In the sub-chapter 3.2, we determined the limits of polymer concentrations and salt concentrations in the polymer solutions for the main group of experiments described in sub-chapter 3.3.

In the sub-chapter 3.3, the relation between selected independent ES parameters and dependent parameters described in theoretical part are studied as the independent parameters were chosen;

- Velocity of spinning roller (rpm)

- Content of salts in the solutions

Two kinds of polymers were selected for the experiments, namely PEO soluble in water and PU soluble in DMF as mentioned in the chapter 2.4. These polymers show different, or even opposite dependence of spinning performance on the content of salt. Generally, two systems polymer-solvent-salt were studied, namely

- a) PU-DMF-Salt
- b) PEO-Water-Salt

Two salts, soluble in both DMF and water were applied in the systems a) and b) namely LiCl and TEAB. These salts differ considerably from each other in the size (and expected movability) of their cations.

3.1. On the measured current in needle- and needleless electrospinning [33]

The measurement of electric current has not yet been applied in roller electrospinning. It is the aim of the present paper to measure the electric current in the process of roller electrospinning and to show the measured data as a potential process characteristic. To maintain continuity with previously presented results [13,26,86,102,103,104,105,107,114,139,156,163,164], some experiments on needle and rod electrospinning will be included.

Poly(ethylene oxide) (PEO) from Aldrich Company having a molecular weight of 400 kDa was used in the following experiments. PEO solutions of 4 wt% concentration were prepared containing 0.1 mol/L of NaCl (Aldrich, quality p.a) and KCl (Lachema, p.a.), respectively. Polymer solutions were then tested in the needle and needleless electrospinning process.

Conductivity (conductivity meter), surface tension (Krüss), and viscosity (Haake RotoVisco1 at 23°C) of the polymer solutions were measured. A digital camera (Sony Full HD NEX-VG10E Handycam, 14.2 megapixel-E18-200 mm Lens) was used.

The needle, rod, and roller electrospinning techniques used for spinning are shown in Figs. 3.1–3.3. The current is evaluated by measuring the voltage on the resistor R placed between the collector electrode and earth. Resistance R is equal to 9811 Ω . The voltage is measured by a 33401A digital multimeter produced by Agilent and stored on a computer at selected points on the time axis (typically 20 records per second).

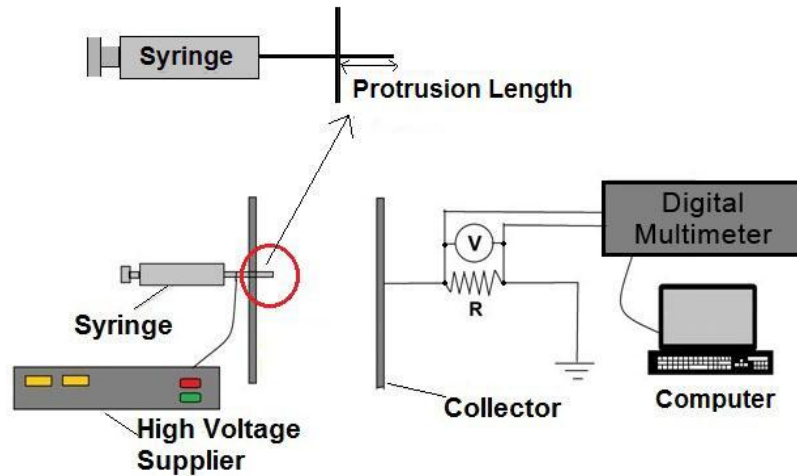


Fig. 3.1. Needle electrospinning system

In the needle electrospinning process a high voltage is used to create an electrically charged jet of polymer solution or melt, which solidifies to leave a polymer fiber. The needle is connected to a high voltage supply while the collector is grounded as shown in Fig. 3.1. The polymer solution at the needle tip is subjected to an electrical field. If the electrical force between needle tip and collector overcomes the surface tension of the polymer solution, a charged jet of fluid is ejected from the tip of the Taylor cone [102]. The process occurs between two parallel plates. The needle penetrates through a small orifice in one plate. It is in touch with the plate so that the plate is charged to the same potential as the needle. The distance between the tip of the needle and the charged plate is called the “needle protrusion length”.

In the needle electrospinning experiments, needles with various inner and outer diameters were used, as shown in Table 3.1.

Table 3.1. Needle diameters

Needle type	Outer diameter (mm)	Inner diameter (mm)	Denominated as
Needle 1	0.8	0.514	0.8
Needle 2	0.6	0.33	0.6
Needle 3	0.4	0.21	0.4

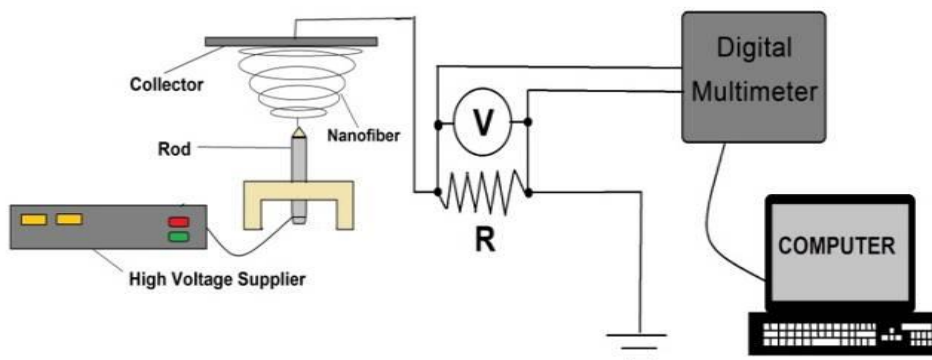


Fig. 3.2. Rod electrospinning system

In the rod electrospinning system (Fig. 3.2), a metal rod 10 mm in diameter linked with a high voltage supply is the spinning electrode. The collector is similar to that used in needle electrospinning. A droplet of polymer solution is placed at the upper end of the rod. Jets develop on the surface of the droplet, mainly close to its periphery.

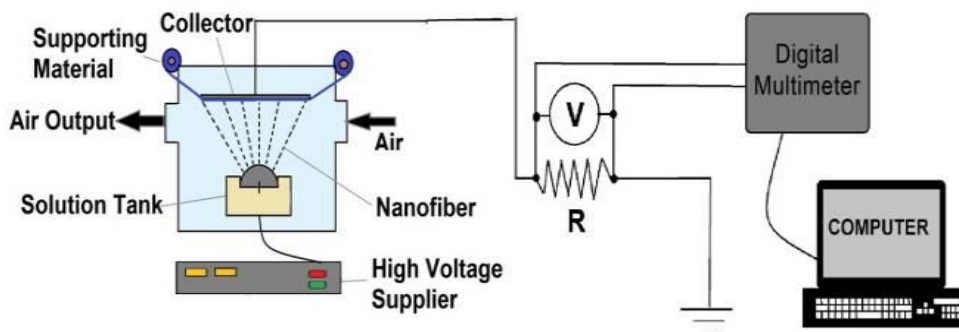


Fig. 3.3. Roller electrospinning system

In the roller electrospinning technology (Fig. 3.3), a rotating roller placed in a solution tank is the spinning electrode. A supporting material (nonwoven web, paper, etc.) moves along the collector electrode. A high voltage is applied to the rotating roller. If the electrical force overcomes the surface tension of the polymer solution, many jets develop on the surface of the roller. A nanofiber layer covers the supporting material. As a result, a continuous nanoweb is formed. In the following experiments, nanofiber layers were collected on a polypropylene spunbond nonwoven fabric.

In the experiments, the effects on the current of the following were studied:

1. in the needle electrospinning process:
 - 1.1. relative humidity
 - 1.2. needle protrusion length
 - 1.3. needle diameter

- 1.4. voltage, feed rate, and conductivity of polymer solution;

2. in the rod electrospinning process:
 - 2.1. time course of current
 - 2.2. relation between number of jets and current;

3. in the roller electrospinning process:
 - 3.1. time course of current
 - 3.2. relation between number of jets and current

The basic properties of polymer solutions are shown in Table 3.2.

Table 3.2. Viscosity, conductivity, and surface tension of PEO polymer solutions.

Polymer	Viscosity (23°C)	Conductivity (21°C)	Surface tension (23°C)
4%PEO + 0.1 M KCl	0.099±0.02 Pa.s	12.2 mS/cm	63.5±1 mN/m
4%PEO + 0.1M NaCl	0.099±0.03 Pa.s	11.8 mS/cm	62.0±1 mN/m

Needle electrospinning

The dependence of the measured current on the ambient relative humidity is shown in Fig. 3.4.

In this experiment, the relative humidity was continuously changed between 20 and 99%. Two measurements were done: with polymer solution and without solution feed. Conditions during the experiment were as follows: needle diameter 0.6 mm, voltage 19 kV, needle protrusion length 8 mm, feed rate 0.6 ml/h, ambient temperature 21 °C, and distance between electrodes 140 mm. The polymer solution was 4 wt% PEO with 0.1 M KCl.

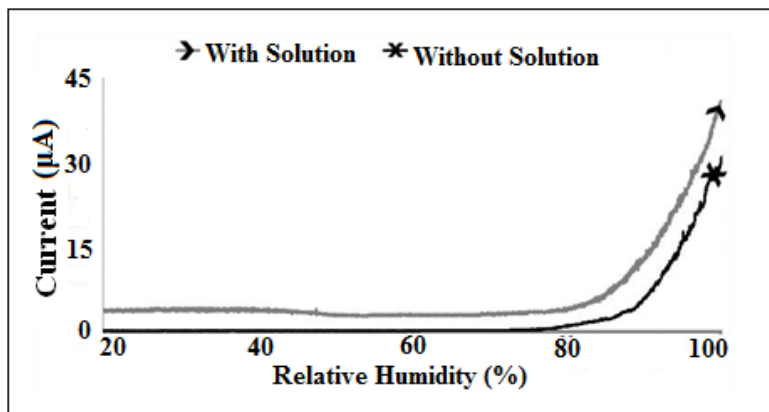


Fig. 3.4. Effect of humidity on current.

The dependence of the current on the needle protrusion length is shown in Fig. 3.5.

In this experiment, 4 wt% PEO with 0.1 M KCl was electrospun at a relative humidity of 39%, temperature of 21.9 °C, and voltage of 19 kV. The feed rate was 0.6 ml/h. Current was measured at various values of the needle protrusion length: namely 18, 16, 14, 12, 10, 8, 6, 4, 2, 1, and 0 mm. The protrusion length was changed by positioning the charged plate against the needle tip while the distance between the tip and the collector electrode was kept constant at 142 mm.

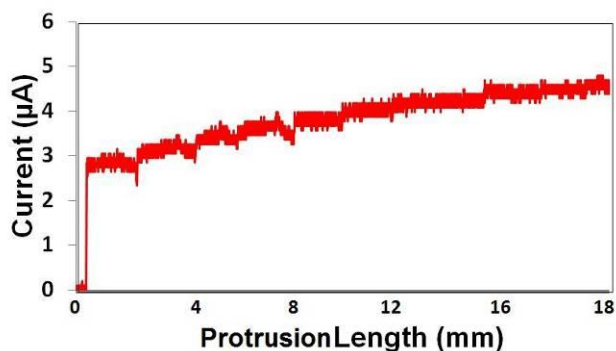


Fig. 3.5. Current vs. protrusion length in needle electrospinning system

To evaluate the effect of needle diameter, the current was measured depending on the voltage at various values of feed rate. The results for the 0.8, 0.6, and 0.4 mm-diameter needles are shown in Figs. 3.6, 3.7, and 3.8. Specific parts of the obtained graphs are labelled (a), (b), (c), and (d), which correspond to different jet regimes according to [163]:

- (a) fluctuating jet
- (b) stable jet
- (c) multiple jet
- (d) stable jet with polymer drops

The conditions of the experiments are listed in Table 3.3.

Table 3.3 Spinning conditions in Experiment 1.3.

Polymer solution	Applied voltage	Distance between electrodes	Feed rate	Protrusion length	Temp./RH
4% PEO + 0.1 M KCl	15, 17, 19, 21, 23, and 25 kV	152 mm	0.2, 0.6, and 1.0 ml/h	8 mm	21.9±2°C/43±2%
4% PEO + 0.1 M NaCl					

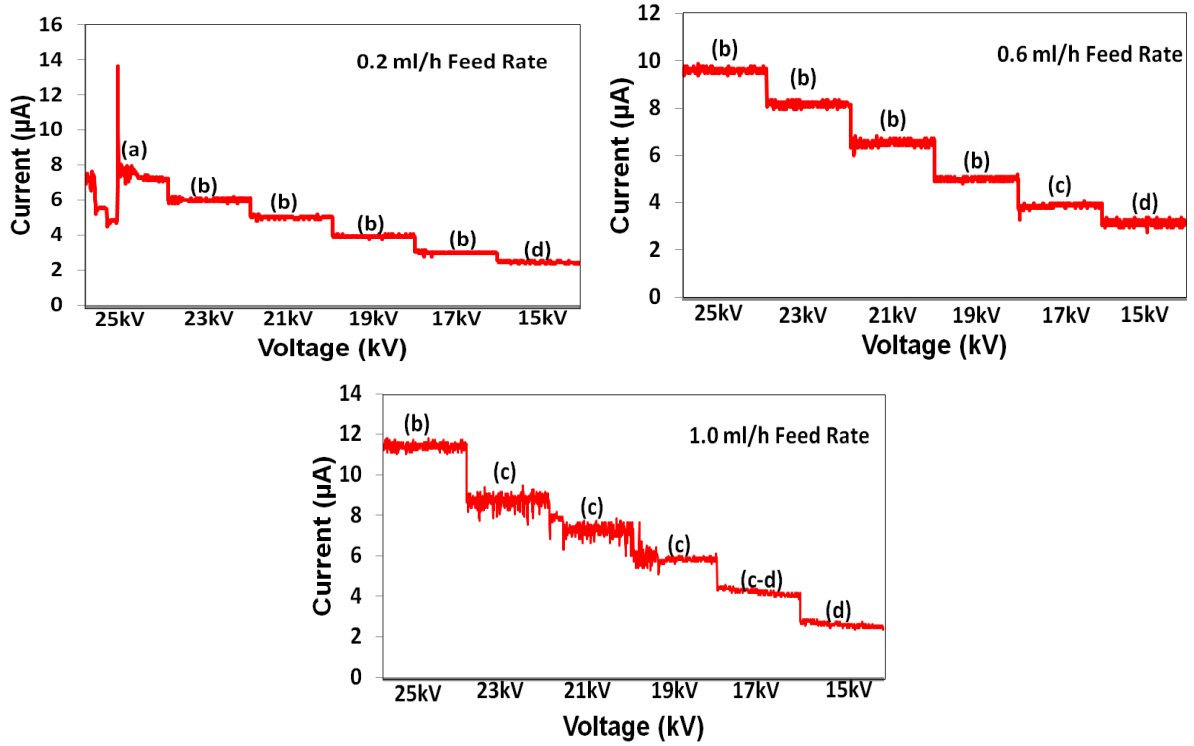


Fig. 3.6. Jet current vs. applied voltage at various feed rates – needle diameter 0.8 mm

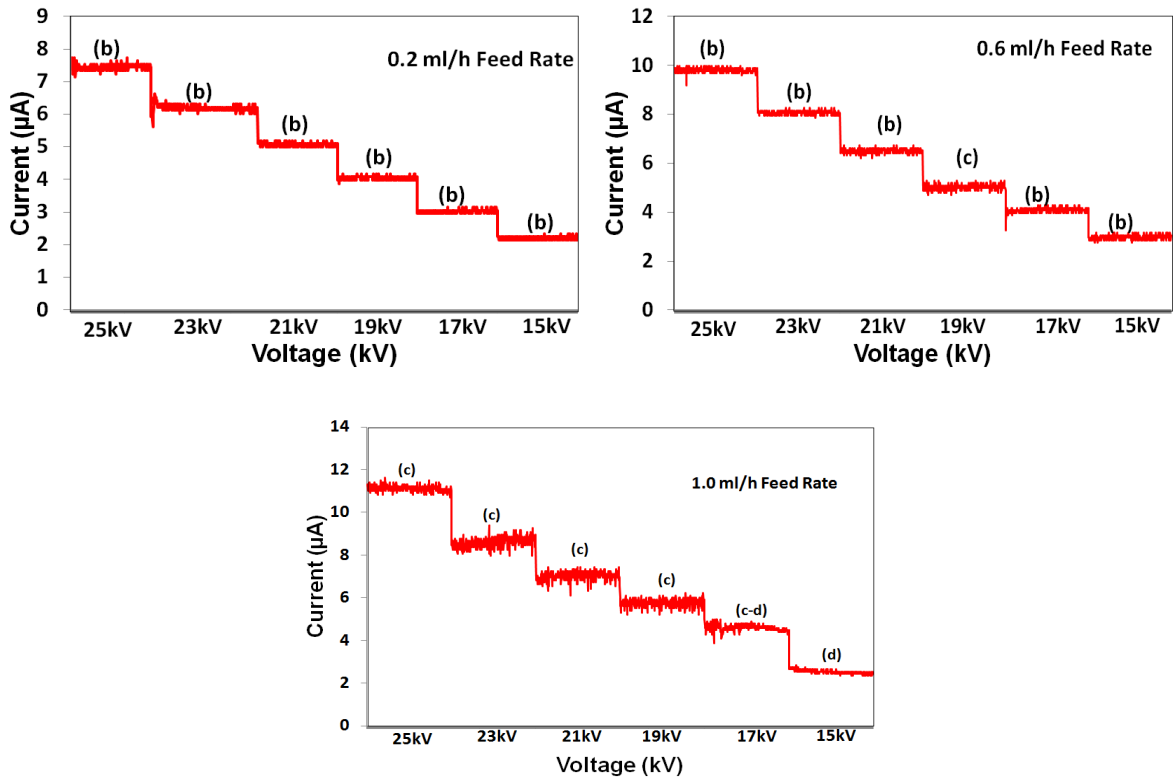


Fig. 3.7. Jet current vs. applied voltage at various feed rates – needle diameter 0.6 mm

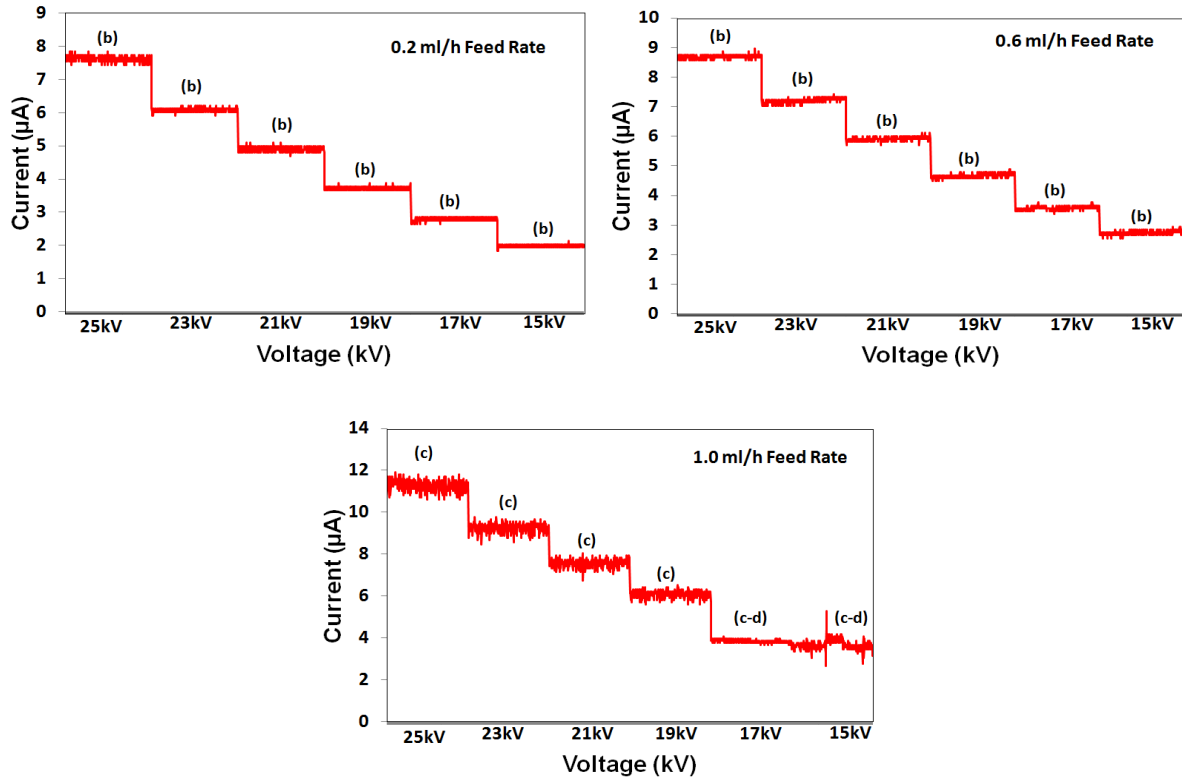


Fig. 3.8. Jet current vs. applied voltage at various feed rates – needle diameter 0.4 mm

A number of measurements were done to examine the results of Bhattacharjee et al. [112] using needles of

various diameters. An example of the results is shown in Fig. 3.9.

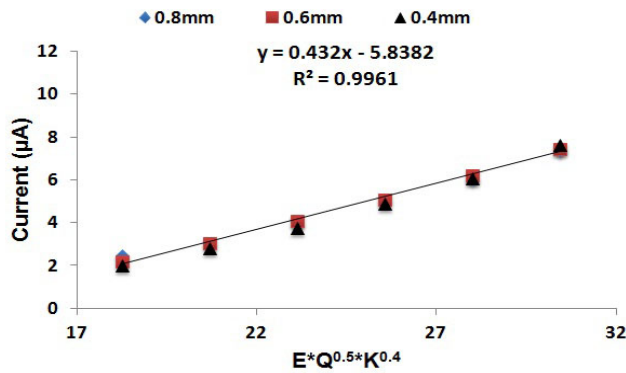


Fig. 3.9. Plot of current vs. $E \cdot Q^{0.5} \cdot K^{0.4}$ at various needle diameters with a feed rate of 0.2 ml/h.

Rod electrospinning

The polymer solutions were electrospun using the rod system under the conditions shown in Table 3.4.

In rod electrospinning, provided that the rod diameter is greater than 6 mm, a number of jets develop at the periphery of the rod. The number of jets depends on various conditions, namely on the size of the droplet of polymer solution. As the droplet becomes smaller during the process, the number of jets decreases. The current tails off correspondingly. When the droplet falls below some limit, the spinning process stops and the value of current falls to zero (see Figs. 3.10 and 3.11).

During the spinning process, the current was measured and the number of jets was recorded using a camera. Tables 3.5 and 3.6 list the values of current per jet.

Table 3.4. Spinning conditions – rod electrospinning experiments

Polymer solution	Distance between electrodes	Applied voltage	Relative humidity	Temperature	Rod diameter
4% PEO + 0.1 M KCl and 4% PEO + 0.1 M NaCl	110 mm	25 kV	25.4±2%	16±2 °C	10 mm

Table 3.5. Number of jets, total current, and current per jet in the rod spinning process.
Solution of PEO with 0.1 mol/L NaCl

Current (μA)	Number of jets	Current per jet (μA)
43.13	8	5.39
36.71	7	5.24
22.27	4	5.57

Table 3.6. Number of jets, total current, and current per jet in the rod spinning process.
Solution of PEO with 0.1 mol/L KCl

Current (μA)	Number of jets	Current per jet (μA)
49.17	7	7.02
44.73	6	7.46
35.26	5	7.05

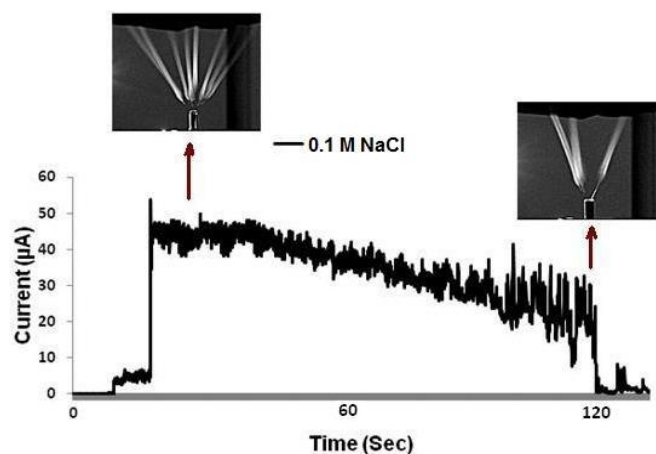


Fig. 3.10. Time course of current and number of jets in the rod electrospinning process.
Solution of PEO with 0.1 mol/L NaCl

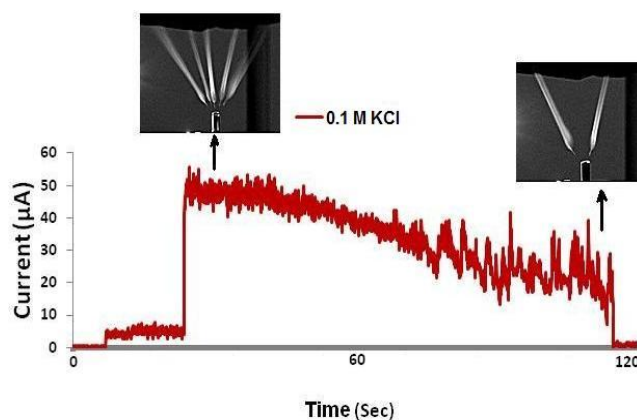


Fig. 3.11. Time course of current and number of jets in rod electrospinning. Solution of PEO with 0.1 mol/L KCl

Roller electrospinning

Polymer solutions were electrospun in the roller electrospinning system as shown in Fig. 3.3. Spinning conditions are shown in Table 3.7.

The current was measured during electrospinning and the total number of jets was recorded using a camera. The total current, number of jets, and current per jet are shown in Figs. 3.12 and 3.13 and in Table 3.8.

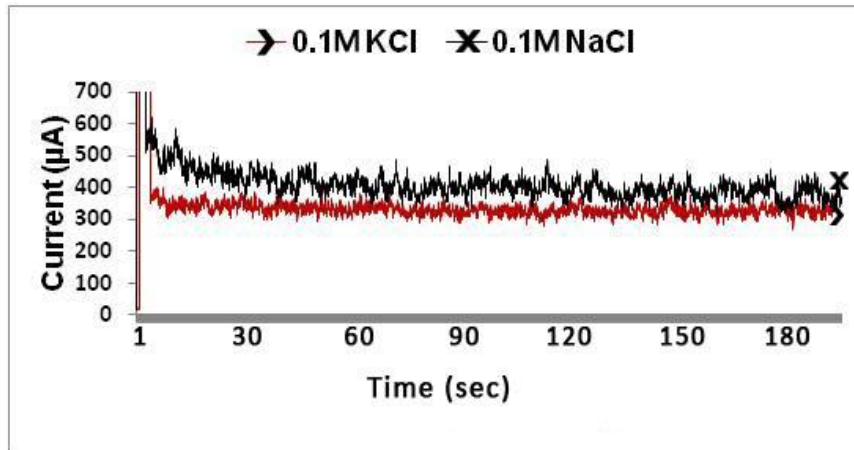


Fig. 3.12. Current vs. time in roller electrospinning

Table 3.7. Spinning conditions of PEO polymer solutions in roller spinning

Polymer solution	Applied voltage	Distance between electrodes	Relative humidity	Temperature	Fabric speed	Roller speed
4% PEO + 0.1 M KCl 4% PEO + 0.1 M NaCl	60 kV	180 mm	25±1%	18.8±2 °C	100 mm/min	5 rpm

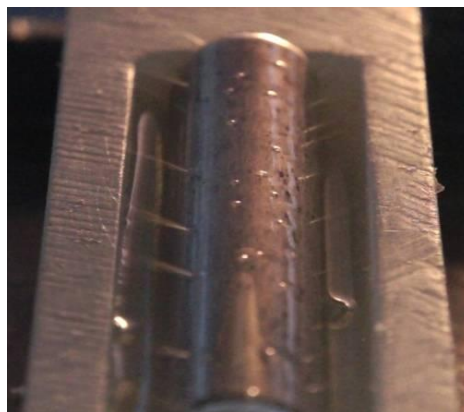


Fig. 3.13. Camera record of roller electrospinning

Table 3.8. Number of jets, total current, and current per jet in roller electrospinning

Polymer solution	Total current (μA)	Number of jets	Current/Jet (μA)
4% PEO + 0.1 M KCl	339.2	30	11.31
4% PEO + 0.1 M NaCl	409.6	37	11.07

3. 2. Determining optimum concentration of solutions

Two polymers were used in the experiments described in chapter 3.3.: the water soluble PEO and water non-soluble PU. Two salts, namely LiCl and TEAB were used as additives for solutions of both the polymers. Concentration limits for the polymers in their solutions as well as for the salts were partly adopted from literature, when available. If this was not the case, the limits were determined based on experiments described in this chapter. In the experiments, basic properties of solutions were measured and the spinning performances as well as the fiber diameters were evaluated. The results served as input data for preparation of solutions as described in chapter 3.3.

Conductivity (conductivity meter), surface tension (Krüss), and viscosity (Haake RotoVisco1 at 23°C) of the polymer solutions were measured. Images of the fibres were taken by SEM (Phenom FEI), and the diameters of the fibres were calculated using the NIS Element AR (NIKON) computer software. A digital camera (Sony Full HD NEX-VG10E Handycam, 14.2 megapixel-E18-200 mm Lens) was used to measure number of jets.

Polyethylene Oxide

The data adopted from literature: Molecular weight 400 kDa, concentration of salts [33,156].

Tested quantity: polymer concentration.

The water soluble polyethylene oxide of molecular weight 400 kDa was purchased from Scientific Polymers. Distilled water was used as a solvent. Tetraethylammonium bromide (TEAB) was used as salt in a constant molar ratio (0.062mol/L). Basic properties of solutions are shown in Table 3.9.

Table 3.9. Properties of PEO solutions

Sample Name	Content of salt in Molar ratio	Viscosity (Pa.s) at 23°C	Conductivity (mS/cm) at 23°C	Surface Tension (mN/m) at 25°C
5%PEO	0.062M TEAB	0.19±0.02	4.98	61.98±1
6%PEO	0.062M TEAB	0.32±0.02	4.74	59.88±1
7%PEO	0.062M TEAB	0.48±0.02	4.33	61.79±1
8%PEO	0.062M TEAB	0.72±0.02	4.18	62.02±1
9%PEO	0.062M TEAB	0.96±0.02	4.11	60.92±1
10%PEO	0.062M TEAB	1.23±0.02	4.12	60.45±1

All the solutions were spun at the same condition shown in the Table 3.10.

Table 3.10. Spinning conditions of PEO polymer solution on roller ES

Voltage(kV)	Distance(mm)	Roller Speed(rpm)	RH(%)	Temp.(C°)	Roller Length (mm)	Roller Diameter (mm)
42	150	1.5	24±1	23±2	145	20

The spinning performance dependent on the solution viscosities is shown in the Fig. 3.14 with error bars at 95% confidence intervals.

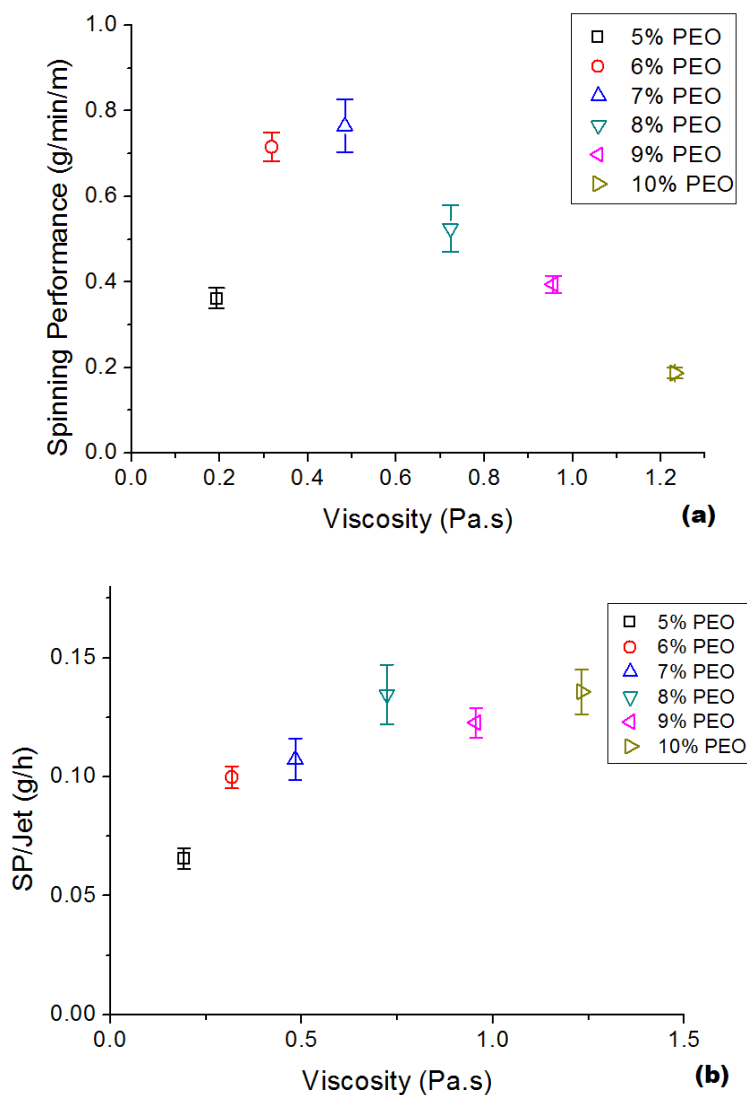


Fig. 3.14. (a) SP and. (b) SP/Jet vs. viscosity of PEO solutions.

Fiber diameters and their dependence on concentration of solutions and SEM images are shown in Fig. 3.15 and 3.16 with error bars at 95% confidence intervals:

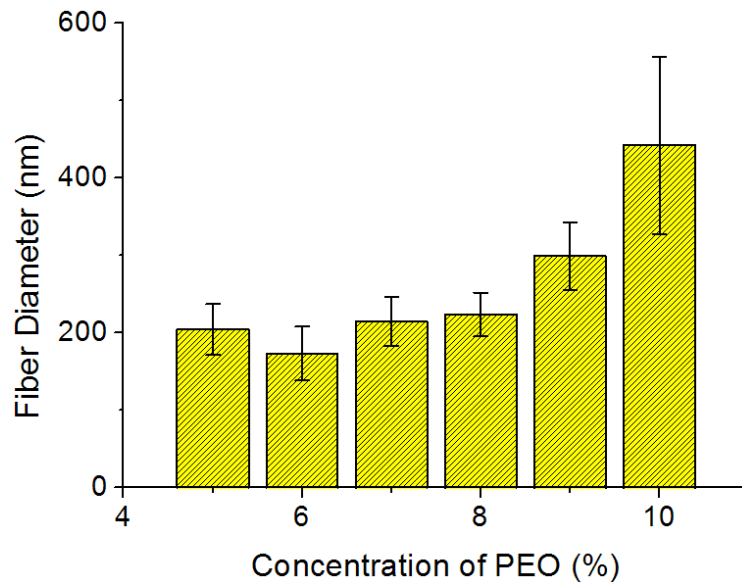


Fig. 3.15. Fiber diameter vs. concentration of PEO solutions

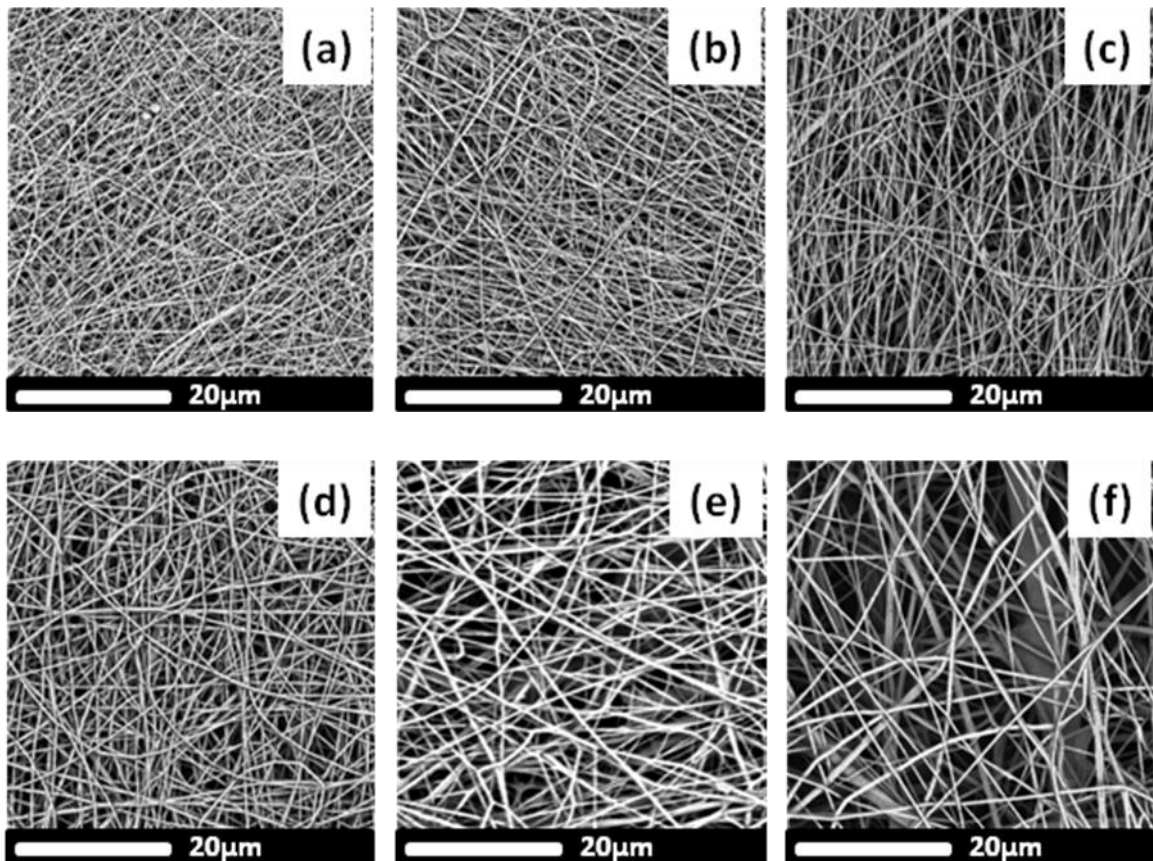


Fig. 3.16. SEM image of PEO solutions (a) 5 % PEO with 0.062 M TEAB. (b) 6 % PEO with 0.062 M TEAB. (c) 7 % PEO with 0.062 M TEAB. (d) 8 % PEO with 0.062 M TEAB. (e) 9 % PEO with 0.062 M TEAB. (f) 10 % PEO with 0.062 M TEAB.

Polyurethane

The data adopted from literature: Polymer concentration 17.5 wt. %. TEAB concentration 0 – 0.056 mol/L [53,149].

Tested quantity: LiCl concentration.

Polyurethane Larithane LS 1086 produced by Novotex. Italy (aliphatic elastomer based on 2000 g/mol linear polycarbonated diol. isophorone diisocyanate and extended by isophorone diamine) was chosen as the second polymer. Dimethylformamide. (DMF). purchased from Fluka. is the solvent.

Basic properties of polymer solutions are in Table 3.11.

Table 3.11. Polymer solution properties of PU.

Sample	Viscosity (Pa.s) at 23°C	Conductivity (mS) at 23°C	Surface Tension (mN/m) at 26°C
17.5% PU+ 0 mol/L LiCl	0.857±0.01	0.038	38.49±2
17.5% PU+ 0.056 mol/L LiCl	1.182±0.01	0.824	39.10±2
17.5% PU+ 0.14 mol/L LiCl	1.457±0.01	1.400	45.7±2
17.5% PU+ 0.28 mol/L LiCl	1.969±0.01	1.880	45.7±2
17.5% PU+ 0.45 mol/L LiCl	1.993±0.01	2.800	47.3±2
17.5% PU+ 0.56 mol/L LiCl	2.340±0.01	3.000	47.8±2

All the solutions were spun under the conditions shown in Table 3.12:

Table 3.12. Spinning conditions of PU solutions on roller ES

Voltage(kV)	Distance(mm)	Roller Speed(rpm)	RH(%)	Temp.(C°)	Roller Length (mm)	Roller Diameter (mm)
62	130	3	22±1	16±2	145	20

The spinning performance and fiber diameters are shown in Fig. 3.17 and 3.18. SEM images are shown in Fig. 3.19 with error bars at 95% confidence intervals:

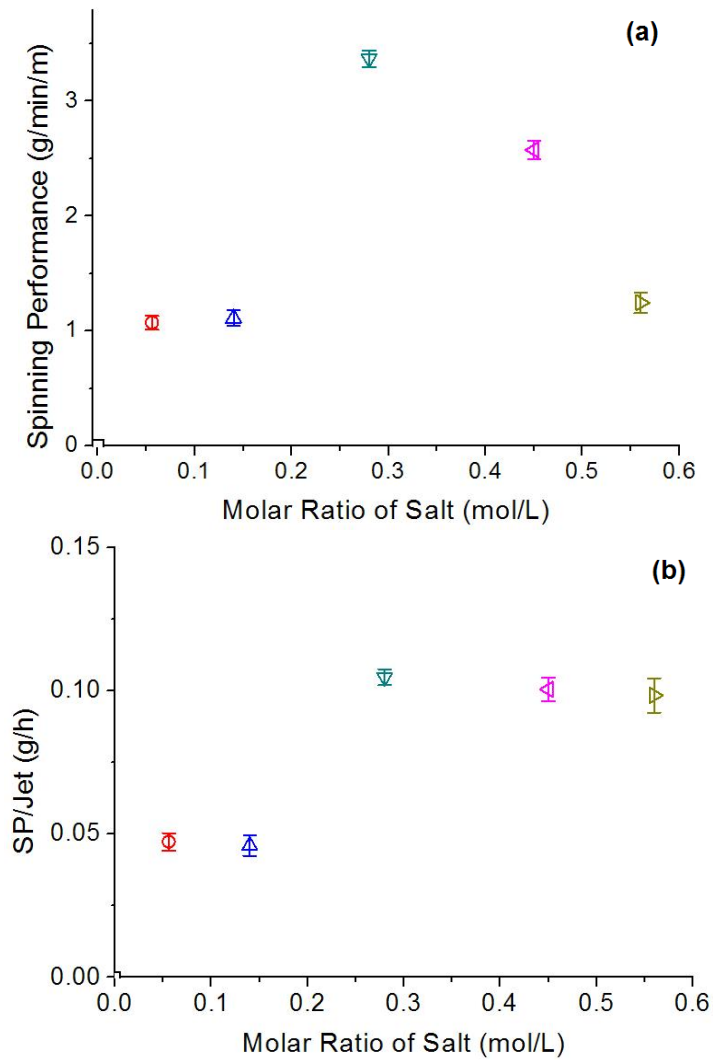


Fig. 3.17. (a) spinning performance. (b) SP/jet vs. viscosity of PU solution

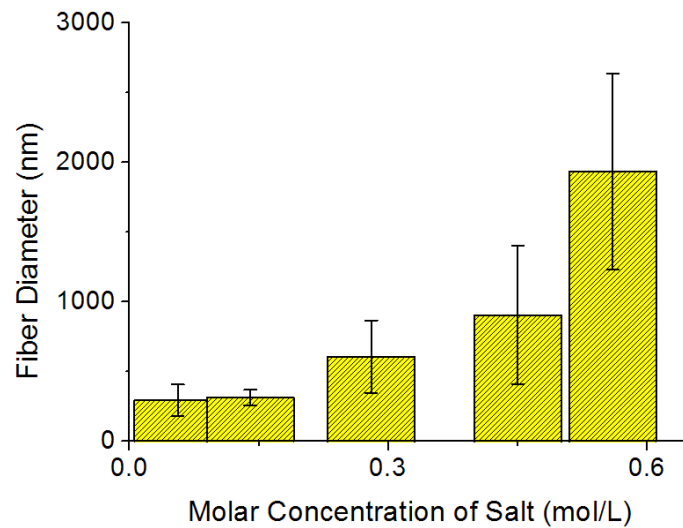


Fig. 3.18. Fiber diameter vs. concentration of PU solutions

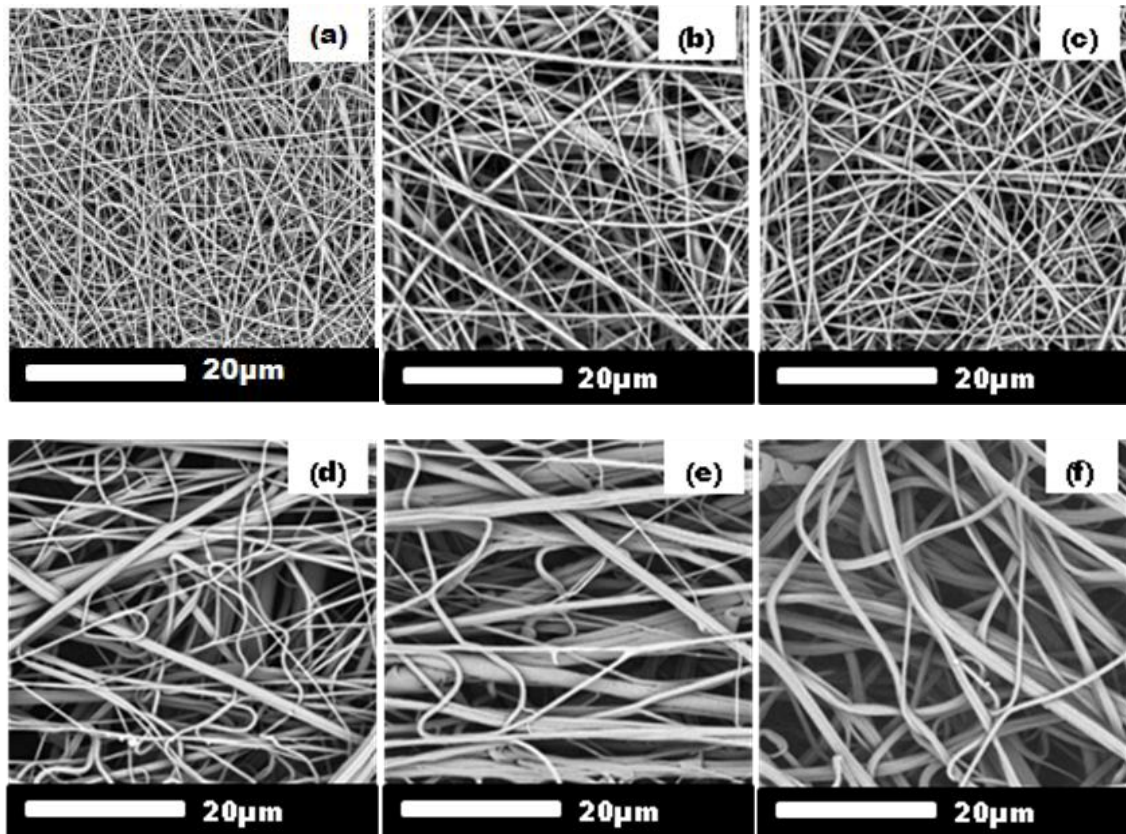


Fig. 3.19. SEM image of PU solutions (a) 17.5% PU. (b) 17.5% PU with 0.056 M LiCl. (c) 17.5% PU with 0.014 M LiCl. (d) 17.5% PU with 0.28 M LiCl. (e) 17.5% PU with 0.45 M LiCl. (f) 17.5% PU with 0.56 M LiCl.

3. 3. Effect of roller velocity and salt concentration on the electrospinning process

Two polymers were used in the following experiments:

- polyethylene oxide 400 kDa as described in the previous chapter as a 6 wt. % solution in distilled water and

- polyurethane as described in the previous chapter as a 17.5 wt. % solution in N,N-dimethylformamide (Fluka) containing 2.2 weight per cent of distilled water. The mixture of polymer solvent/non-solvent was chosen based on the earlier experiments [46, 131]. Adding a non-solvent to the solvent increases the number of entanglements, viscosity and spinnability of some polymers as shown in Fig. 3.20. Two salts soluble in both water and DMF were used:

- tetraethylammonium bromide from Fluka and

- LiCl from Lach-Ner. s r.o.. Czech Republic.

The concentrations of the salts in the solutions were set based on the preliminary experiments described in the previous chapter [53,149] and in the chapter 3.2.

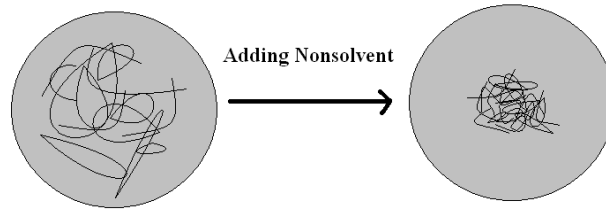


Fig. 3.20. Effect of nonsolvent on chain entanglements of macromolecules.

3.3.1. Nomenclature and symbols of solutions

PEO solutions in the water. polymer concentration 6 wt. % ;

-0 concentration of salts (PEO-▷)

-0.024 mol/L TEAB (tetraethylammonium bromide) (PEOT1-□)

-0.062 mol/L TEAB (tetraethylammonium bromide) (PEOT2-○)

-0.124 mol/L TEAB (tetraethylammonium bromide) (PEOT3-△)

-0.024 mol/L LiCl (lithium chloride) (PEOL1 -▽)

-0.062 mol/L (lithium chloride) (PEOL2-◇)

-0.124 mol/L (lithium chloride) (PEOL3-◁)

PU solutions in the DMF. polymer concentration 17.5 wt. % ;

-0 concentration of salts (PU-▶)

-0.022 mol/L TEAB (tetraethylammonium bromide) (PUT1-■)

-0.044 mol/L TEAB (tetraethylammonium bromide) (PUT2-●)

-0.071 mol/L TEAB (tetraethylammonium bromide) (PUT3-▲)

-0.014 mol/L LiCl (lithium chloride) (PUL1-▼)

-0.028 mol/L LiCl (lithium chloride) (PUL2-◆)

-0.056 mol/L LiCl (lithium chloride) (PUL3-◀)

3.3.2. Methods and results

Spinning conditions

The solutions were spun using a spinning device as shown in Fig. 3.25. All the measured results in Figs. are with error bars at 95% confidence intervals. Spinning conditions of PEO and PU are shown in Table 3.13 and 3.14:

Table 3.13. Spinning conditions of PEO solutions on roller ES

Sample	Voltage(kV)	Distance(mm)	Roller speed(rpm)	RH (%)	Temp.(C°)	Roller Length (mm)	Roller Diameter (mm)
6% PEO+ salt series	42	150	1-1.5-2-3	28.5±2	23±1	145	20

Table 3.14. Spinning conditions of PU solutions on roller ES

Sample	Voltage(kV)	Distance(mm)	Roller speed(rpm)	RH (%)	Temp.(C°)	Roller Length (mm)	Roller Diameter (mm)
17.5%PU+ salt series	62	130	1-3-5-7-9-14-62	24.5±2	16±1	145	20

In the case of PEO it is impossible to increase roller speed over 3 rpm. otherwise the fiber bundles starts to fly in the surround and fabric surface become hairy as shown in Fig. 3.21.

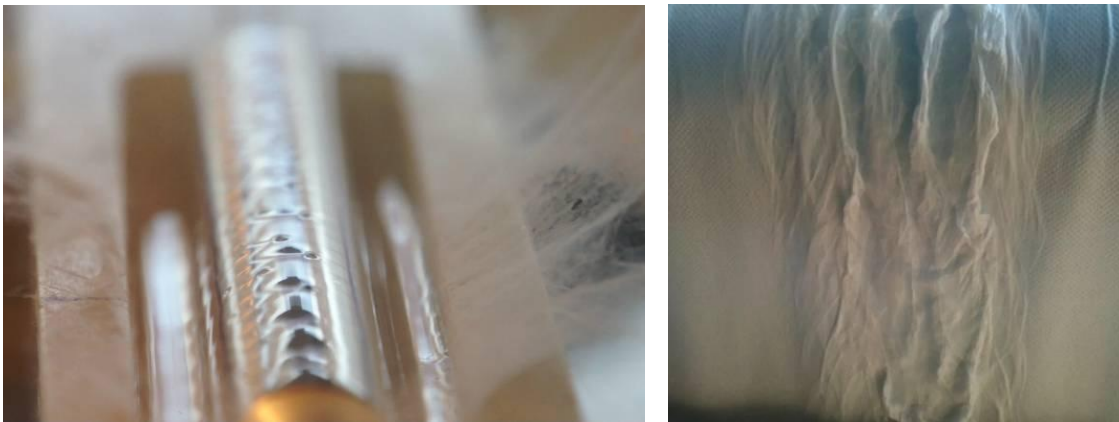


Fig. 3.21. Fiber bundles and unevenness on the take up fabric surface

- Measurement of surface tension: The measurement carried out using KRÜSS Tensiometers at at 25°C and their software LabDesk by using plate method and illustrated in Fig. 3.22. All dash lines indicate the connection of the points.

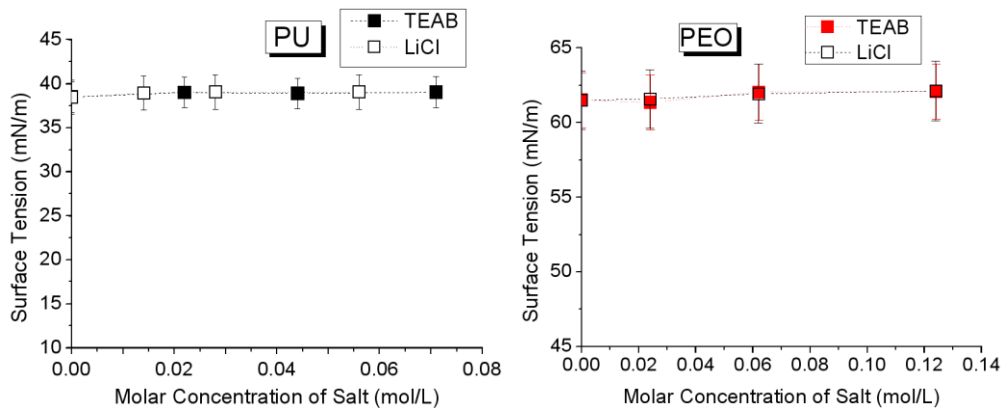


Fig. 3.22. Surface tension of polymer solutions

- Measurement of viscosity: The zero-shear viscosities of solutions were measured by Haake RotoVisco1 at 23 °C and illustrated in Fig. 3.23.

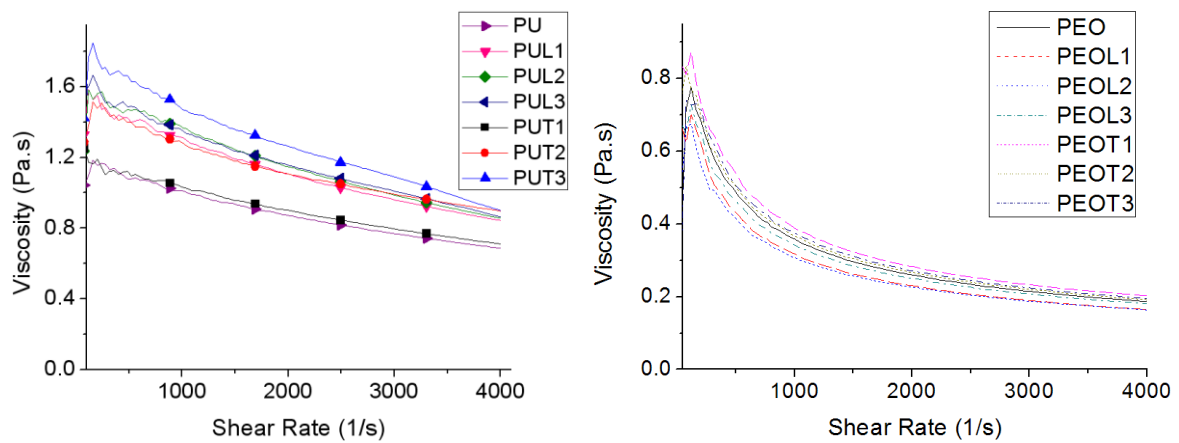


Fig. 3.23. Viscosity of polymer solutions

- Measurement of conductivity: The conductivities of polymer solutions were measured at 23 °C by conductivity meter OK-102/1 branded Radelkis and illustrated in Fig. 3.24.

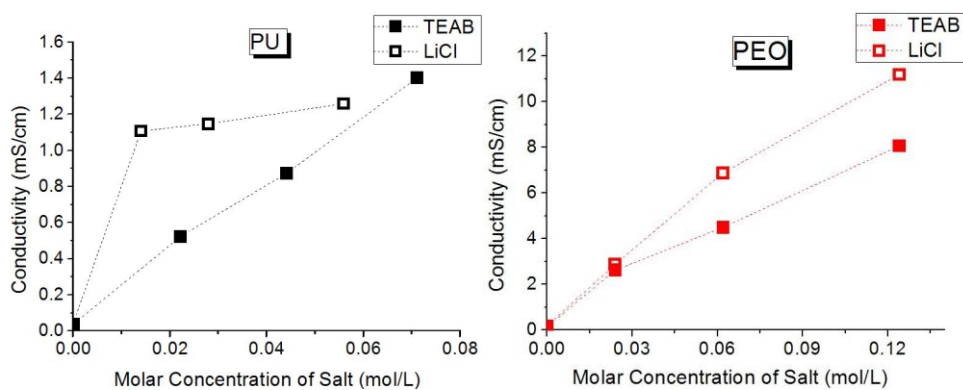


Fig. 3.24. Conductivities of polymer solutions with content of salts (dot lines indicate connection of points).

- Measurement of launching time of jets

Launching time of jets is the time between switching on the voltage and the moment when the first jet appears on the surface of spinning roller. Launching time was measured using two methods:

- the first jet was indicated on the camera record
 - the first jet was indicated as the jump on the current-time record.
- The results of both the methods were identical.

The launching time was measured in two different electrospinning arrangements:

- the device as shown in Fig. 3.25
- the device with a grounded wire as shown in Fig. 3.26.

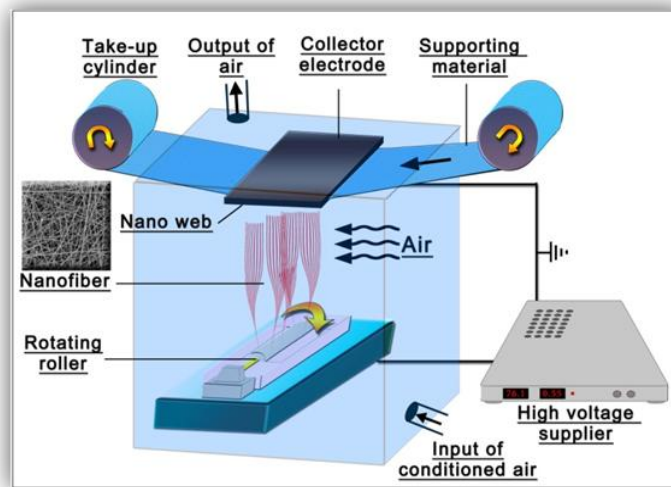


Fig. 3.25. Diagram of roller electrospinning system

The latter arrangement was studied based on the experience gained in previous experiments. The grounded wire placed close to the spinning electrode deforms the electric field. This many times helped to create Taylor's cones of polymer solutions with a difficult spinnability.

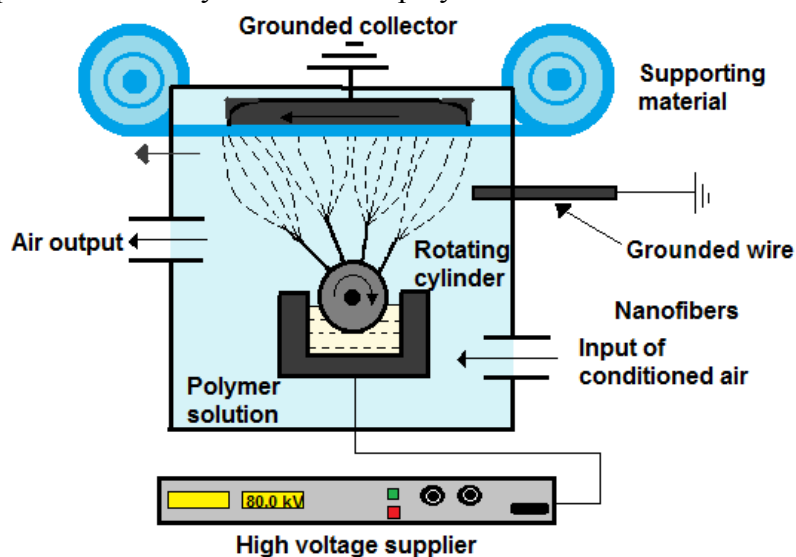


Fig. 3.26. Wire between roller and collector (distance of the tip of wire from roller surface is 95mm).

Camera and current measurement were used simultaneously. The results are in Tables 3.15-3.16.

Table 3.15. Launching time of cones for PU polymer solutions (in second).

Number of experiment	PU	PUT1	PUT2	PUT3	PUL1	PUL2	PUL3
1	>300	4.9	9.5	4	5.7	6.2	8.9
2	>300	13.6	16.6	12.9	>300	3.8	116
3	>300	89.9	4.6	12	7.7	5.5	8.1
4	>300	91.6	14.3	9.1	>300	2.9	14.9
5	>300	7	27.1	7	6.2	67.2	33.8
6	>300	162	4.8	14.6	>300	46.7	112.2
7	>300	10.4	30.9	8.4	279	30.1	46.7
8	>300	88.2	107.1	3.8	4	4.2	5.9
9	>300	96.2	7.5	4	3.6	>300	4.2
10	>300	8	63.5	10.8	180	182.6	8.2

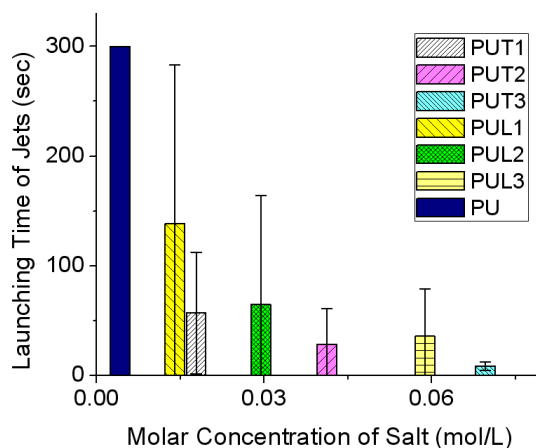


Fig. 3.27. Launching time of PU solutions

Table 3.16. Launching time of cones for PEO polymer solutions (in second)

Number of experiment	PEO	PEOT1	PEOT2	PEOT3	PEOL1	PEOL2	PEOL3
1	2.5	28.7	9.8	5.7	2.4	2.1	7.1
2	3	225.7	11.6	3.2	274.4	2.2	3.7
3	3.5	2.8	3	2.3	100.8	2.3	2.6
4	4.2	31.6	24.8	2.9	40.6	2.4	2.8
5	131.5	62.5	40.6	2.5	124.4	3.3	2.5
6	9	>300	211.9	2.5	>300	3.6	2.5
7	153.4	24.9	64.1	2.7	4.2	4.7	2.7
8	2.2	50	127.5	2.6	>300	3.3	2.7
9	>300	>300	5.2	2.4	288.3	3.3	2
10	57.8	88.7	6.2	2.4	>300	3.8	2.2

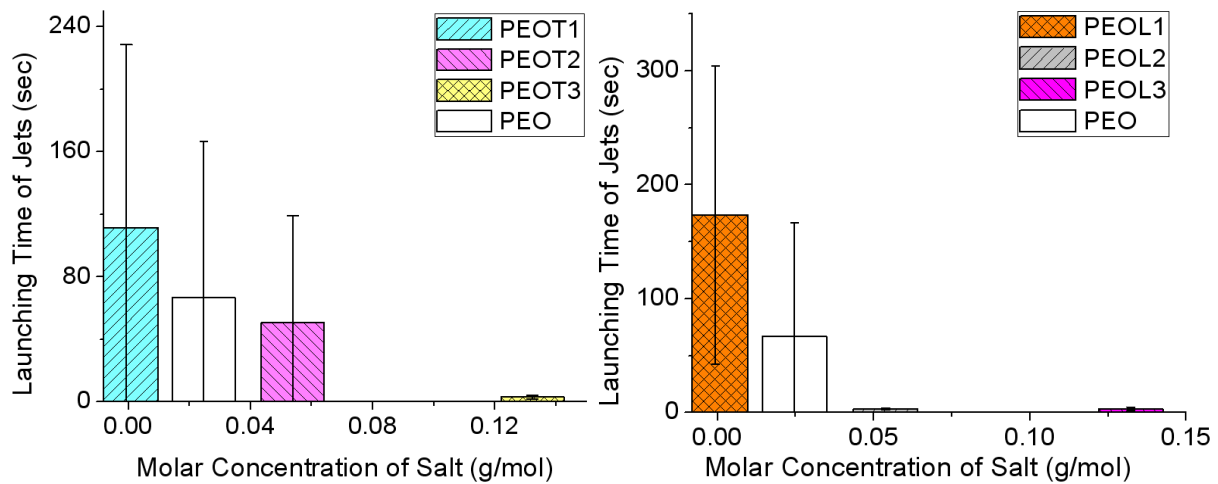


Fig. 3.28. Launching time of PEO solutions

Launching time of cones was measured 10 times as it mentioned in Chapter 2. Results are shown in Table 3.15 and 3.16 in the unit **second**. Some of them took more than 5 minutes to start which shown as “>300 “.

At the time we replaced wire between collector and roller for PU solutions. suddenly cones were formed in a few seconds and it started to spin on the middle of roller.

At the time grounded wire used between collector and roller surface. results of PEO with and without salt is shown in Table 3.17. Two unstable solutions were chosen for this experiment.

Table 3.17. Launching time of jet with the grounded wire (in seconds).

Number of experiment	PEO	PEOL1
1	3	2.1
2	3.8	2.0
3	4.3	2.5
4	4	2.7
5	3	2.2
6	8.3	2.1
7	2.6	3.8
8	8.5	2.4
9	8.1	3.2
10	7.1	2.6

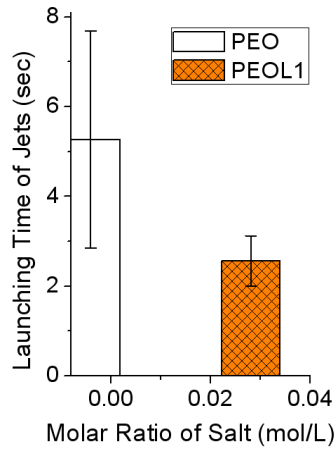


Fig. 3.29. Launching time of selected PEO solutions

- Measurement of number of jets and spinning area: A Sony Full HD NEX-VG10E Handy cam-E18-200 mm Lens camera was used in the experiments. Spinning area was determined by taking image from camera and using NIS-elements software. Results are illustrated in Figs. 3.30-3.31. For measurement of jet length a rod with 10 mm diameter electrospinning system was used. The length of jet was measured on the record of camera [165].

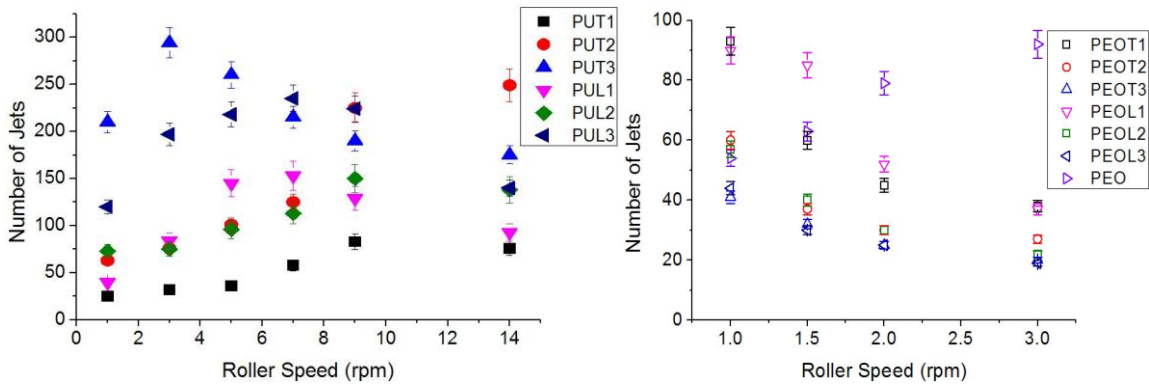


Fig. 3.30. Number of jets on the roller.

At 62 rpm; the number of jets of PUT1 solution was zero and the other solutions (PUT2-PUT3-PUL1-PUL2-PUL3) had fewer number of jets on the surface than 14 rpm.

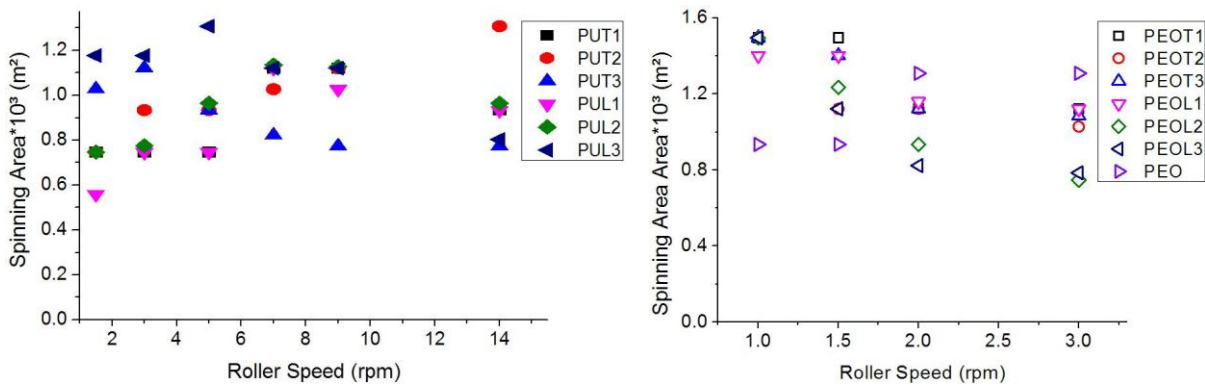


Fig. 3.31. Spinning area

At 62 rpm ; the spinning area of PU solutions was smaller than that at 14 rpm.

- Measurement of current and current/jet:

Roller electrospinning technique used for spinning is shown in Fig. 3.32. The current is evaluated by measuring the voltage on the resistor R placed between the collector electrode and earth. Resistance R is equal to 9811 Ω . The voltage is measured by a 33401A digital multimeter produced by Agilent and the values are stored in a computer at selected points on the time axis (typically 20 records per second).

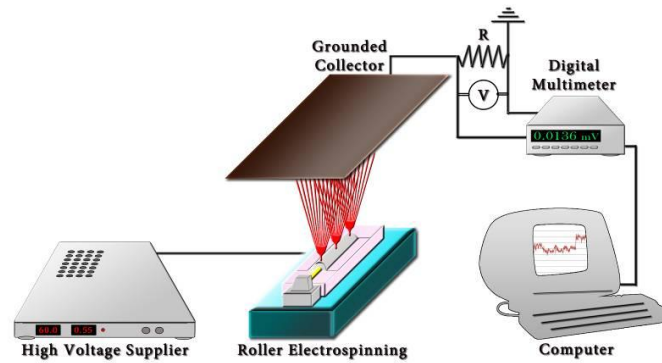


Fig. 3.32. Measurement of current on roller electrospinning system

The results are illustrated in Figs. 3.33-3.34. At 62 rpm; the current and current/jet of PUT1 solution was zero and the other solutions (PUT2-PUT3-PUL1-PUL2-PUL3) had fewer total current than 14 rpm while current/jet was further.

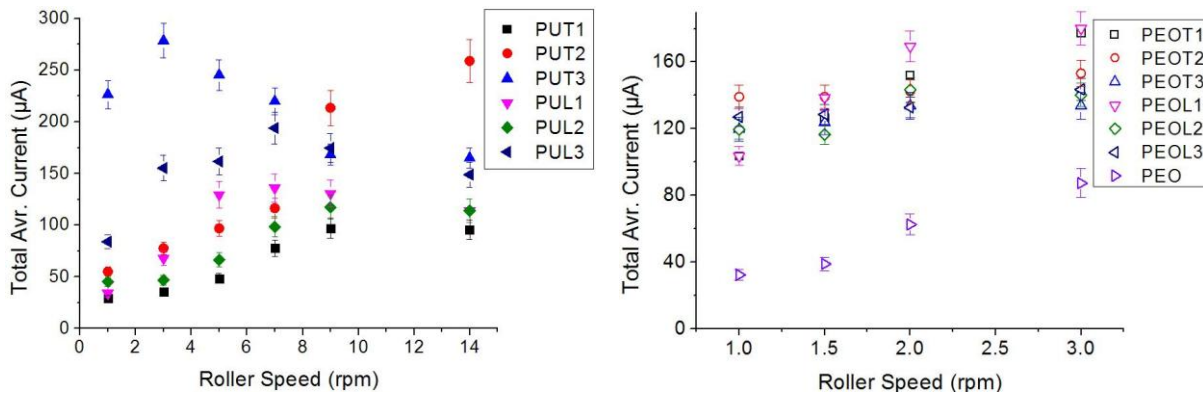


Fig. 3.33. Total current vs. roller speed

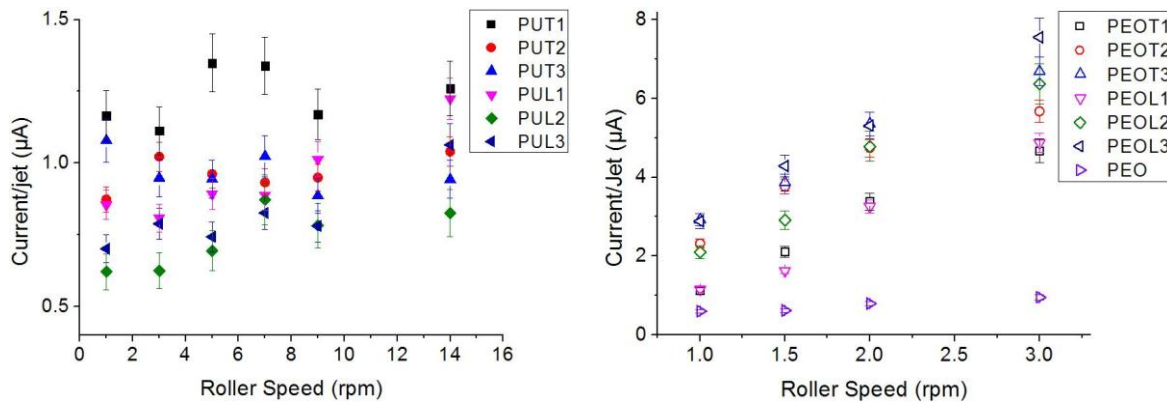


Fig. 3.34. Current/jet vs. roller speed

- Measurement of distance between neighboring jets: It was determined by taking image from camera and then calculating spinning area. Using Eqn. 2.30. number of jets were determined and illustrated in Fig. 3.35. At 62 rpm; the distance between jets of PUT1 solution was zero and the other solutions (PUT2-PUT3-PUL1-PUL2-PUL3) had the same distance of jets with 14 rpm.

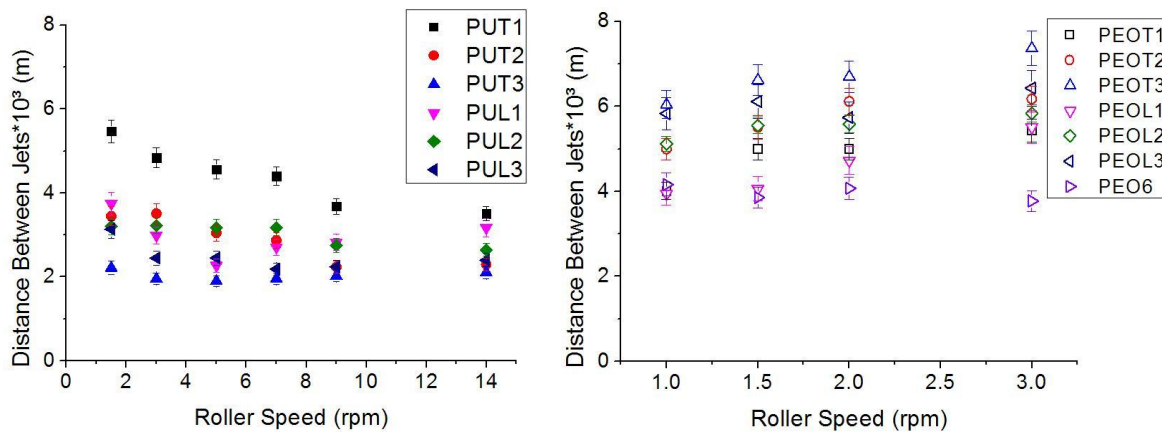


Fig. 3.35. Distance between jets vs. roller speed

- Measurement of spinning performance and performance/jet: 10x10 cm² nanofiber webs were prepared and measured on a balance. The calculations were done according to Eqns. 2.13-2.14. At 62 rpm; the SP of PUT1 solution was zero and the other solutions (PUT2-PUT3-PUL1-PUL2-PUL3) had fewer SP than 14 rpm.

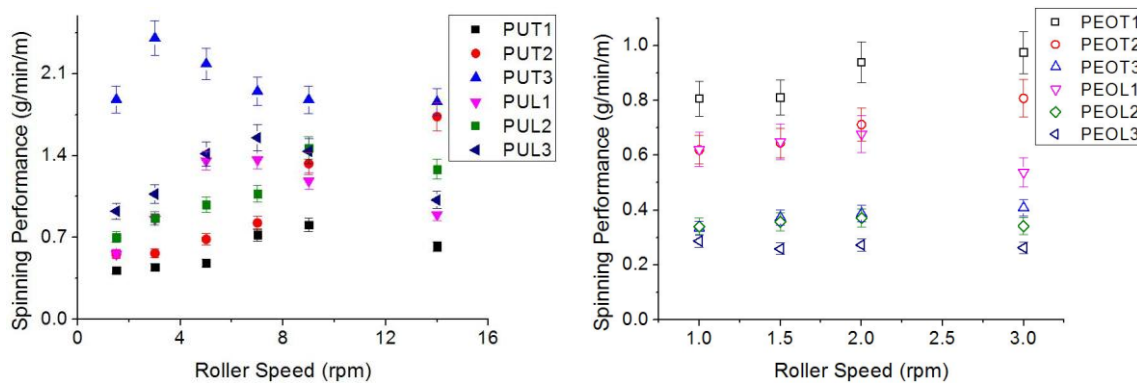


Fig. 3.36. Spinning performance of PU and PEO nanofibers in various rpm.

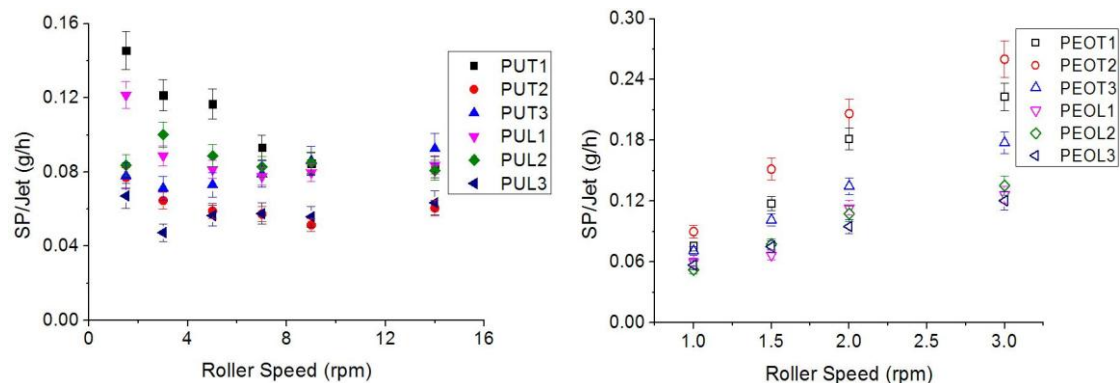


Fig. 3.37. SP/jet of PU and PEO nanofibers in various rpm.

At 62 rpm ; the SP/jet of PU solutions were almost the same with the result of 14 rpm.

- Measurement of fiber diameter and diameter distribution: Images of microstructure of nanofibers membrane were taken by scanning electron microscope (SEM) branded by Feico (Fig. 3.38). SEM images are shown in the Appenndix Part. NIS-elements software was used to determine fiber diameter and diameter distribution. At 62 rpm; the fiber diameter and diameter distribution of PU solutions were very high.

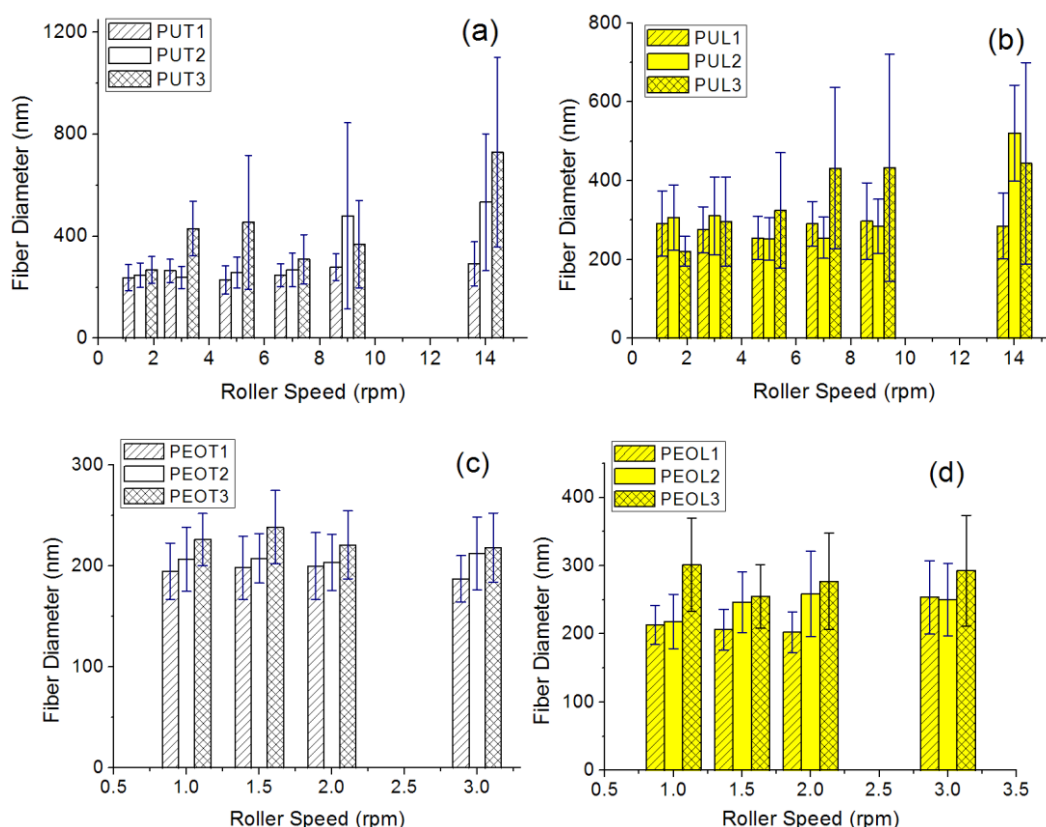


Fig. 3.38. Fiber diameter vs. roller speed (a) PU with TEAB salt. (b) PU with LiCl salt. (c) PEO with TEAB salt. (d) PEO with LiCl salt.

- Measurement of non-fibrous area: Using SEM images and NIS-elements software. non-fibrous areas were calculated (Fig. 3.39). At 62 rpm. the non-fibrous area of PU solutions was extremely high.

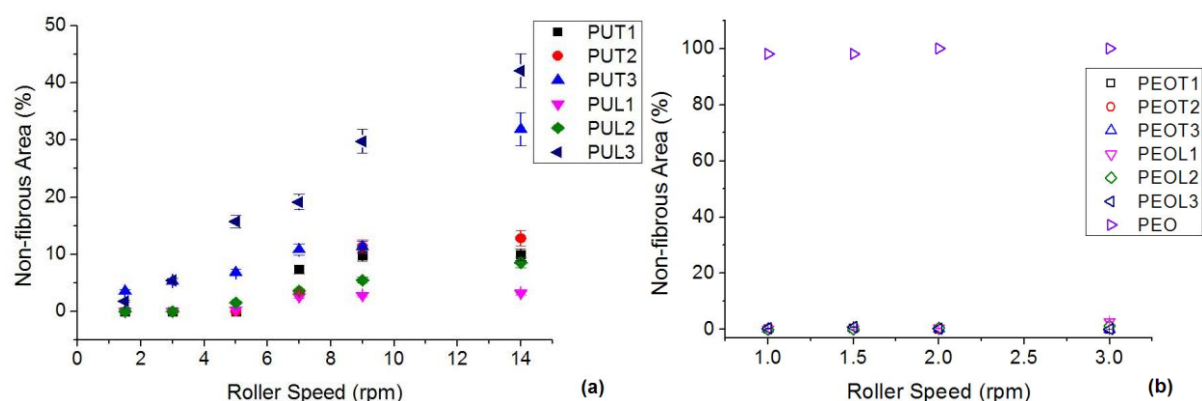


Fig. 3.39. Non-fibrous area vs. roller speed (a) PU. (b) PEO nanofibers

- Measurement of length of jets: A Sony Full HD NEX-VG10E Handy cam (14.2 megapixels)-E18-200 mm Lens camera was used in the experiments. Results are illustrated in Fig. 3.40. For measurement of jet length a rod with 10 mm diameter electrospinning system was used. The length of jet was measured on the record of camera [165].

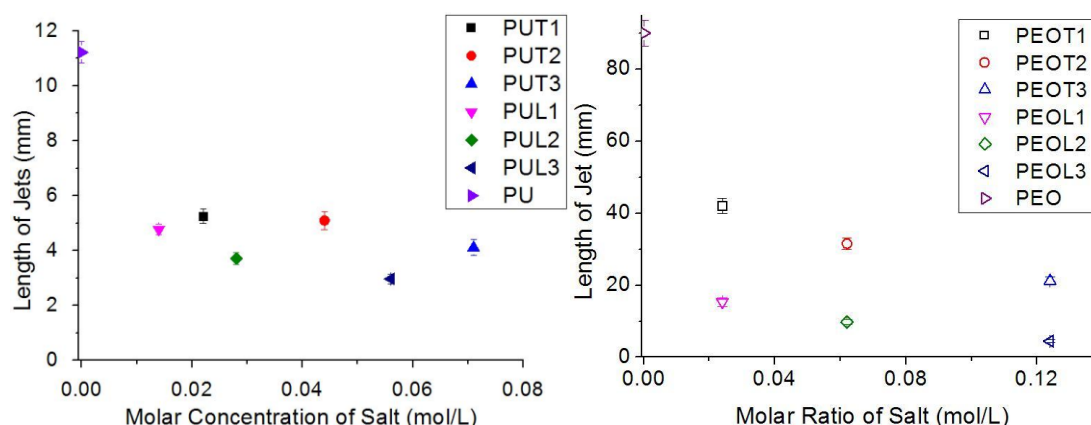


Fig. 3.40. Length of jets vs. molar ratio of salt

4. DISCUSSION

This chapter is divided into three parts corresponding to the three parts of the previous chapter.

4.1. On the Measured Current in Needle- and Needleless Electrospinning

The aim of this work was to study the effects of various conditions during the electrospinning process on the current and current per jet. respectively. As a result of the study. suitable quantities should be suggested to characterize the roller electrospinning of polymer solutions and melts.

In the needle electrospinning, the effects of relative humidity, needle protrusion length, and needle diameter were studied.

Relative humidity does not influence the value of current except for extremely high humidity (over 80%), when the air becomes conductive (Fig. 3.4). The difference between the values of current with and without polymer solution is constant within broad limits of relative humidity. The effect of relative humidity on current could not be directly studied in the roller electrospinning process as it is not clear whether the number of jets or throughput per jet is constant when the humidity varies.

The current increases with increasing needle protrusion length (Fig. 3.5). Undoubtedly, the intensity of the electric field at the tip of the needle, which grows with increasing needle protrusion length, is responsible for the rise in current.

In the roller electrospinning, the electric field intensity at the places of origin of the jets is probably rather low, close to that at a zero value of needle protrusion length in Fig. 3.5. It corresponds with the generally lower spinnability of any polymer solution on the roller compared with needle spinning.

The needle diameter does not influence values of current in needle electrospinning (Experiment 1.3; Figs. 3.6–3.8). On the other hand, all the four jet regimes described by Samatham and Kim [106] were observed depending on the values of feed rate, voltage, and needle diameter. The fluctuating jet regime was observed in only one case: at high voltage with the lowest feed rate and maximum needle diameter. The small-diameter needles, due to high linear flow velocity, seem to support a stable process even at the high ratio of voltage/feed rate.

The validity of the equation of Bhattacharjee et al. [112] was tested using the experimental results as shown in one example in Fig. 3.9. In all cases, the results obeyed the equation independently of the needle diameter and type of polymer solution.

A comparison of the current and camera records illustrated in Figs. 3.10 and 3.11 and in Tables 3.4 and 3.5 shows that the value of current per jet does not depend on the number of jets. In other words, the value of current is approximately the same in all the jets occurring simultaneously in the specific spinning experiment. This result suggests that the same situation can be expected in the roller electrospinning process. The solution containing KCl showed a higher value of current per jet, which corresponds with its higher conductivity.

The results of the roller electrospinning process (Figs. 3.12 and 3.13; Table 3.7) show that the current as well as the number of jets is rather constant during the spinning process.

The number of Taylor's cones (or jets) per spinning area is determined using a camera record (Fig. 3.13). Then, the current per jet is calculated by dividing the total current by the number of jets. Another significant process characteristic can be determined from the camera record, namely the distances between adjoining Taylor's cones.

Both the PEO solutions show almost the same value of current per jet but the more conductive solution containing KCl creates fewer jets on the roller than the other one. This corresponds to the experience with electrospinning of some polymers, namely poly(vinyl alcohol) and poly(ethylene oxide) from water solutions: the addition of salts increasing conductivity of solutions leads to lower throughput, better regularity of the nanofiber web, and smaller fiber diameters (see also the discussion in the part 4.3.).

The values of current per jet in the studied spinning systems are similar: 1–10 μA in the needle spinning process, 5–7 μA in the rod spinning process, and ca. 11 μA in the roller electrospinning process.

4.2. Determining optimum concentration of solutions

Polyethylene Oxide

The results illustrated in Table 3.9 show that the differences in electric conductivity and surface tension of studied solutions are not significant. Conditions of electrospinning were the same for all the materials. Therefore, only the concentration of solutions and related solution viscosity influenced the spinning performance and fiber diameters.

Spinning performance (Fig. 3.14) shows its maximum at the solution concentration of 7%. The graphs in Fig. 3.15 show that the average fiber diameters increase with increasing concentration and the standard deviation of fiber diameters also increases. The increase in fiber diameters with solution viscosity had been proved in many earlier works. SEM images of PEO solutions are illustrated in Fig. 3.16.

Polyurethane

The results illustrated in Table 3.11 show that the differences in surface tension of studied solutions are changed significantly; the viscosity and conductivity are affected by addition of salt. Conditions of electrospinning were the same for all the materials. We can assume that viscosity and conductivity of solutions are responsible for significant differences in spinnability, throughput and fiber quality. Solution viscosity shows an important effect on the fiber diameter and morphology of nanofiber layer.

Spinning performance of PU solution by adding LiCl salt is illustrated in Fig. 3.17. Both viscosity and conductivity have positive effect on PU spinnability up to a certain limit. At high viscosity spinning performance decreased. Spinning performance per one jet shows the same tendency as the total spinning performance.

It has been found that with the increase of electrical conductivity of the solution, there is a significant decrease in the diameter of the electrospun nanofibers. In these experiments, the solution viscosity and conductivity increases simultaneously. Fig. 3.18 illustrated that fiber diameter increases with salt content due to high viscosity. This can be seen from SEM images of samples as shown in Fig. 3.19.

4.3. Effect of roller velocity and salt on electrospinning process

Solutions of PU in DMF and of PEO in water containing salts TEAB and LiCl were employed in the experiments in the part 3.3. These solutions and their concentrations were chosen for following reasons:

1. PU and PEO show considerably different behavior in ES process, namely opposite influence of added salts on their spinnability;
2. The solutions allow a comparison between the aqueous and non-aqueous systems;
3. Concentration limits of polymers and salts in the solutions were determined in the chapter 3.2;
4. Both salts have different effect with polymer solutions which is very difficult to explain.

Basic properties of the solutions measured and described in the chapter 3.3. show that:

1. Surface tension of the solutions corresponds to that of used solvents and is not significantly dependent on the content of salts. Thus, the surface tension was not an influencing independent parameter in the experiments;

2. Viscosity of the solutions as a function of share rate shows considerably different character of both the polymers: Effective viscosity of PEO strongly depends on share rate, that of PU shows only moderate dependence. Thus, the macromolecules of PEO 400 kDa show high degree of mechanical entanglement and highly macromolecular character. The strength of PEO jets as a necessary requirement for spinnability is satisfactorily high at relatively low polymer concentration and corresponding viscosity. On the other hand, spinnability of PU requires rather high polymer concentration and corresponding viscosity. Viscosity of PU solutions grows with content of salts which is not the case in PEO solutions.

3. Conductivity of the solutions of the both TEAB and LiCl in water as well as in DMF is generally high and all the values are surprisingly close to each other. TEAB shows the same conductivity in water as LiCl does in spite of its evidently bigger ions. The values of conductivity in DMF are, again surprisingly, close to those in water which refers to a high degree of dissociation of the salts in DMF. On the other hand, the conductivities of polymer solutions containing salts differ from each other to some extent. The PEO solutions show higher conductivity than PU solutions due to their lower viscosity and corresponding greater movability of ions in direct electric field. The PU solutions containing LiCl are more conductive than those with TEAB as their ions are more movable in the highly viscous liquid.

4. The other basic properties of the solutions were not measured but there are probably a number of differences between the solutions which may cause their different behaviour in the ES process. For instance, the kind and concentration of polar groups in polymers, solvents and in the systems polymer-solvent-salt are certainly responsible for interactions of the solutions of their components with the electric field. Character and content of polar groups influences dielectric constant of materials. Water, DMF and PEO show high values of permittivity (80, 38 and 39, respectively) [157,158]. On the other hand the permittivity of PU is rather low (5-7) which may be the reason for its poor spinnability. Spinnability of PU grows considerably with addition of salts [53]. This may be caused by the interactions between DMF and TEAB [145] or between PU and salts [53,58] as follows in Fig. 4.1 and 4.2:

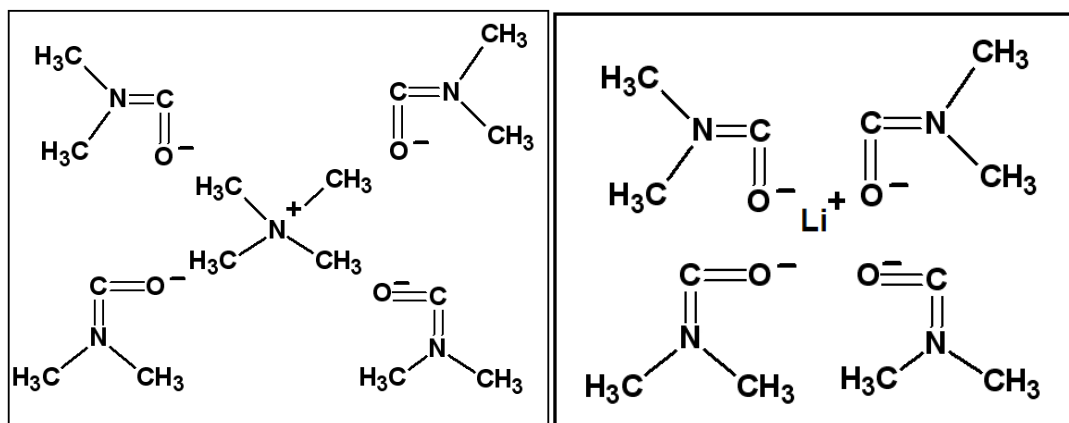


Fig. 4.1. Computed structure of the tetramethylammonium ion and lithium ion complexed to four N,N-dimethylformamide molecules [145].

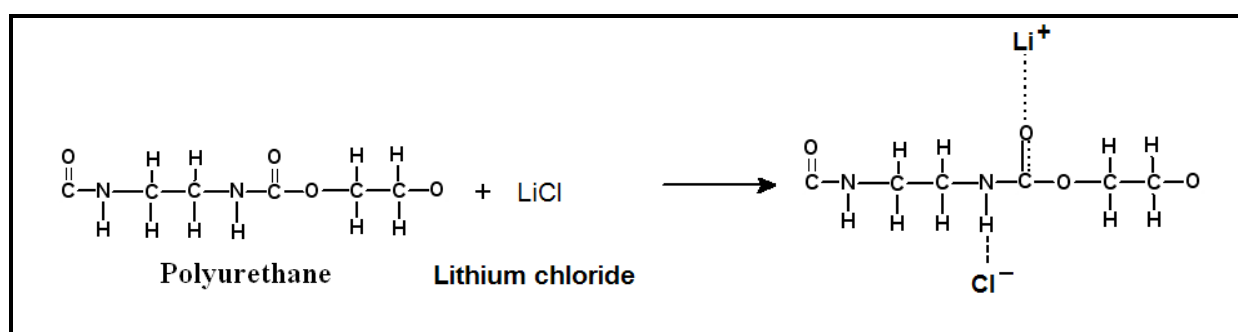


Fig. 4.2. Chemical interaction of LiCl salt with PU polymer.

Due to these interactions, the DMF-TEAB, DMF-LiCl and PU-Li systems may show substantially stronger ionic character and stronger attractive response in electric field.

Stronger jets of more viscous PU solutions containing salts are probably the second reason for better spinnability of such solutions.

To explain the complex relations shown in the chapter 3.3, let us first discuss the dependencies of some new ES parameters described in the chapter 2.3, on the independent process parameters.

The launching time of jets (Figs. 3.27-3.28 and Tables 3.15-3.16) depends significantly on the content of salts in the polymer solutions. With increasing salt concentration the launching time decreases in the case of PU as well as PEO. If the electric field is deformed by the grounded wire, launching time also decreases significantly due to high local concentration of electric field (Fig. 3.29 and Table 3.17).

The launching time appears to be significant at the beginning of the spinning process only. Video records show that after the voltage has been switched on, the first jets appear on the surface of spinning roller in the time described as launching time. Repeated measurements with one polymer solution show a wide distribution of launching times (Tables 3.15-3.16). Nevertheless, as soon as the first jet appeared, the other jets follow in a short time. After a jet disappears due to its breakage, a new jet appears immediately close to the broken one. The number of jets on the roller surface develops and reaches the final value in a short time after

the first jet appeared. The number of jets is then almost constant in the following time of spinning process.

The video records show that the formation of new jets is strongly evoked by disturbances of the solution surface caused by any reason such as movement of another jet, breakage of a jet etc.

The dependence of the launching time on studied independent ES parameters differs from that of number of jets and spinning performance. Therefore, we conclude that the launching time influences the spinning process at its beginning only. After reaching the constant number of jets, the process does not depend on launching time any more.

Measurement of the *jet length* shows significant differences between PU and PEO behavior. The jets of electrospun PEO are much longer than those of PU. This fact can explain some other differences in the spinning process of both the polymers as discussed later.

The length of the jets and its dependence on the salt content and viscosity was discussed by Dao [32] (see chapter 2.3.1.2.2.). Nevertheless, his theory does not explain the significant differences in the jet length between PU and PEO solutions. These are probably caused by considerably greater interactions of PEO with electric field when compared with those of PU due to more polar character of PEO. Stronger interactions lead to a faster jet deformation and resulting jet length.

In ES, PU and PEO show essential differences in their behavior, namely in *the number of jets* on the spinning roller (and in the spinning performance as discussed below).

First, the number of jets is considerably larger at PU. Two attempts have been done to explain this difference:

- a) The theory of shielding effect of conducting lightning rods was taken into account [166]. According to this theory, the electric field is screened out in the conical space having a tip at the end of conductor and a top angle about 45° to 60° (Fig. 4.3) [167,168,169,170,171,172,173]. We supposed that the distance between cones is proportional to the length of jets as shown in Fig. 4.4 and only one jet can be formed within the area of this cone base. The standard deviation of length of jets and distance between jets were illustrated in Figures 3.35 and 3.40. Fig. 4.4 illustrates average values. The shielding angles were calculated from the values of the jet lengths and corresponding jet to jet distances as shown in Tables 4.1 and 4.2. The results in Tables 4.1 and 4.2 did not confirm applicability of the shielding theory in this case. Probably, the theory requires highly conductive metal rods.

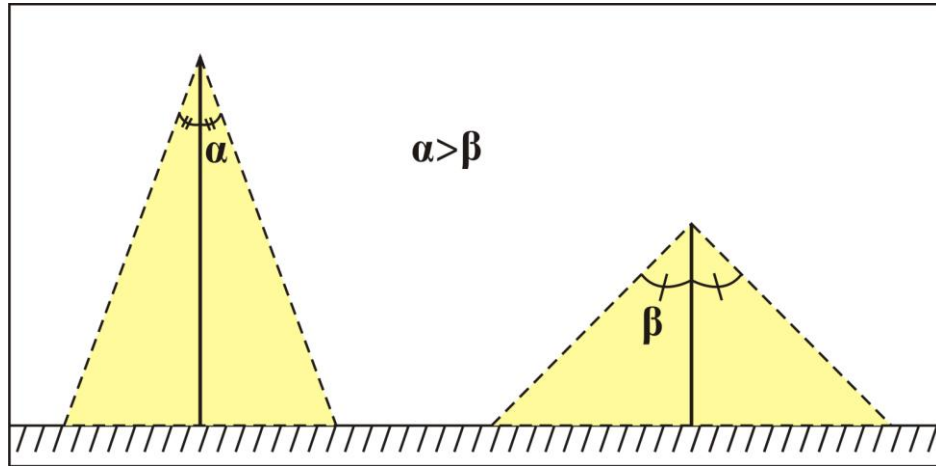


Fig. 4.3. The shielding effect of rods in different length.

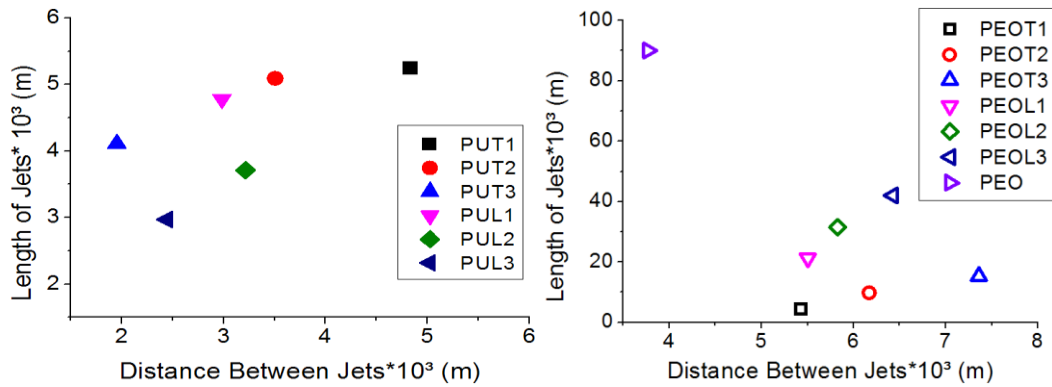


Fig. 4.4. Length of jets vs. Distance between jets at 3 rpm roller speed

Table 4.1. Shielding angle of PU jets

rpm	Shielding angle of PU jets (in degree)					
	PUT1	PUT2	PUT3	PUL1	PUL2	PUL3
1.5	27.50±1.10	18.68±0.74	15.06±0.60	21.37±0.85	23.32±0.93	27.80±1.11
3	24.71±0.98	18.99±0.75	13.36±0.53	17.32±0.69	23.42±0.93	22.36±0.89
5	23.45±0.93	16.62±0.66	12.98±0.52	13.35±0.53	23.14±0.92	22.40±0.86
7	22.72±0.90	15.72±0.62	13.38±0.53	15.81±0.63	23.12±0.92	20.18±0.80
9	19.29±0.77	12.36±0.49	13.79±0.55	16.45±0.53	20.28±0.81	20.63±0.82
14	18.46±0.73	12.68±0.50	14.34±0.57	18.34±0.73	19.61±0.78	21.96±0.87

Table 4.2. Shielding angle of PEO jets

rpm	Shielding angle of PEO jets (in degree)						
	PEOT1	PEOT2	PEOT3	PEOL1	PEOL2	PEOL3	PEO6
1	2.73±0.08	4.53±0.13	8.10±0.24	7.32±0.22	14.67±0.44	32.98±0.99	1.32±0.04
1.5	3.40±0.10	4.99±0.15	8.87±0.26	7.53±0.22	15.84±0.47	34.24±1.02	1.22±0.03
2	3.40±0.10	5.54±0.16	8.97±0.27	8.74±0.26	15.92±0.47	32.56±0.97	1.29±0.04
3	3.70±0.11	5.59±0.16	9.84±0.29	10.16±0.30	16.59±0.49	35.59±1.06	1.20±0.03

- b) Lukas [35,41,174] calculated the distance between jets by calculating inter-jet distance called the critical wavelength. This parameter allows estimation of the relative productivity of the electrospinning process. Calculation of the critical wavelength λ_c can be done using the equation:

$$\lambda_c = 2\pi a \quad (4.1)$$

where a denotes the capillary length. It can be expressed in the form:

$$a = \sqrt{\frac{\gamma}{\rho g}}, \quad (4.2)$$

where ρ is liquid mass density. γ is linear force of surface tension and g gravitational acceleration.

The calculation of PU and PEO inter-jet distance are tabulated in Tables 4.3 and 4.4.

Table 4.3. Inter-jet distance of PU solution

Polymer	Inter-jet distance (m)
PUT1	0.01252
PUT2	0.01249
PUT3	0.01253
PUL1	0.01251
PUL2	0.01253
PUL3	0.01254

Table 4.4. Inter-jet distance of PEO solution

Polymer	Inter-jet distance (m)
PEOT1	0.01573
PEOT2	0.01578
PEOT2	0.01580
PEOL1	0.01570
PEOL2	0.01579
PEOL3	0.01580
PEO	0.01572

Second. the number of PU cones grows with the content of salt in the solution. On the contrary, the number of PEO cones falls with growing salt concentration. This effects seem to be difficult to explain as the role of salts is multiple:

1. Salt (TEAB more than LiCl) creates complex structures (Fig. 4.2) with PU which leads to changes in the interactions macromolecule – macromolecule and macromolecule – solvent. This causes an increase in viscosity, related entanglement number and stronger jets. Thus, the effect of salts in the PU solutions is following:

- stronger jets result in longer average life of jets [58];

-the jets are shorter due to higher content of ions and greater viscosity [32]. the number of jets grows.

These effects of salts do not occur in the PEO solutions as the salts do not create complex structures with PEO.

2. Salts increase the conductivity of the polymer solutions. Increase in the conductivity changes the character of the polymer solution from a semi-conductor to a conductor so that the solution is losing the character of a „leaky model“ (see chapter 2.3.1.1.3.). This leads to the loss of ability to create Taylor's cones.

Apparently the effect of salts according to 2. works against that in 1. In the case of PU. the effects described in 1. predominate those in 2. In the case of PEO. only effects according to 2. apply.

The differences between the PU and PEO behavior are also based on different polymer characteristics. namely:

1. PEO 400 kDa has the molecular weight high enough to create strong jets even at the low concentration and corresponding viscosity. It is not the case of PU. PU needs an increase in entanglement level using a salt.
2. PEO contains strongly polar groups so that it shows strong interactions with electric field. This is expressed by a high value of dielectric constant. Again. this is not the case of PU. PU needs an increase in polarity via creating complexes with salts.

The spinning performance (Fig 3.36) shows in principle the same tendencies as the number of jets. Nevertheless **the spinning performance per jet** (Fig 3.37) is not an independent quantity. The amount of polymer solution flowing through one Taylor's cone depends on the viscosity of solution. on the thickness of solution layer and on the drawing force of electric field. dependent on dielectric properties of the polymer or polymer solution.

The total average current shows the same tendencies as the spinning performance does (Fig. 4.5). On the other hand. the plot of the current per jet vs. spinning performance per jet does not show clear relation (Fig. 4.6). When a jet breaks up into secondary jets. the additional ions are transferred from the polymer solution into the air in the vicinity of the jet [155]. Several reports have suggested that charge carriers are transported in the atmosphere surrounding fluid jet [112,175,176]. Therefore. measured current grows with spinning performance and with the amount of salts in the polymer solutions. The current is probably not transported from one to the other electrode primarily with the polymer or solvent. The mechanism of current in ES was studied separately in more detail [165] and the results are not a part of this work.

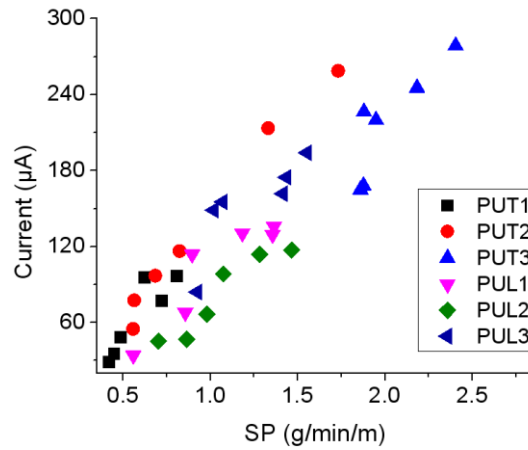


Fig.4.5. Average total current vs. spinning performance (PU)

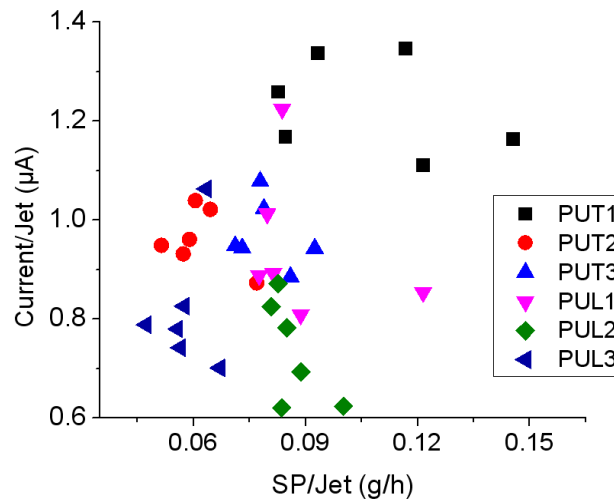


Fig. 4.6. Current per jet vs. spinning performance per jet (PU)

To explain rather complex and non-monotonous dependencies of studied dependent ES parameters on the *spinning roller velocity*, the video records of the spinning process were carefully studied and following velocities compared:

\vec{v} - velocity of roller surface (ms^{-1})

\vec{v}_{j1} - velocity of jets against static collector electrode

\vec{v}_{j2} - velocity of jets against the surface of moving roller electrode.

The situations depending on the movement of roller are shown in Fig. 4.7.

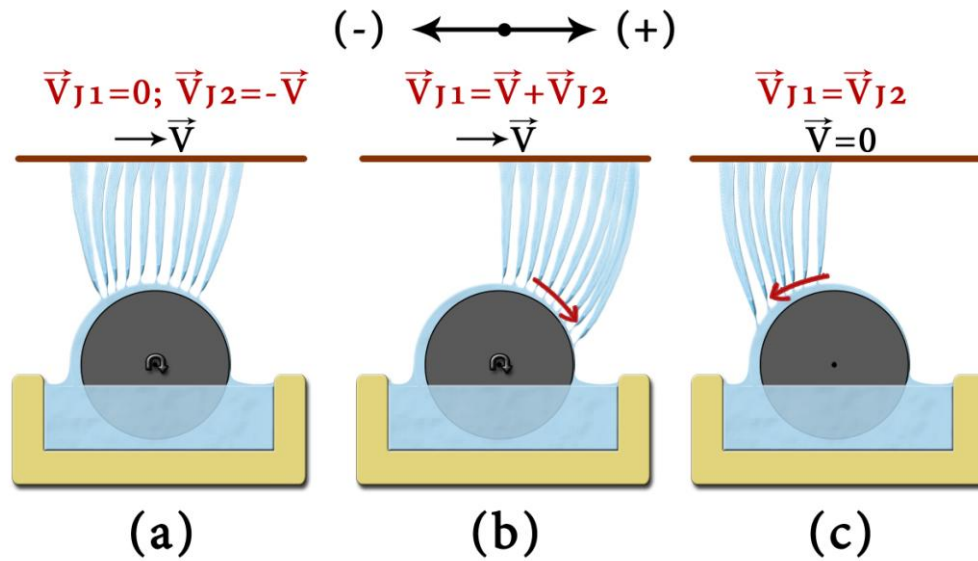


Fig. 4.7. Movement of roller and position of jets.

A. Low roller velocity (Fig. 4.7.a): The jets move against the moving surface of roller and keep stable positions against the collector electrode.

$$\vec{v}_{j2} = -\vec{v} \quad \text{and} \quad \vec{v}_{j1} = 0 \quad (4.3)$$

B. High roller velocity (Fig. 4.7.b): The jets move in the direction of \vec{v} and reach the solution bath.

$$\vec{v}_{j1} = \vec{v} + \vec{v}_{j2} \quad (\vec{v}_{j2} \text{ being negative}) \quad (4.4)$$

C. Roller stops suddenly (Fig. 4.7.c): The jets start moving against the former direction of roller movement.

$$\vec{v} = 0 \quad \text{and} \quad \vec{v}_{j1} = \vec{v}_{j2} < 0 \quad (4.5)$$

The case C illustrates crucial importance of the strength of jets in the ES process. It also shows that the jets have their „roots“ inside the solution layer. the „roots“ being moving, partially oriented macromolecules of dissolved polymer.

The border velocity \vec{v} separating the cases A and B depends on movability of jets against the surface of spinning roller is a complex function of solution viscosity, thickness of solution layer and drawing electric force F . The Eqn. (2.43) is probably applicable in description of the jets movability as well as in the throughput per jet.

Using the above described observations, the dependencies of measured ES parameters on the roller velocity can be explained as follows:

Generally, the dependence of the number of jets, spinning area and spinning performance on the roller velocity is non-monotonous for following reason:

If the roller velocity is low, then the solution feed and the thickness of solution layer on the roller are small. This is limiting the values of above mentioned dependent parameters. Also, the jets move against the surface of the roller and keep stable positions against the static collector electrode as shown in Fig. 4.7.a. If the roller velocity exceeds a critical value, the limited movability of jets leads to their movement towards the solution bath (Fig. 4.7.b). This causes a reduction in spinning area and number of jets but not necessarily that of spinning performance. Spinning performance can be kept more or less constant or even slightly grow with increasing roller velocity as the loss of the number of jets is compensated by greater throughput per jet due to increase in the thickness of solution layer. The critical value of the roller velocity depends on the viscosity of polymer solution and probably on some other properties of polymer solution such as its spinnability. In the case of PEO, the critical value is lying at the low roller velocity (below 1 rpm) as the movability of jets is limited due to rather thin solution layer. Therefore, the non-monotonous character of above mentioned dependencies is not apparent from the experimentally found data.

Quality of produced nanofibers and nanofiber layers was tested in the experiments, namely fiber diameters (Fig. 3.38) and non-fibrous area (Fig. 3.39), though this was not an important part of the work. In the PU ES, the highest content of salts leads to an increase in viscosity and bigger fiber diameters connected with it. High salt content also leads to lower quality of PU nanofiber layers. On the contrary, PEO nanofiber diameters and quality of nanofiber layers do not significantly depend on the content of salt if this lays above a certain limit.

There are some dependencies found in the experimental results which were not explained by performed experiments and their explanation requires specific studies. The dependence of jet lengths on the roller velocity (Fig. 3.40) is one of examples.

5. CONCLUSIONS

New independent and dependent ES parameters were introduced and studied by author, namely:

- velocity of rotating roller and related quantities – secondary independent parameters (thickness of solution layer, feeding rate of polymer solution, time available for Taylor's cones formation). The relations between the roller velocity and secondary independent parameters were calculated and/or measured;
- average electric current in roller ES and current per jet;
- spinning area and positions of jets;
- number of Taylor's cones per spinning area and the average distance between neighbouring cones;
- polymer solution throughput per Taylor's cone was calculated.

Above mentioned parameters were introduced and studied with the aim of better understanding the ES mechanism. In the previous studies focused on a limited number of parameters such as molecular weight of polymer, solution concentration and viscosity, spinning performance), some ES phenomena remained unexplained.

The main results of experiments:

- total electric current in the roller ES is more or less proportional to the spinning performance. On the contrary, the current per jet is not proportional to the spinning performance per jet. This discrepancy evoked a more thorough investigation of the phenomenon. The results were separately published [165] and are not a part of this work;

- the dependence of number of jets and the dependence of spinning performance on the roller velocity is generally non-monotonous. Thickness of solution layer and feed rate versus movability of jets against the roller surface are the main influencing factors of this complex relation;

the launching time of jets does not influence the number of jets on the spinning roller and spinning performance significantly. It only can influence the starting period of the spinning process. As soon as the spinning process becomes stable, the number of jets depends on other parameters and is principally stable;

the experimentally found distance between jets is in a reasonably good agreement with theoretical conclusions of Lukas, nevertheless, it depends on some more variables than Lukas considered, namely on the conductivity of polymer solution;

spinning area mainly depends on movement of roller. Experimental results of PEO showed that increasing roller rpm decrease spinning area except PEO without salt. The relationship between spinning area and spinning performance is related with number of jets. Higher number of jets means larger spinning area which also means higher SP;

the length of jets mainly depends on the amount of salt which is related with conductivity and the viscosity of solution. The length of PEO solutions' jets is much greater than that of PU solutions which was explained in the chapter 4.3. There is no relation between SP and length of jets;

the effect of rotating roller on fiber surface morphology shows that increasing roller speed increase the fiber diameter and non-fibrous area. It is necessary to optimize roller speed to obtain proper fiber diameter and minimum non-fibrous area for every polymer solution;

- salts may influence entanglement number and polarity of macromolecules when creating complex bonds with them. On the other hand, the salts increase the conductivity of solutions which may cross the limits supposed by the model of a „leaky dielectric“;

- PEO 400 kDa with its high polarity and high entanglement number (strength of jets) shows high spinning performance. This is reduced by the increase in conductivity;

- in the case of PU, the salts creating complex bonds with the polymer, increase the low polarity as well as the entanglement number which causes an increase in the spinning performance. Further addition of salts would probably lead to reduced spinning performance. Nevertheless it cannot be proved because of extreme increase in the solution viscosity.

Future works

The results of this thesis should be seen as initial works focused on definitions of parameters of needleless electrospinning, introducing new parameters and on development of methods to measure these new parameters. This thesis also brings the results of studies influence of some selected independent parameters, for instance, velocity of roller spinning electrode and

content of salt in polymer solutions on electrospinning process. In future. I suggest continued studies focused on:

- There is not enough work about permittivity effect on electrospinning. Theoretical studies leading to full explanation and complete description of electrospinning process involving effects of permittivity on dependent parameters. such as. length of jet. distance between jets. current on a jet. spinning performance. fiber diameter. life time of jets. spinning area.
- Full understanding of relations between independent and dependent parameters

6. REFERENCES

- [1] T. Lin, H.X. Wang, X.G. Wang, Self-crimping bicomponent nanoribers electrospun from polyacrylonitrile and elastomeric polyurethane, *Advanced Materials* 17 (2005) 2699-+.
- [2] S.W. Bail DH, Khalighi K, Seboldt H., Temporary wound covering with a silicon sheet for the soft tissue defect following open fasciotomy. Technical note., *J Cardiovasc Surg (Torino)* 39 (1998) 587-591.
- [3] R.M. Nerem, A. Sambanis, Tissue engineering: from biology to biological substitutes, *Tissue Eng* 1 (1995) 3-13.
- [4] X.H. Zong, K. Kim, D.F. Fang, S.F. Ran, B.S. Hsiao, B. Chu, Structure and process relationship of electrospun bioabsorbable nanofiber membranes, *Polymer* 43 (2002) 4403-4412.
- [5] P. Taepaiboon, U. Rungsardthong, P. Supaphol, Drug-loaded electrospun mats of poly(vinyl alcohol) fibres and their release characteristics of four model drugs, *Nanotechnology* 17 (2006) 2317-2329.
- [6] K. Kosmider, J. Scott, Polymeric nanofibres exhibit an enhanced air filtration performance, *Filtration & Separation* 39 (2002) 20-22.
- [7] K.H. Hong, Preparation and properties of electrospun poly (vinyl alcohol)/silver fiber web as wound dressings, *Polymer Engineering and Science* 47 (2007) 43-49.
- [8] J.S. Choi, K.W. Leong, H.S. Yoo, In vivo wound healing of diabetic ulcers using electrospun nanofibers immobilized with human epidermal growth factor (EGF), *Biomaterials* 29 (2008) 587-596.
- [9] A.C. Patel, S. Li, J.M. Yuan, Y. Wei, In situ encapsulation of horseradish peroxidase in electrospun porous silica fibers for potential biosensor applications, *Nano Letters* 6 (2006) 1042-1046.
- [10] X.M. Mo, C.Y. Xu, M. Kotaki, S. Ramakrishna, Electrospun P(LLA-CL) nanofiber: a biomimetic extracellular matrix for smooth muscle cell and endothelial cell proliferation, *Biomaterials* 25 (2004) 1883-1890.
- [11] J.J. Stankus, L. Soletti, K. Fujimoto, Y. Hong, D.A. Vorp, W.R. Wagner, Fabrication of cell microintegrated blood vessel constructs through electrohydrodynamic atomization, *Biomaterials* 28 (2007) 2738-2746.
- [12] T. Ondarcuhu, C. Joachim, Drawing a single nanofibre over hundreds of microns, *Europhysics Letters* 42 (1998) 215-220.
- [13] O. Jirsak, F. Sanetnik, D. Lukas, V. Kotek, L. Martinova, J. Chaloupek, A Method of Nanofibers Production from a Polymer Solution Using Electrostatic Spinning and a Device for Carrying Out the Method, EP1673493, Czech Republic, 2005.
- [14] G. Taylor, Electrically Driven Jets, *Proceedings of the Royal Society of London Series a-Mathematical and Physical Sciences* 313 (1969) 453-&.
- [15] W. Gilbert, (Ed.), *On the Magnet and Magnetic Bodies, and on That Great Magnet the Earth*, John Wiley & Sons, Newyork, 1893.
- [16] L. Rayleigh, On the Equilibrium of Liquid Conducting Masses charged with Electricity, *Philosophical Magazine* 14 (1882) 184-186.
- [17] C.V. Boys, On the Production, Properties, and some suggested Uses of the Finest Threads, *Proceedings of the Physical Society of London* 9 (1887) 8.
- [18] J.F. Cooley, Apparatus for Electrically Dispersing Fluids, US Patent 1902.
- [19] W.J. Morton, Method of Dispersing Fluids, US Patent 1902.
- [20] J. Zeleny, The Electrical Discharge from Liquid Points, and a Hydrostatic Method of Measuring the Electric Intensity at Their Surfaces, *Phys. Rev.* 3 (1914) 69-91.

- [21] J. Zeleny, The Discharge of Electricity from Pointed Conductors Differing in Size, *Physical Review (Series I)* 25 (1907) 305-333.
- [22] A. Formhals, Production of artificial fibers from fiber forming liquids, US Patent, US2323025 A, United States, 1943.
- [23] F. Anton, Process and apparatus for preparing artificial threads, Richard, Schreiber Gastell, Anton, Formhals, United States, 1934.
- [24] A. Formhals, Production of Artificial Fibers, US Patent, United State, 1937.
- [25] A. Formhals, Method and apparatus for the production of fibers, US Patent, US2116942 A, United State, 1938.
- [26] A. Formhals, Artificial Thread and Method of Producing Same, US Patent, US2187306 A, United State, 1940.
- [27] W.A. Macky, Some Comparisons of the Invigorating Effect of the Climate in Different Parts of New Zealand, *New Zealand Journal of Science & Technology* 19 (1930) 164-172.
- [28] W.A. Macky, Some investigations on the deformation and breaking of water drops in strong electric fields, *Proceedings of the royal society, series A: mathematical physical and engineering sciences* 133 (1931) 565-587.
- [29] C.N. Norton, United States Patent, 1936.
- [30] G.I. Taylor, Disintegration of water drops in an electric field, *Proceedings of the Royal Society A: Mathematical, Physical and Engineering Sciences* 280 (1964) 383-397.
- [31] J.R. Melcher, E.P. Warren, Electrohydrodynamics of a Current-Carrying Semi-Insulating Jet, *Journal of Fluid Mechanics* 47 (1971) 127-&.
- [32] A.T. Dao, The Role Of Rheological Properties Of Polymer Solutions In Needleless Electrostatic Spinning, *Nonwoven*, Technical University of Liberec, Liberec, 2010, pp. 80.
- [33] F. Yener, B. Yalcinkaya, O. Jirsak, On the Measured Current in Needle- and Needleless Electrospinning, *Journal of Nanoscience and Nanotechnology* 13 (2013) 4672-4679.
- [34] A.L. Yarin, E. Zussman, Upward needleless electrospinning of multiple nanofibers, *Polymer* 45 (2004) 2977-2980.
- [35] D. Lukas, A. Sarkar, P. Pokorny, Self-organization of jets in electrospinning from free liquid surface: A generalized approach, *Journal of Applied Physics* 103 (2008).
- [36] O.O. Dosunmu, G.G. Chase, W. Kataphinan, D.H. Reneker, Electrospinning of polymer nanofibres from multiple jets on a porous tubular surface, *Nanotechnology* 17 (2006) 1123-1127.
- [37] X. Wang, H.T. Niu, T. Lin, X.G. Wang, Needleless Electrospinning of Nanofibers With a Conical Wire Coil, *Polymer Engineering and Science* 49 (2009) 1582-1586.
- [38] H.T. Niu, T. Lin, X.G. Wang, Needleless Electrospinning. I. A Comparison of Cylinder and Disk Nozzles, *Journal of Applied Polymer Science* 114 (2009) 3524-3530.
- [39] L. Tonks, A Theory of Liquid Surface Rupture by a Uniform Electric Field, *Physical Review* 48 (1935) 562-568.
- [40] L.D. Landau, *Electrodynamics of continuous media* / by L.D. Landau and E.M. Lifshitz ; translated from the Russian by J.B. Skyes and J.S. Bell, Pergamon Press ; Addison-Wesley, Oxford : Reading, Mass, 1960.
- [41] D. Lukáš, A. Sarkar, L. Martinová, K. Vodsed'álková, D. Lubasová, J. Chaloupek, P. Pokorný, P. Mikeš, J. Chvojka, M. Komárek, Physical principles of electrospinning (Electrospinning as a nano-scale technology of the twenty-first century), *Textile Progress* 41 (2009) 59-140.
- [42] L. Torobin, R. Findlow, Method and Apparatus for Producing High Efficiency Fibrous Media Incorporating Discontinuous Sub-Micron Diameter Fibers and Web Media Formed Thereby, U.S. Patent, 2001.

- [43] A. Fabbriante, G. Ward, T. Fabbriante, Micro-Denier Nonwoven Materials Made Using Modular Die Units, U.S. Patent, 2000.
- [44] <http://www.hillsinc.net/articles/Polymeric.htm>, Polymeric Nanofibers Fantasy or Future?, 2013.
- [45] M.A. Hassan, B.Y. Yeom, A. Wilkie, B. Pourdeyhimi, S.A. Khan, Fabrication of nanofiber meltblown membranes and their filtration properties, *Journal of Membrane Science* 427 (2013) 336-344.
- [46] M. Dauner, Ullrich, A. & Reiter, F. , Nanofibers by Centrifuge Spinning to Improve Filter Media, in: P.o.t.W.F. Congress (Ed.), (WFC10), Leipzig, Germany, 2008.
- [47] P. Mellado, H.A. McIlwee, M.R. Badrossamay, J.A. Goss, L. Mahadevan, K.K. Parker, A simple model for nanofiber formation by rotary jet-spinning, *Applied Physics Letters* 99 (2011).
- [48] M.P. Rutter, Inspired by cotton candy, engineers put new spin on nanofibers, 2010.
- [49] K. Mie, S. Tsuyoshi, N. Suguru, T. Kengo, Development and application of high-strength polyester nanofibers, *Polymer Journal* 44 (2012) 987-994.
- [50] R. Pike, Super Fine Microfiber Nonwoven Web, U.S. Patent, 1999.
- [51] A.S. Nain, J.C. Wong, C. Amon, M. Sitti, Drawing suspended polymer micro-/nanofibers using glass micropipettes, *Applied Physics Letters* 89 (2006).
- [52] Elmarco, Electrospinning devices, <http://www.elmarco.com/nanofiber-equipment/electrospinning-devices-nslab200-nslab500/>, Liberec, 2004-2012.
- [53] F. Cengiz, O. Jirsak, The effect of salt on the roller electrospinning of polyurethane nanofibers, *Fibers and Polymers* 10 (2009) 177-184.
- [54] F. Yener, O. Jirsak, Improving Performance of Polyvinyl Butyral Electrospinning, *Nanocon 2011* (2011) 356-361.
- [55] F. Yener, O. Jirsak, Comparison between the Needle and Roller Electrospinning of Polyvinylbutyral, *Journal of Nanomaterials* (2012).
- [56] F. Cengiz-Çallioğlu, O. Jirsak, M. Dayik, Electric current in polymer solution jet and spinnability in the needleless electrospinning process, *Fibers and Polymers* 13 (2012) 1266-1271.
- [57] F. Cengiz, T.A. Dao, O. Jirsak, Influence of solution properties on the roller electrospinning of poly(vinyl alcohol), *Polymer Engineering & Science* 50 (2010) 936-943.
- [58] F. Cengiz-Callioğlu, O. Jirsak, M. Dayik, Investigation into the relationships between independent and dependent parameters in roller electrospinning of polyurethane, *Textile Research Journal* 83 (2013) 718-729.
- [59] J.O. Cengiz F., Dayik M., An Investigation the Effects of Ambient Humidity on the Roller Electrospinning of Nanofiber Production, *Electronic Journal of Textile Technologies* 3 (2009) 24-32.
- [60] S.L. Shenoy, W.D. Bates, H.L. Frisch, G.E. Wnek, Role of chain entanglements on fiber formation during electrospinning of polymer solutions: good solvent, non-specific polymer-polymer interaction limit, *Polymer* 46 (2005) 3372-3384.
- [61] W.W. Graessley, Polymer-Chain Dimensions and the Dependence of Viscoelastic Properties on Concentration, Molecular-Weight and Solvent Power, *Polymer* 21 (1980) 258-262.
- [62] R.G.C. Bahattarjee P.K., Electrospinning and Polymer Nanofibers: Process Fundamentals, *Comprehensive Biomaterials* 1 (2011) 497-512.
- [63] G.H. McKinley, T. Sridhar, Filament-Stretching Rheometry, *Ann. Rev. Fluid Mechanics* 34 (2002) 375-415.

- [64] H.A. Barnes, *A Handbook of Elementary Rheology*, University of Wales Institute of Non-Newtonian Fluid Mechanics, University of Wales, Institute of Non-Newtonian Fluid Mechanics, Aberystwyth, 2000.
- [65] G.W.S. Blair, *A Survey of General and Applied Rheology*, Pitman; 1st edition, 1944.
- [66] K.W. Kim, K.H. Lee, M.S. Khil, Y.S. Ho, H.Y. Kim, The effect of molecular weight and the linear velocity of drum surface on the properties of electrospun poly(ethylene terephthalate) nonwovens, *Fibers and Polymers* 5 (2004) 122-127.
- [67] C.J. Buchko, L.C. Chen, Y. Shen, D.C. Martin, Processing and microstructural characterization of porous biocompatible protein polymer thin films, *Polymer* 40 (1999) 7397-7407.
- [68] C. Mit-uppatham, M. Nithitanakul, P. Supaphol, Ultrafine Electrospun Polyamide-6 Fibers: Effect of Solution Conditions on Morphology and Average Fiber Diameter, *Macromolecular Chemistry and Physics* 205 (2004) 2327-2338.
- [69] M.M. Demir, I. Yilgor, E. Yilgor, B. Erman, Electrospinning of polyurethane fibers, *Polymer* 43 (2002) 3303-3309.
- [70] P.K. Bhattacharjee, J.P. Oberhauser, G.H. McKinley, L.G. Leal, T. Sridhar, Extensional rheometry of entangled solutions, *Macromolecules* 35 (2002) 10131-10148.
- [71] N. Bhardwaj, S.C. Kundu, Electrospinning: A fascinating fiber fabrication technique, *Biotechnology Advances* 28 (2010) 325-347.
- [72] K.F. Seeram Ramakrishna, Wee-Eong Teo, Teik-Cheng Lim, Zuwei Ma, *An Introduction to Electrospinning and Nanofibers*, World Scientific Publishing Co., 2005.
- [73] H. Fong, I. Chun, D.H. Reneker, Beaded nanofibers formed during electrospinning, *Polymer* 40 (1999) 4585-4592.
- [74] Y. Filatov, A. Budyka, V. Kirichenko, *Electrospinning of Micro-and-Nanofibers: Fundamentals and Applications in Separation and Filtration Process*, Bgell House Inc, 2007.
- [75] Y.X. Li, X.F. Lu, X.C. Liu, C.C. Zhang, X.A. Li, W.J. Zhang, C. Wang, Ultra-low dielectric performance of polymer electrospun nanofiber mats, *Applied Physics - Materials Science & Processing* 100 (2010) 207-212.
- [76] S.J. Kim, C.K. Lee, S.I. Kim, Effect of ionic salts on the processing of poly(2-acrylamido-2-methyl-1-propane sulfonic acid) nanofibers, *Journal of Applied Polymer Science* 96 (2005) 1388-1393.
- [77] P. Heikkilä, A. Harlin, Electrospinning of polyacrylonitrile (PAN) solution: Effect of conductive additive and filler on the process, *Express Polymer Letters* 3 (2009) 437-445.
- [78] F. Yener, O. Jirsak, Development of New Methods for Study of Mechanism of Electrospinning, in: S.g.c.o.F.o.T.E.a.F.o.M. Engineering (Ed.), Workshop, Technical University of Liberec, Světlanka, 2012.
- [79] J.R. Melcher, G.I. Taylor, Electrohydrodynamics - a Review of Role of Interfacial Shear Stresses, *Annual Review of Fluid Mechanics* 1 (1969) 111-&.
- [80] D.R. Lide, *CRC Handbook of Chemistry and Physics*, 90th Edition (CRC Handbook of Chemistry & Physics), CRC Press, 2009.
- [81] Ž. Voršič, Polyurethane as an Isolation for Covered Conductors InTech (2012).
- [82] G.P. Industries, Dielectric constant, in: I. Global Polymer Industries (Ed.), http://globalpolymer.com/documents/uhtm_specs.pdf, 2013.
- [83] J. Zeleny, Instability of Electrified Liquid Surfaces, *Phys. Rev.* 10 (1917) 1-6.
- [84] A.L. Yarin, S. Koombhongse, D.H. Reneker, Taylor cone and jetting from liquid droplets in electrospinning of nanofibers, *Journal of Applied Physics* 90 (2001) 4836-4846.
- [85] Baumgart.Pk, Electrostatic Spinning of Acrylic Microfibers, *Journal of Colloid and Interface Science* 36 (1971) 71-&.

- [86] J.M. Deitzel, J. Kleinmeyer, D. Harris, N.C.B. Tan, The effect of processing variables on the morphology of electrospun nanofibers and textiles, *Polymer* 42 (2001) 261-272.
- [87] M.M. Hohman, M. Shin, G. Rutledge, M.P. Brenner, Electrospinning and electrically forced jets. II. Applications, *Physics of Fluids* 13 (2001) 2221-2236.
- [88] Y.M. Shin, M.M. Hohman, M.P. Brenner, G.C. Rutledge, Electrospinning: A whipping fluid jet generates submicron polymer fibers, *Applied Physics Letters* 78 (2001) 1149-1151.
- [89] X.Y. Yuan, Y.Y. Zhang, C.H. Dong, J. Sheng, Morphology of ultrafine polysulfone fibers prepared by electrospinning, *Polymer International* 53 (2004) 1704-1710.
- [90] X.Y. Geng, O.H. Kwon, J.H. Jang, Electrospinning of chitosan dissolved in concentrated acetic acid solution, *Biomaterials* 26 (2005) 5427-5432.
- [91] Z.Z. Zhao, J.Q. Li, X.Y. Yuan, X. Li, Y.Y. Zhang, J. Sheng, Preparation and properties of electrospun poly(vinylidene fluoride) membranes, *Journal of Applied Polymer Science* 97 (2005) 466-474.
- [92] C.X. Zhang, X.Y. Yuan, L.L. Wu, Y. Han, J. Sheng, Study on morphology of electrospun poly(vinyl alcohol) mats, *European Polymer Journal* 41 (2005) 423-432.
- [93] C. Mit-uppatham, M. Nithitanakul, P. Supaphol, Ultrathin electrospun polyamide-6 fibers: Effect of solution conditions on morphology and average fiber diameter, *Macromolecular Chemistry and Physics* 205 (2004) 2327-2338.
- [94] S. Megelski, J.S. Stephens, D.B. Chase, J.F. Rabolt, Micro- and nanostructured surface morphology on electrospun polymer fibers, *Macromolecules* 35 (2002) 8456-8466.
- [95] H.T. Niu, X.G. Wang, T. Lin, Upward Needleless Electrospinning of Nanofibers, *Journal of Engineered Fibers and Fabrics* 7 (2012) 17-22.
- [96] H.T. Niu, X.G. Wang, T. Lin, Needleless electrospinning: influences of fibre generator geometry, *Journal of the Textile Institute* 103 (2012) 787-794.
- [97] H.T. Niu, T. Lin, Fiber Generators in Needleless Electrospinning, *Journal of Nanomaterials* (2012).
- [98] J. Rebicek, M. Pokorny, V. Velebny, Aligned nano fiber deposition onto a patterned rotating drum collector by electrospinning, *Nanocon*, Brno, 2011.
- [99] J. Chvojka, D. Lukas, Electrospun Nanoyarns Produced Using Special Collectors, in: T. Ltd. (Ed.), 1st Nacocon International Conference, Roznov pod Radhostem, Czech Republic, 2009, pp. 207-210.
- [100] L. Vyslouzilova, J. Chvojka, D. Lukas, Oriented Nanofibrous Layers, in: C. Binetruy, F. Boussu (Eds.), *Recent Advances in Textile Composites*, Destech Publications, Inc, Lancaster, 2010, pp. 187-193.
- [101] J. Chvojka, J.P. Hinestroza, D. Lukas, Production of Poly(vinylalcohol) Nanoyarns Using a Special Saw-like Collector, *Fibres & Textiles in Eastern Europe* 21 (2013) 28-31.
- [102] Y.M. Shin, M.M. Hohman, M.P. Brenner, G.C. Rutledge, Experimental characterization of electrospinning: the electrically forced jet and instabilities, *Polymer* 42 (2001) 9955-9967.
- [103] S.A. Theron, E. Zussman, A.L. Yarin, Experimental investigation of the governing parameters in the electrospinning of polymer solutions, *Polymer* 45 (2004) 2017-2030.
- [104] J.H. He, Y.Q. Wan, J.Y. Yu, Scaling law in electrospinning: relationship between electric current and solution flow rate, *Polymer* 46 (2005) 2799-2801.
- [105] C.K. Lee, S.I. Kim, S.J. Kim, The influence of added ionic salt on nanofiber uniformity for electrospinning of electrolyte polymer, *Synthetic Metals* 154 (2005) 209-212.
- [106] R. Samatham, K.J. Kim, Electric current as a control variable in the electrospinning process, *Polymer Engineering and Science* 46 (2006) 954-959.

- [107] D. Fallahi, M. Rafizadeh, N. Mohammadi, B. Vahidi, Effects of feed rate and solution conductivity on jet current and fiber diameter in electrospinning of polyacrylonitrile solutions, *E-Polymers* (2009).
- [108] M.M. Munir, F. Iskandar, Khairurrijal, K. Okuyama, A constant-current electrospinning system for production of high quality nanofibers, *Review of Scientific Instruments* 79 (2008).
- [109] D. Fallahi, M. Rafizadeh, N. Mohammadi, B. Vahidi, Effect of LiCl and non-ionic surfactant on morphology of polystyrene electrospun nanofibers, *E-Polymers* (2008).
- [110] M.M. Munir, A.B. Suryamas, F. Iskandar, K. Okuyama, Scaling law on particle-to-fiber formation during electrospinning, *Polymer* 50 (2009) 4935-4943.
- [111] D. Fallahi, M. Rafizadeh, N. Mohammadi, B. Vahidi, Effect of Applied Voltage on Surface and Volume Charge Density of the Jet in Electrospinning of Polyacrylonitrile Solutions, *Polymer Engineering and Science* 50 (2010) 1372-1376.
- [112] P.K. Bhattacharjee, T.M. Schneider, M.P. Brenner, G.H. McKinley, G.C. Rutledge, On the measured current in electrospinning, *Journal of Applied Physics* 107 (2010).
- [113] C.J. Angamma, S.H. Jayaram, Analysis of the Effects of Solution Conductivity on Electrospinning Process and Fiber Morphology, *Ieee Transactions on Industry Applications* 47 (2011) 1109-1117.
- [114] P. Pokorny, P. Mikes, D. Lukas, Measurement of Electric Current in Liquid Jet, in: T. Ltd. (Ed.), 2nd Nanocon International Conference, Tanger Ltd., Olomouc, Czech Republic, 2010, pp. 282-286.
- [115] J.M. Deitzel, C. Krauthauser, D. Harris, C. Pergantis, J. Kleinmeyer, Key parameters influencing the onset and maintenance of the electrospinning jet, *Polymeric Nanofibers* 918 (2006) 56-73.
- [116] L. Vysloužilová, P. Pokorný, P. Mikeš, M. Bílek, R. Deliu, E. Amler, K.G. Kornev, D. Lukáš, Characteristic hydrodynamic time of elctrospinning, *Journal: Physical Review E*, (in press) (2013).
- [117] M.B. Khumalo, O. Jirsak, Roller Electrospinning With Regards To Roller Movement, Nonwoven Dept., Technical University of Liberec, Liberec, 2012, pp. 60.
- [118] A.L. Frenkel, A.J. Babchin, B.G. Levich, T. Shlang, G.I. Sivashinsky, Annular Flows can Keep Unstable Films from Breakup-Nonlinear Saturation of Capillary Instability, *Journal of Colloid and Interface Science* 115 (1987) 225-233.
- [119] O.H. Campanella, R.L. Cerro, Viscous-Flow on the Outside of a Horizontal Rotating Cylinder-The Roll Coating Regime with a Single Fluid, *Chemical Engineering Science* 39 (1984) 1443-1449.
- [120] J.S. Tsai, C.I. Hung, C.K. Chen, Nonlinear hydromagnetic stability analysis of condensation film flow down a vertical plate, *Acta Mechanica* 118 (1996) 197-212.
- [121] P.J. Cheng, C.K. Chen, H.Y. Lai, Nonlinear stability analysis of thin viscoelastic film flow traveling down along a vertical cylinder, *Nonlinear Dynamics* 24 (2001) 305-332.
- [122] P.J. Cheng, D.T.W. Lin, Surface waves on viscoelastic magnetic fluid film flow down a vertical column, *International Journal of Engineering Science* 45 (2007) 905-922.
- [123] H.I. Andersson, E.N. Dahl, Gravity-driven flow of a viscoelastic liquid film along a vertical wall, *Journal of Physics D-Applied Physics* 32 (1999) 1557-1562.
- [124] B.S. Dandapat, A.S. Gupta, Solitary waves on the surface of a viscoelastic fluid running down an inclined plane, *Rheologica Acta* 36 (1997) 135-143.
- [125] K. Walters, The motion of an elastic-viscous liquid contained between coaxial cylinders, *J. Mech. Appl. Math.* 13 (1960) 444-461.
- [126] J. Ashmore, A.E. Hosoi, H.A. Stone, The effect of surface tension on rimming flows in a partially filled rotating cylinder, *Journal of Fluid Mechanics* 479 (2003) 65-98.

- [127] P.L. Evans, L.W. Schwartz, R.V. Roy, Steady and unsteady solutions for coating flow on a rotating horizontal cylinder: Two-dimensional theoretical and numerical modeling, *Physics of Fluids* 16 (2004) 2742-2756.
- [128] O.E. Jensen, The thin liquid lining of a weakly curved cylindrical tube, *Journal of Fluid Mechanics* 331 (1997) 373-403.
- [129] A.E. Hosoi, L. Mahadevan, Axial instability of a free-surface front in a partially filled horizontal rotating cylinder, *Physics of Fluids* 11 (1999) 97-106.
- [130] L.W. Schwartz, D.E. Weidner, Modelling of Coating Flows on Curved Surfaces, *Journal of Engineering Mathematics* 29 (1995) 91-103.
- [131] M. Chugunova, R.M. Taranets, Qualitative Analysis of Coating Flows on a Rotating Horizontal Cylinder, *International Journal of Differential Equations* 2012 (2012) 30.
- [132] R.L. Cerro, L.E. Scriven, Rapid Free-Surface Film Flows-Integral Approach, *Industrial & Engineering Chemistry Fundamentals* 19 (1980) 40-50.
- [133] V.V. Pukhnachev, Motion of a liquid film on the surface of a rotating cylinder in a gravitational field, *Journal of Applied Mechanics and Technical Physics* 18 (1977) 344-351.
- [134] E.B. Hansen, M.A. Kelmanson, Steady, viscous, free-surface flow on a rotating cylinder, *Journal of Fluid Mechanics* 272 (1994) pp 91-108.
- [135] M.A. Kelmanson, On inertial effects in the Moffatt-Pukhnachov coating-flow problem, *Journal of Fluid Mechanics* 633 (2009) 327-353.
- [136] D.F. Benjamin, T.J. Anderson, L.E. Scriven, Multiple Roll Systems- Steady-State Operation, *Aiche Journal* 41 (1995) 1045-1060.
- [137] D.H. Reneker, I. Chun, Nanometre diameter fibres of polymer, produced by electrospinning, *Nanotechnology* 7 (1996) 216-223.
- [138] S.J. Kim, K.M. Shin, S.I. Kim, The effect of electric current on the processing of nanofibers formed from poly(2-acrylamido-2-methyl-1-propane sulfonic acid), *Scripta Materialia* 51 (2004) 31-35.
- [139] O. Jirsak, K. Frana, F. Yener, Electrospinning studies: Jet forming Force, in: T. Faculty (Ed.), *Strutex, Liberec, 2012*, pp. 97.
- [140] M. Bellis, 1937 to 1949 - Invention, Research and Development, *Polyurethanes Business Group - Bayer Industries, 2013*.
- [141] T.H. Meyer, Keurentjes, J., *Handbook of Polymer Reaction Engineering*, WILEY-VCH Verlag GmbH & Co. KGaA, Weinheim, 2005.
- [142] J.E. Mark, *Polymer Data Handbook*, Oxford University Press, Inc., 1999.
- [143] K.H. Lee, H.Y. Kim, Y.J. Ryu, K.W. Kim, S.W. Choi, Mechanical behavior of electrospun fiber mats of poly(vinyl chloride)/polyurethane polyblends, *Journal of Polymer Science Part B-Polymer Physics* 41 (2003) 1256-1262.
- [144] D.N. Rockwood, K.A. Woodhouse, J.D. Fromstein, D.B. Chase, J.F. Rabolt, Characterization of biodegradable polyurethane microfibers for tissue engineering, *Journal of Biomaterials Science, Polymer Edition* 18 (2007) 743-758.
- [145] A.J. Fry, Tetraalkylammonium ions are surrounded by an inner solvation shell in strong electron pair donor solvents, *Electrochemistry Communications* 11 (2009) 309-312.
- [146] P.P. Rastogi, A Study on Ion-Dipole Interaction Energy of some Alkali Metal Cations, Halide Anions and Symmetrical Tetraalkylammonium Ions in Different Solvents, *Zeitschrift für Physikalische Chemie* 75 (1971) 202-206.
- [147] O.V. Erokhina, A.V. Artemov, L.S. Gal'braikh, G.A. Vikhoreva, A.A. Polyutov, State of lithium cation in a solution of polyurethane in diethylformamide, *Fibre Chemistry* 38 (2006) 447-449.

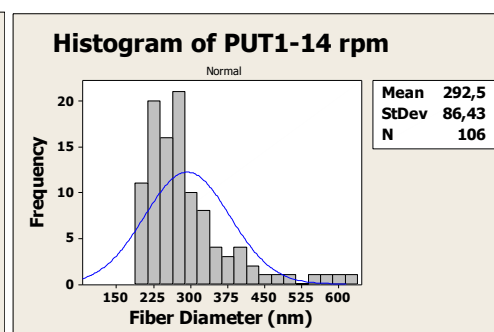
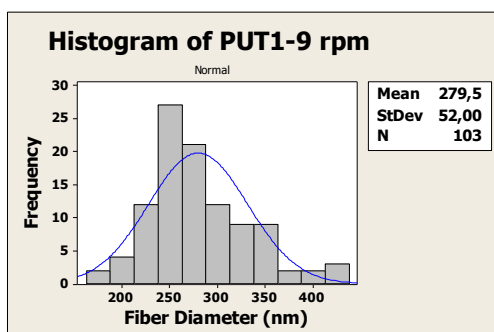
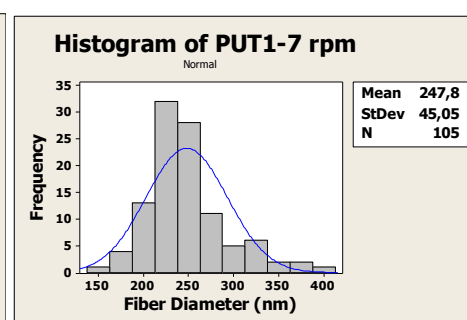
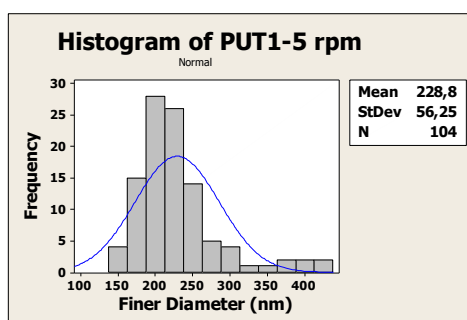
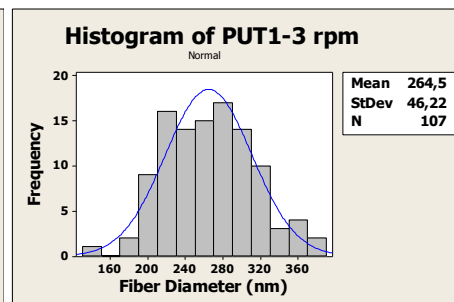
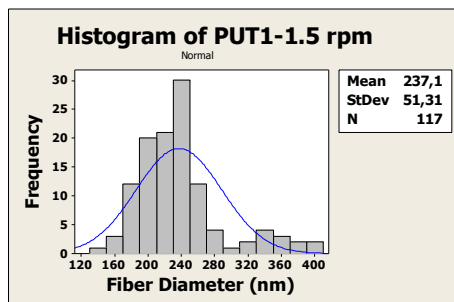
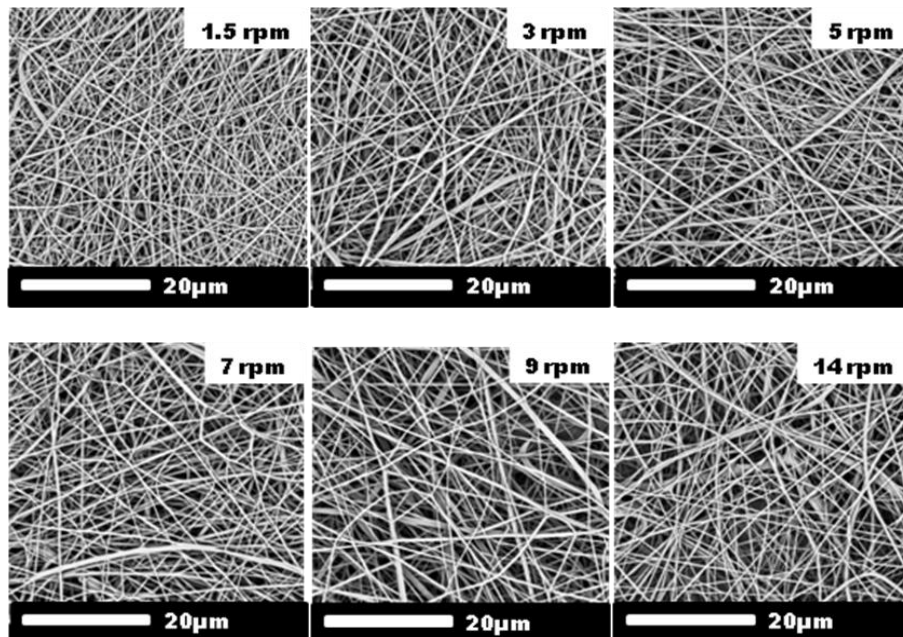
- [148] C.F. Cengiz, O. Jirsak, The Effect of Polymer and Salt Concentration on Fiber Properties in Electrospinning of Polyurethane Nanofibers *Journal of Textiles and Engineer* 20 (2013) 90.
- [149] B. Yalcinkaya, Analysis of Taylor Cone Structure and Jet Life on the Nanofiber Production with Needle and Needle-less Electrospinning Methods, *Textile Engineering*, Suleyman Demirel University, Isparta, 2012, pp. 144.
- [150] F. Sheikh, N.M. Barakat, M. Kanjwal, A. Chaudhari, I.-H. Jung, J. Lee, H. Kim, Electrospun antimicrobial polyurethane nanofibers containing silver nanoparticles for biotechnological applications, *Macromolecular Research* 17 (2009) 688-696.
- [151] C.T. Laurencin, A.M.A. Ambrosio, M.D. Borden, J.A. Cooper, Tissue engineering: Orthopedic applications, *Annual Review of Biomedical Engineering* 1 (1999) 19-46.
- [152] G. Verreck, I. Chun, J. Rosenblatt, J. Peeters, A.V. Dijk, J. Mensch, M. Noppe, M.E. Brewster, Incorporation of drugs in an amorphous state into electrospun nanofibers composed of a water-insoluble, nonbiodegradable polymer, *J Control Release* 92 (2003) 349-360.
- [153] J.D. Ferry, *Viscoelastic Properties of Polymers*, Wiley, Newyork, 1980.
- [154] A. Karmakar, A. Ghosh, Dielectric permittivity and electric modulus of polyethylene oxide (PEO)-LiClO₄ composite electrolytes, *Current Applied Physics* 12 (2012) 539-543.
- [155] G. Collins, J. Federici, Y. Imura, L.H. Catalani, Charge generation, charge transport, and residual charge in the electrospinning of polymers: A review of issues and complications, *Journal of Applied Physics* 111 (2012) 044701.
- [156] A.A. Mazari, O. Jirsak, Relationship Between Needle and Needle-less Electrospinning, MSc. Thesis, Nonwoven, Technical University of Liberec, Liberec, 2011, pp. 66.
- [157] H. Kliem, K. Schroder, W. Bauhofer, High dielectric permittivity of polyethylene oxide in humid atmospheres, in: *IEEE (Ed.), Electrical Insulation and Dielectric Phenomena*, 1996, pp. 12-15 vol.11.
- [158] C. Fanggao, G.A. Saunders, E.F. Lambson, R.N. Hampton, G. Carini, A. Bartolotta, M. Lanza, Frequency dependence of the complex dielectric constant of poly(ethylene oxide) under hydrostatic pressure, *Il Nuovo Cimento D* 16 (1994) 855-864.
- [159] R. Konwarh, N. Karak, M. Misra, Electrospun cellulose acetate nanofibers: The present status and gamut of biotechnological applications, *Biotechnology Advances* 31 (2013) 421-437.
- [160] J.S. Im, J. Yun, J.G. Kim, Y.S. Lee, Preparation and Applications of Activated Electrospun Nanofibers for Energy Storage Materials, *Current Organic Chemistry* 17 (2013) 1424-1433.
- [161] D. Rodoplu, Y. Sen, M. Mutlu, Modification of Quartz Crystal Microbalance Surfaces via Electrospun Nanofibers Intended for Biosensor Applications, *Nanoscience and Nanotechnology Letters* 5 (2013) 444-451.
- [162] M.M.G. Fouda, M.R. El-Aassar, S.S. Al-Deyab, Antimicrobial activity of carboxymethyl chitosan/polyethylene oxide nanofibers embedded silver nanoparticles, *Carbohydrate Polymers* 92 (2013) 1012-1017.
- [163] P. Pokorny, P. Mikes, D. Lukas, Electrospinning jets as X-ray sources at atmospheric conditions, *Epl* 92 (2010).
- [164] J.M. Deitzel, J. Kleinmeyer, D. Harris, N.C. Beck Tan, The effect of processing variables on the morphology of electrospun nanofibers and textiles, *Polymer* 42 (2001) 261-272.
- [165] B. Yalcinkaya, F. Yener, O. Jirsak, F. Cengiz-Callioglu, On the Nature of Electric Current in the Electrospinning Process, *Journal of Nanomaterials*, ID 538179 (2013) 10.

- [166] M.W. Jernegan, Benjamin Franklin's 'Electrical Kite' and Lightning Rod, *The New England Quarterly* 1 (1928) 180-196.
- [167] V. Cooray, *Lightning Protection*, The Institution of Engineering and Technology, 2009.
- [168] J.L.G. Lussac, *Instruction Sur Les Paratonnerres*, Kessinger Publishing, LLC, Paris, 1824.
- [169] M. Nayel, Investigation of Lightning Rod Shielding Angle, in: Ieee (Ed.), *Ieee Industry Applications Society Annual Meeting*, New York, 2010.
- [170] A.V. Rakov, M.A. Uman, *Lightning: Physics and Effects* Cambridge University Press 2003.
- [171] M.A. Uman, *All about Lightning*, Dover Publications, Newyork, 1987.
- [172] C.F. Wagner, G.D. McCann, G.L. MacLane, Shielding of transmission lines, *Electrical Engineering* 60 (1941) 313-328.
- [173] X. Zhang, L. Dong, J. He, S. Chen, R. Zeng, Study on the Effectiveness of Single Lightning Rods by a Fractal Approach, *Journal of Lightning Research* 1 (2009) 1-8.
- [174] M. Komarek, L. Martinova, T. Ltd, Design and Evaluation of Melt-Electrospinning Electrodes, in: T. Ltd. (Ed.), *2nd Nanocon International Conference*, Olomouc, Czech Republic, 2010, pp. 72-77.
- [175] S. Tripatanasuwan, D.H. Reneker, Corona discharge from electrospinning jet of poly(ethylene oxide) solution, *Polymer* 50 (2009) 1835-1837.
- [176] F.J. Higuera, Ion evaporation from the surface of a Taylor cone, *Physical Review E* 68 (2003).

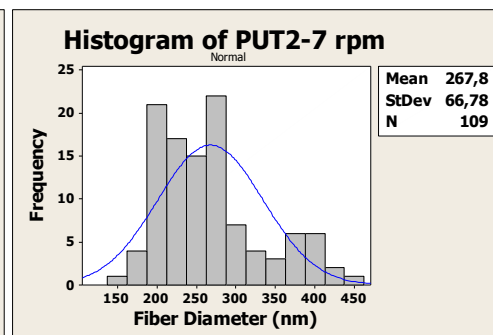
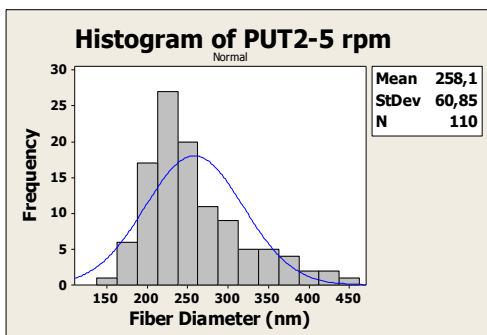
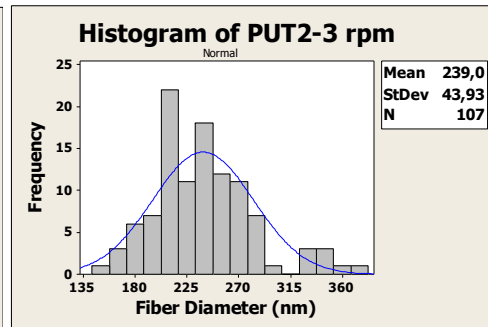
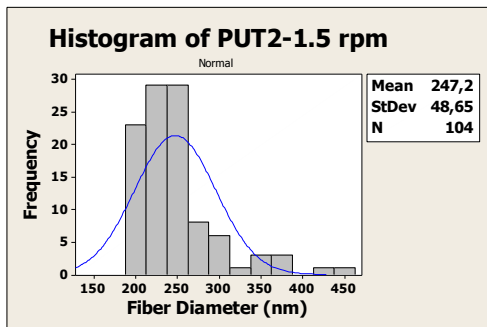
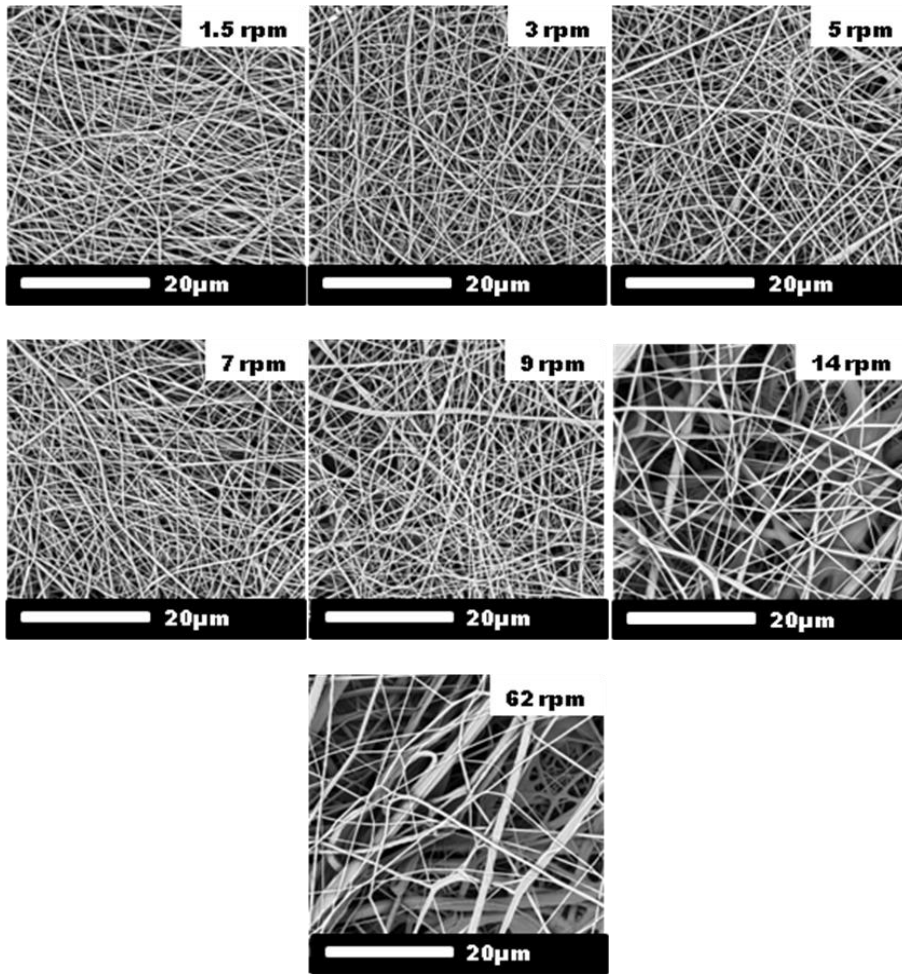
7. APPENDIX

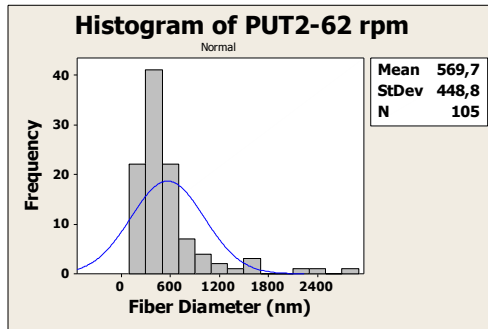
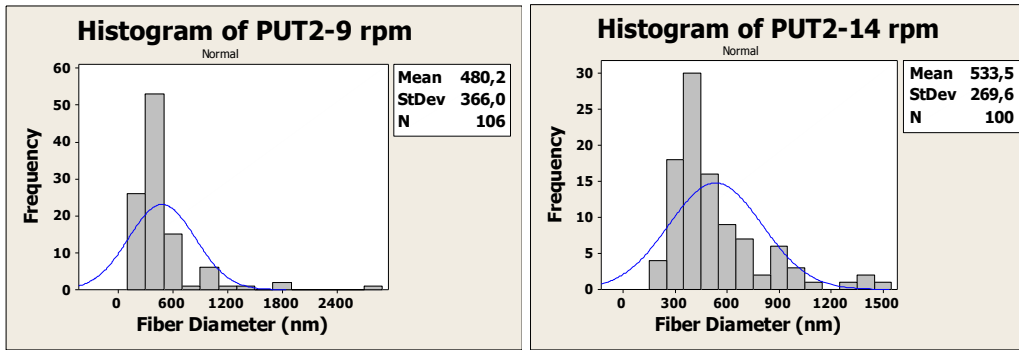
Appendix A: SEM pictures of samples

PUT1 in various rpm:

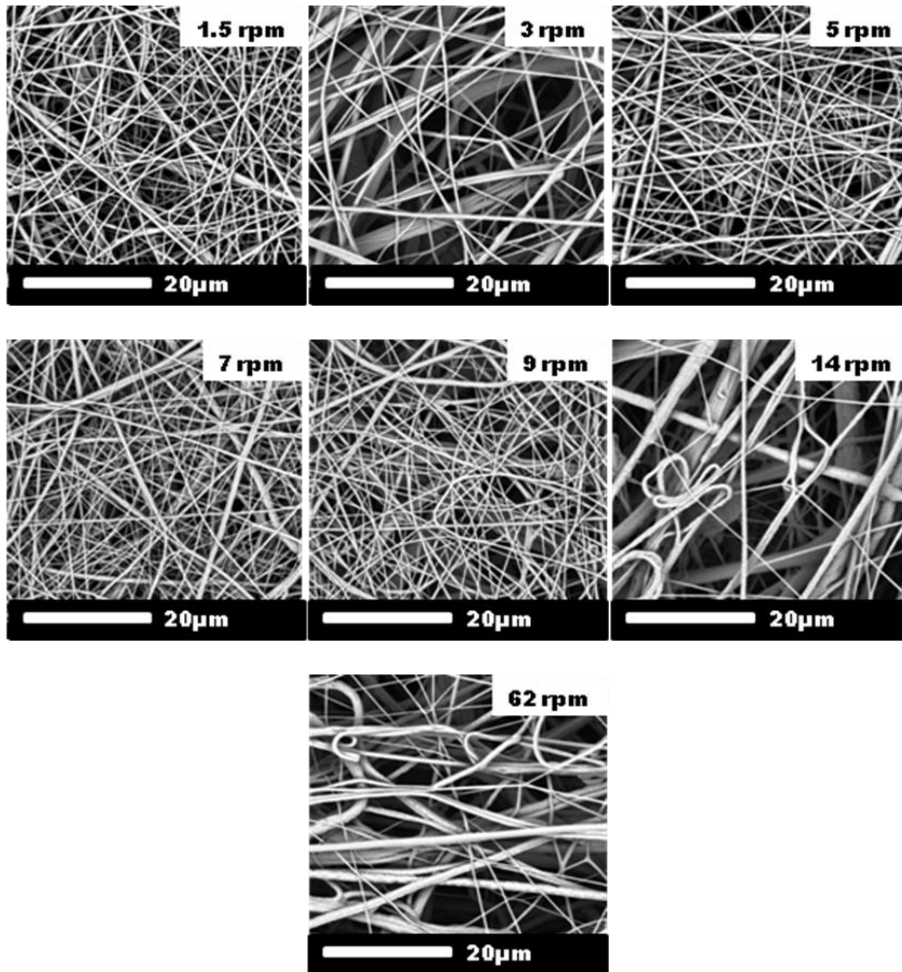


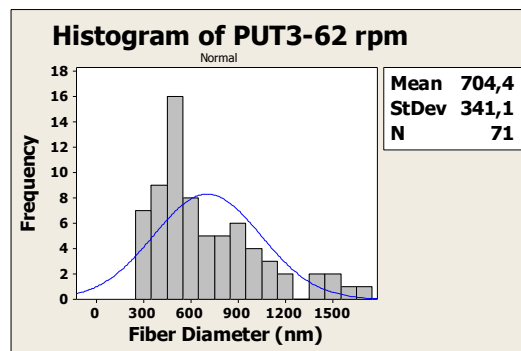
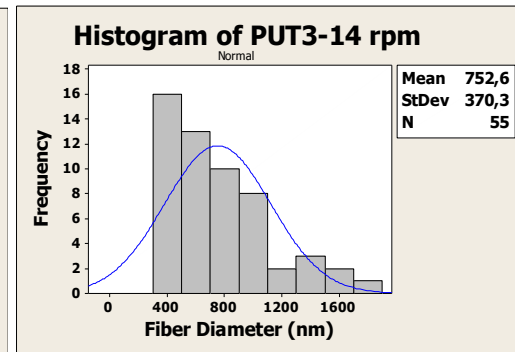
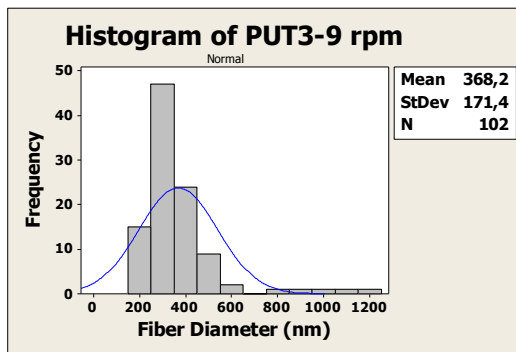
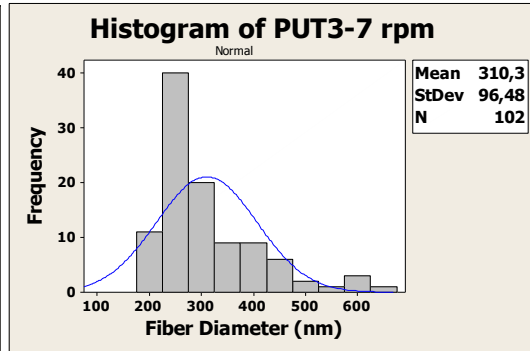
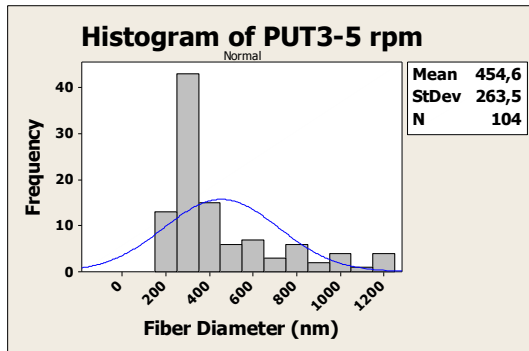
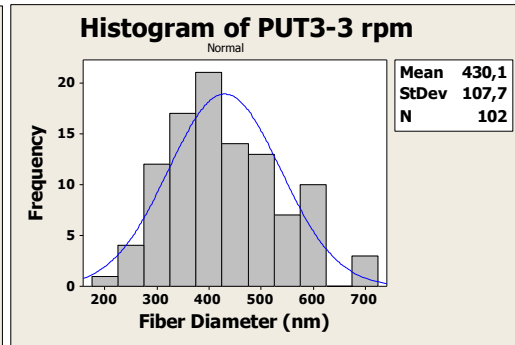
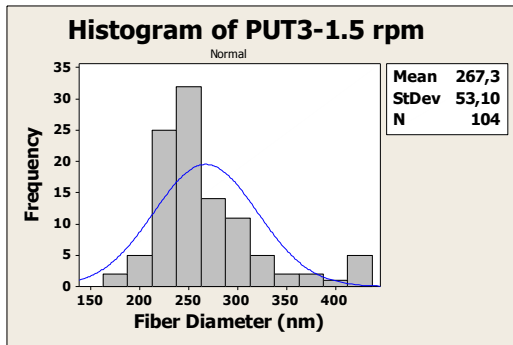
PUT2 in various rpm:



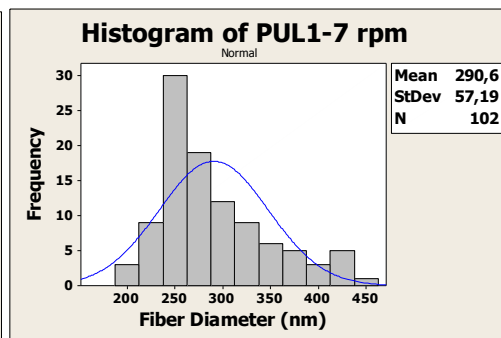
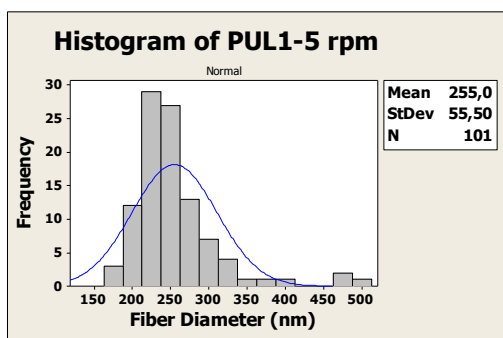
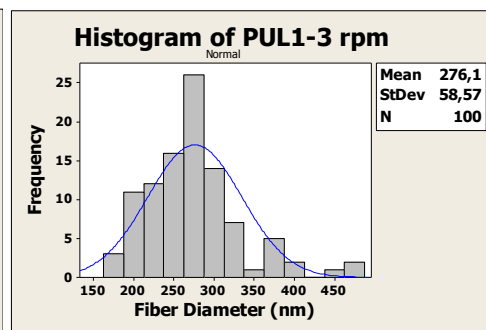
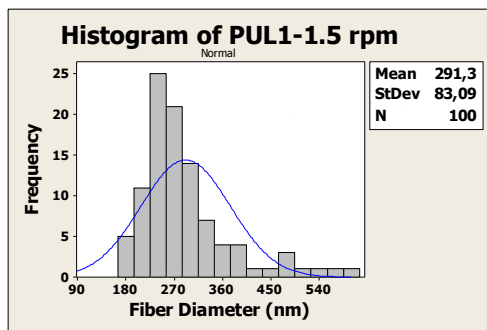
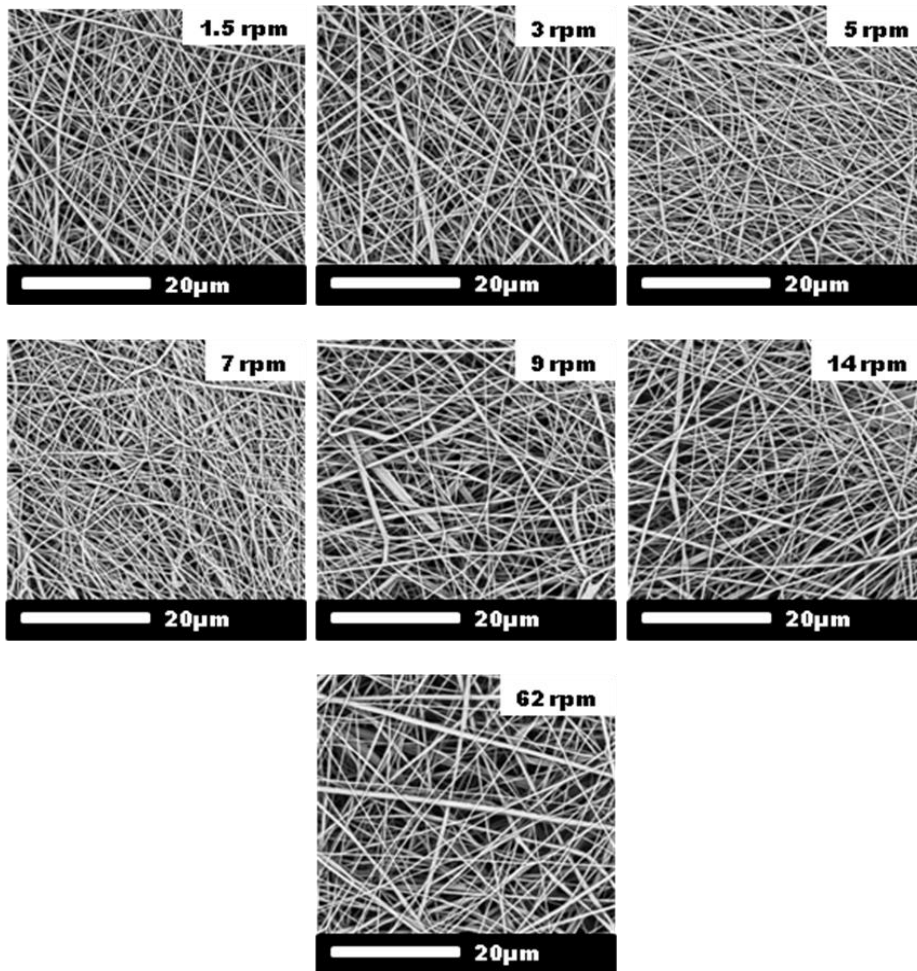


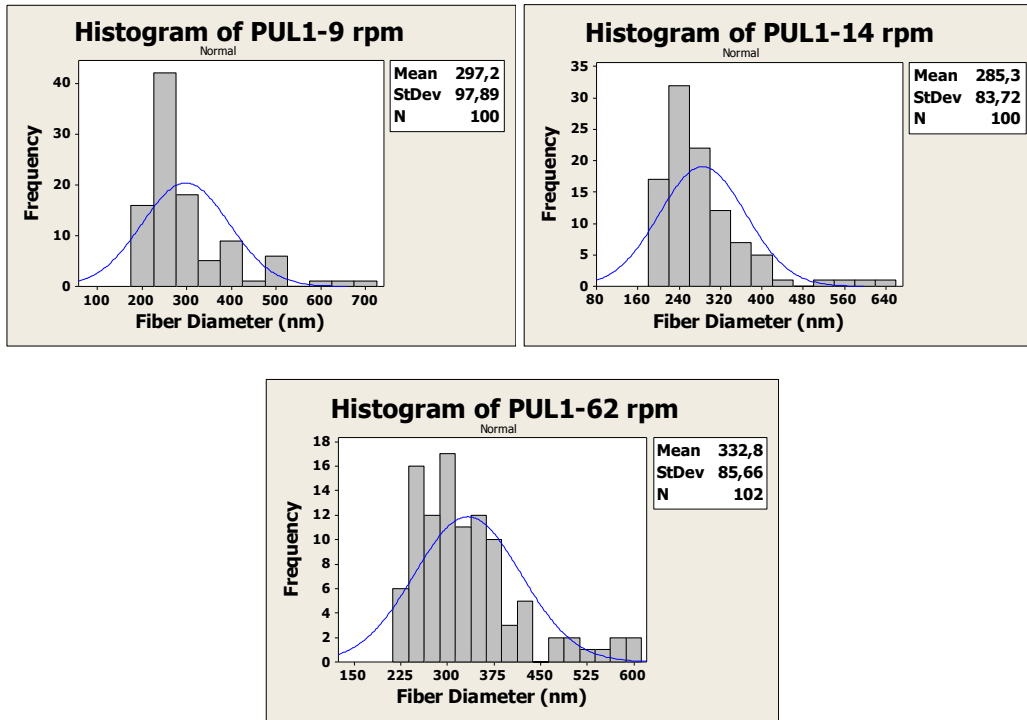
PUT3 in various rpm:



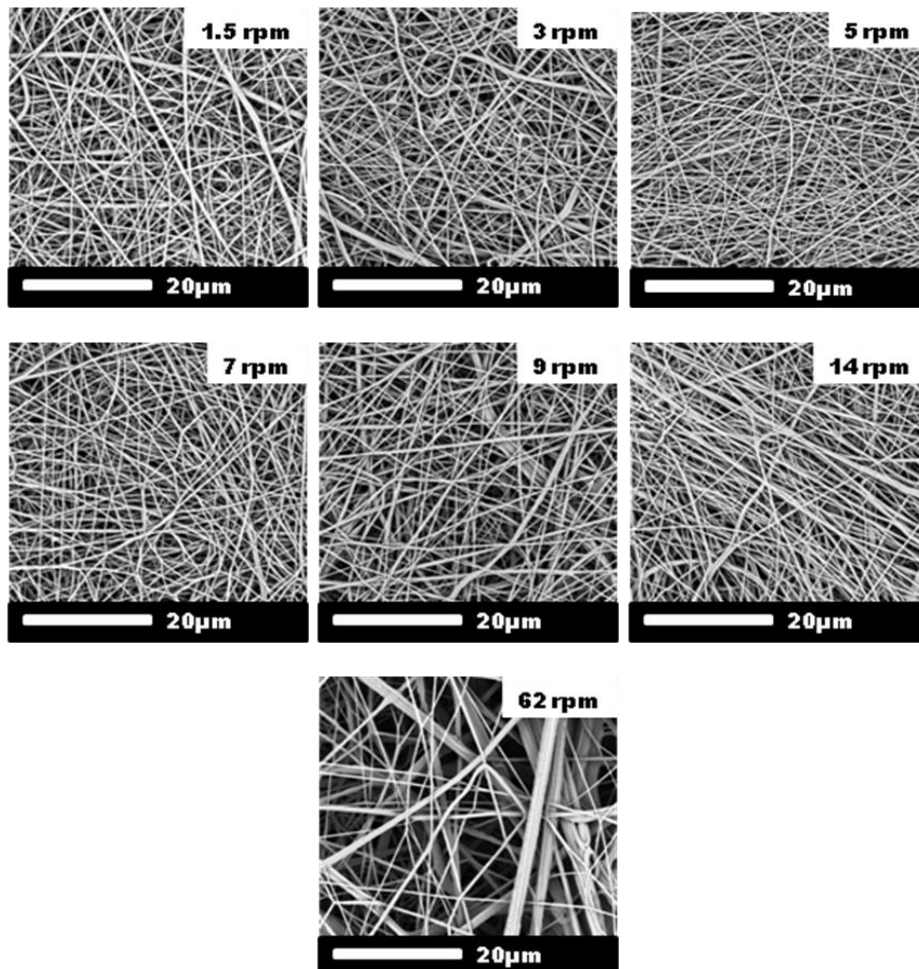


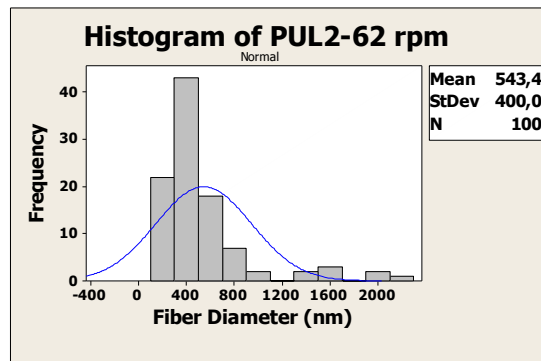
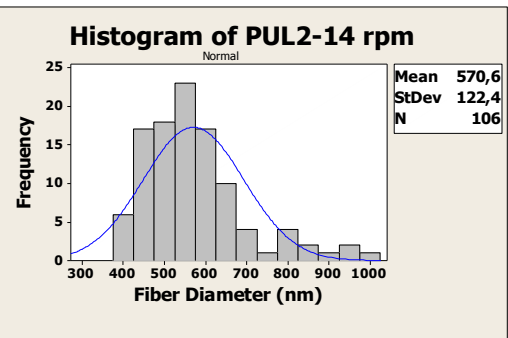
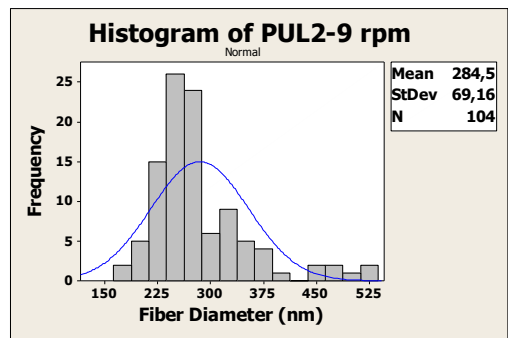
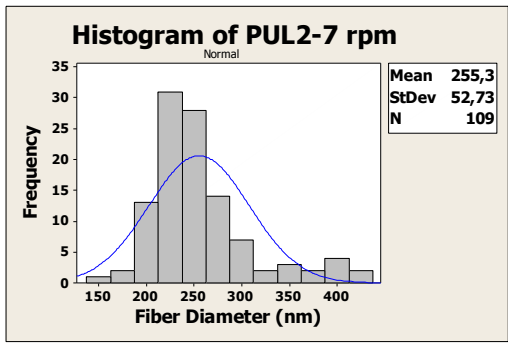
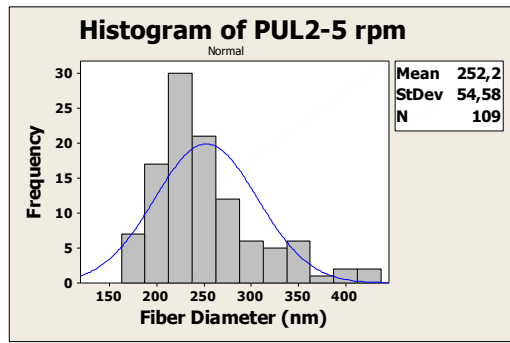
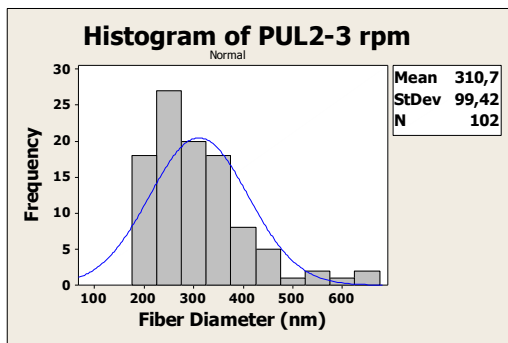
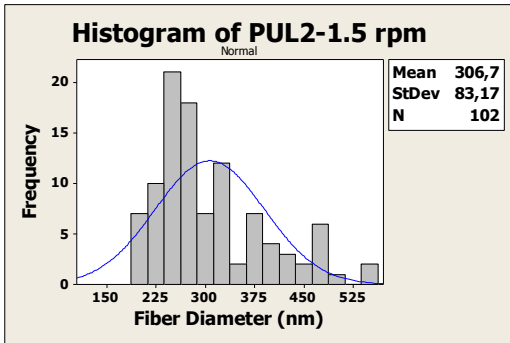
PUL1 in various rpm:



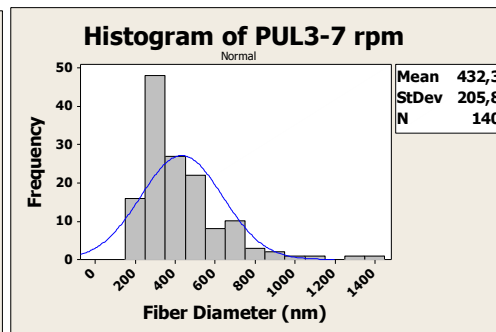
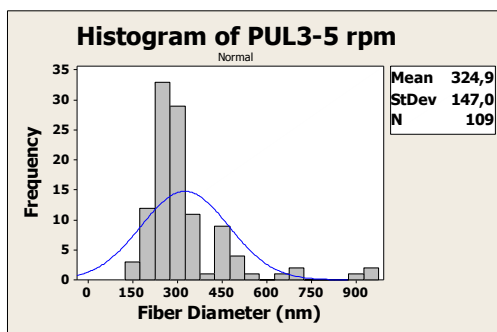
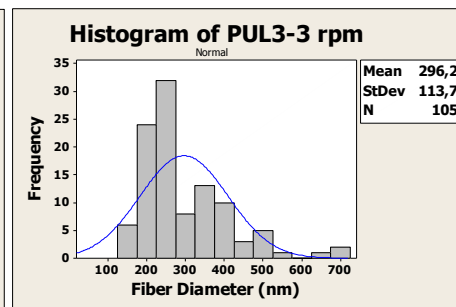
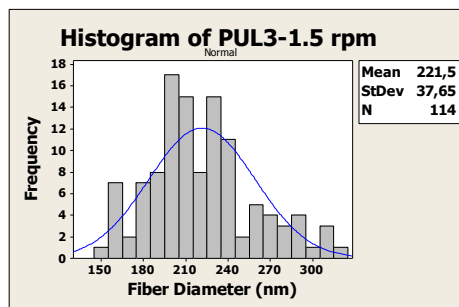
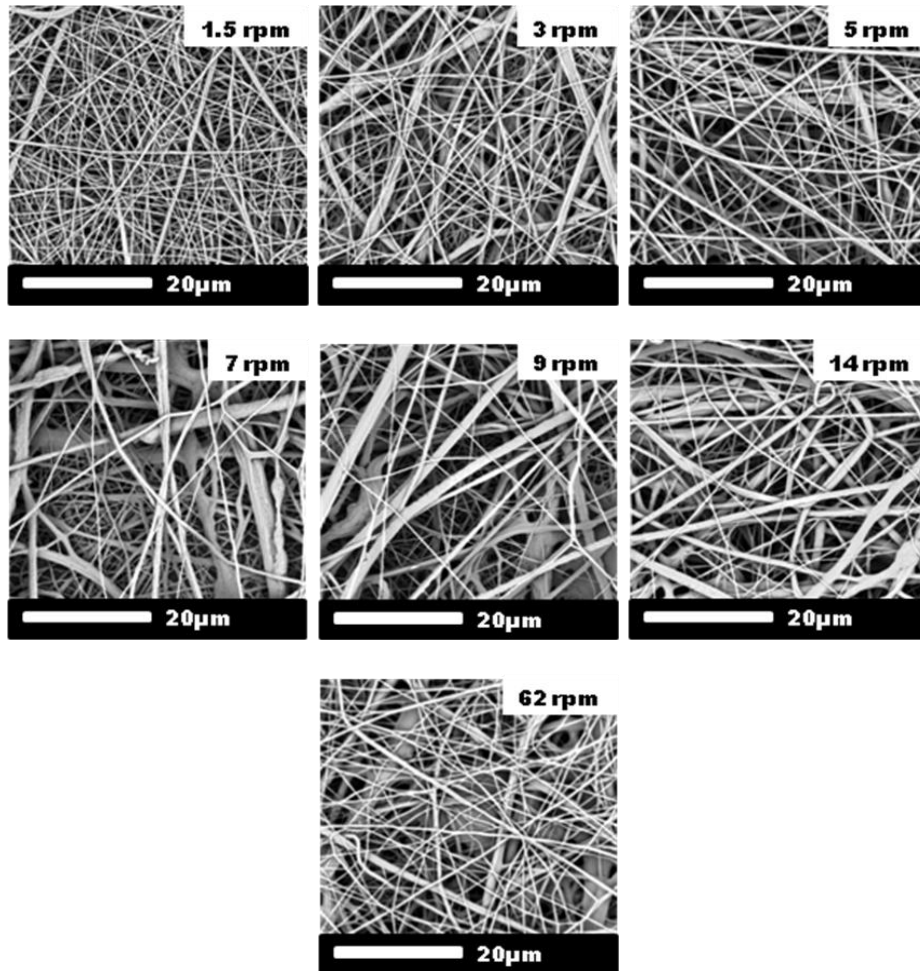


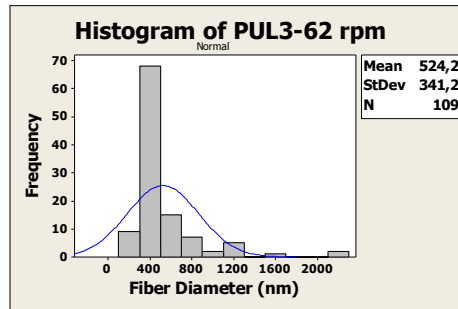
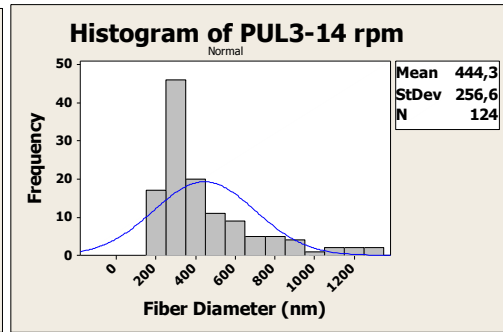
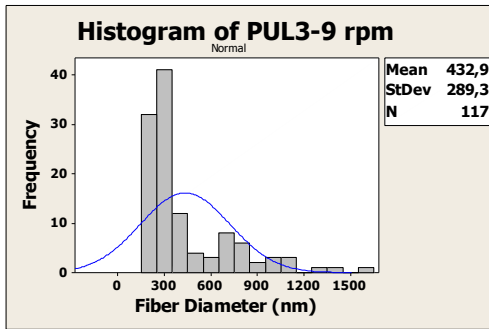
PUL2 in various rpm:



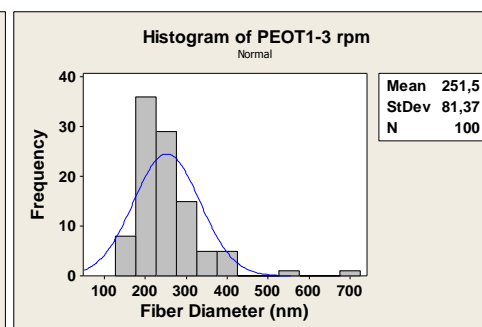
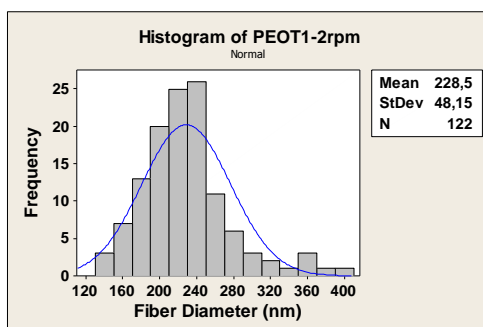
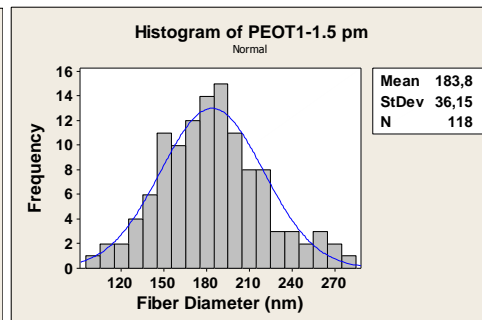
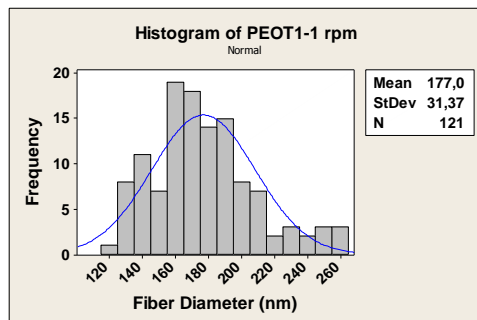
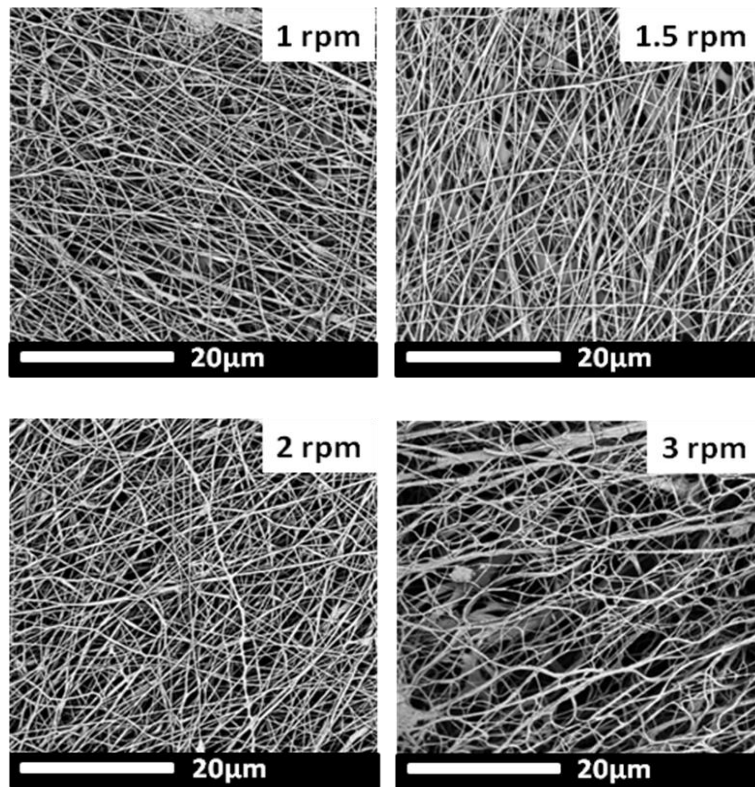


PUL3 in various rpm:

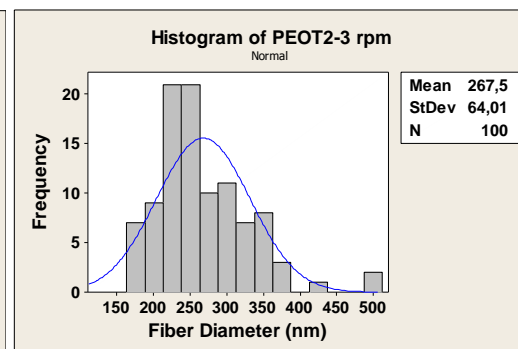
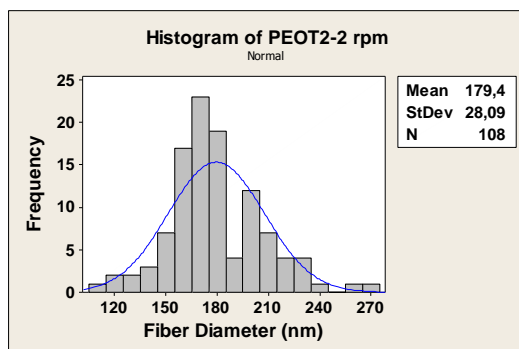
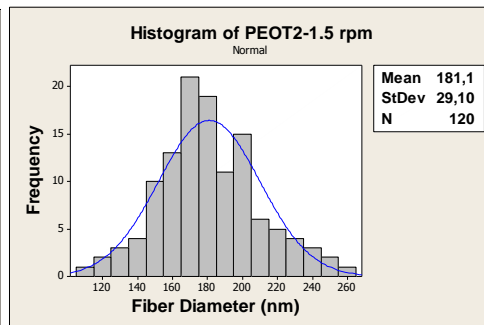
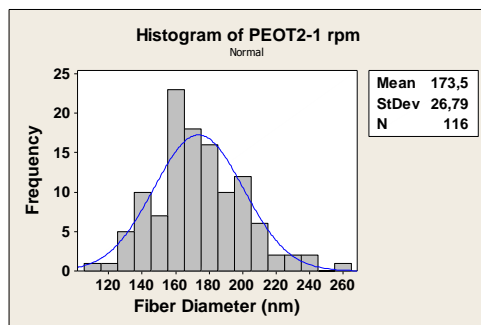
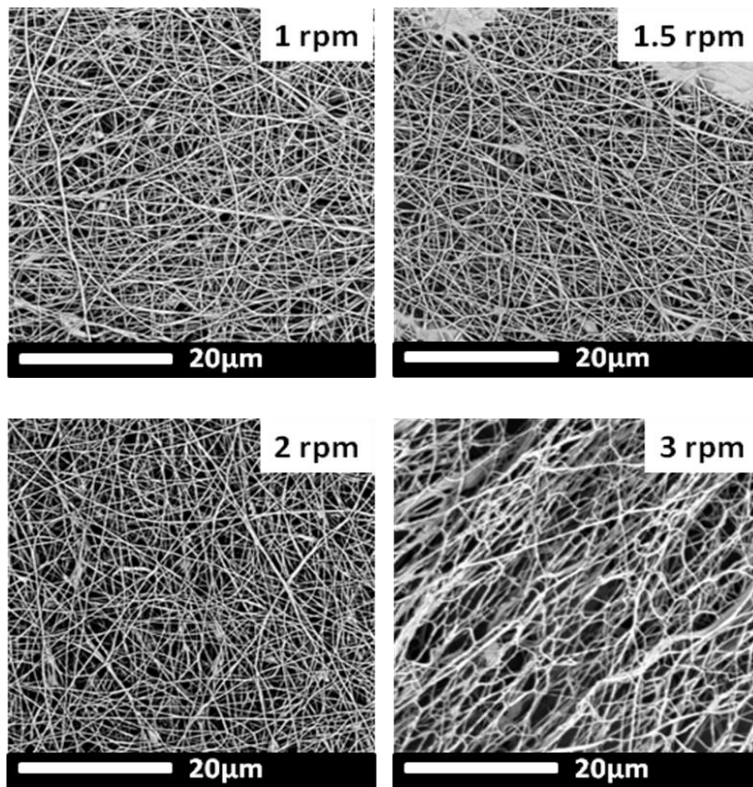




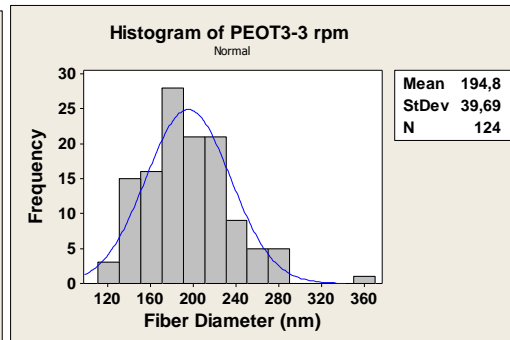
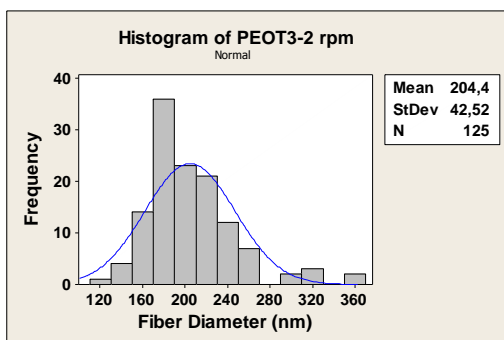
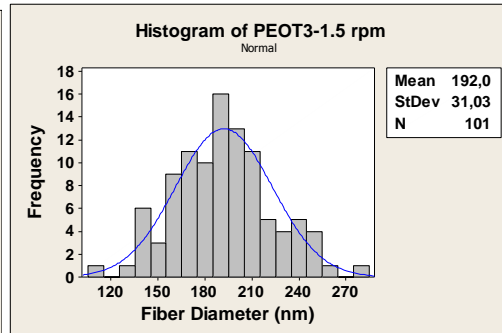
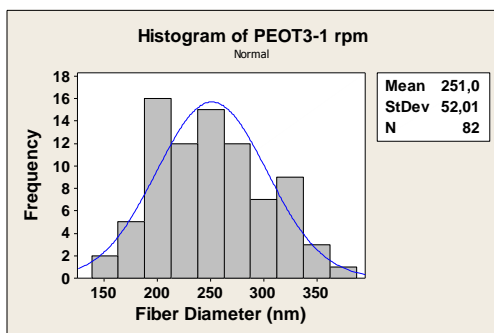
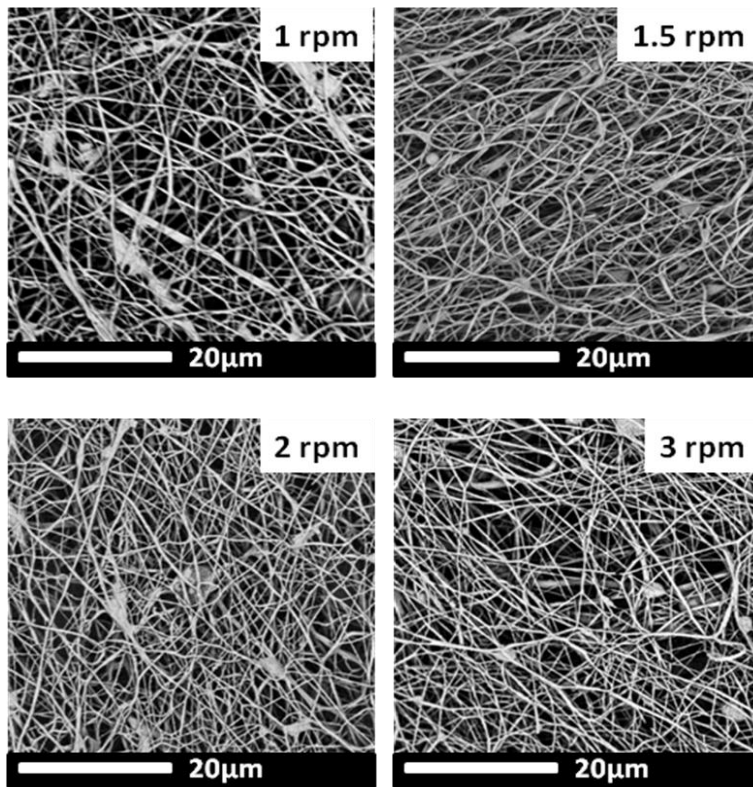
PEOT1 in various rpm:



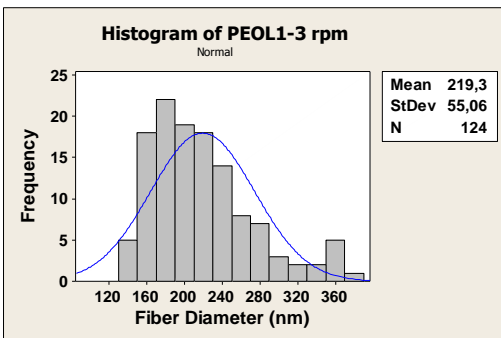
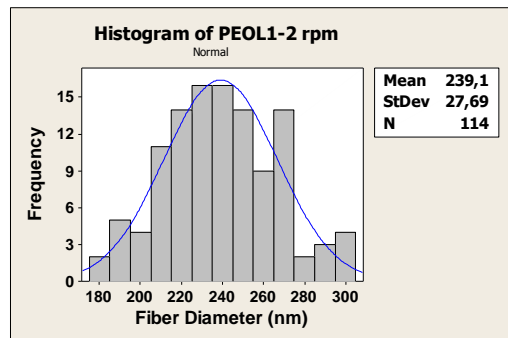
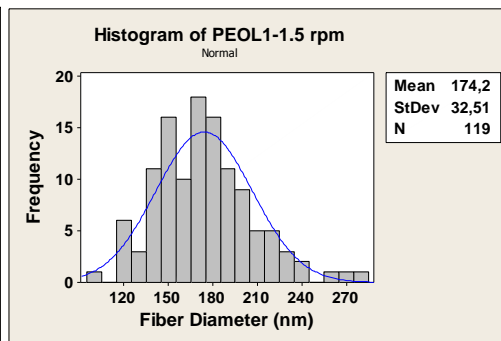
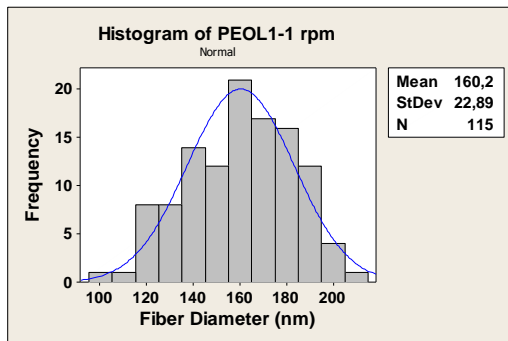
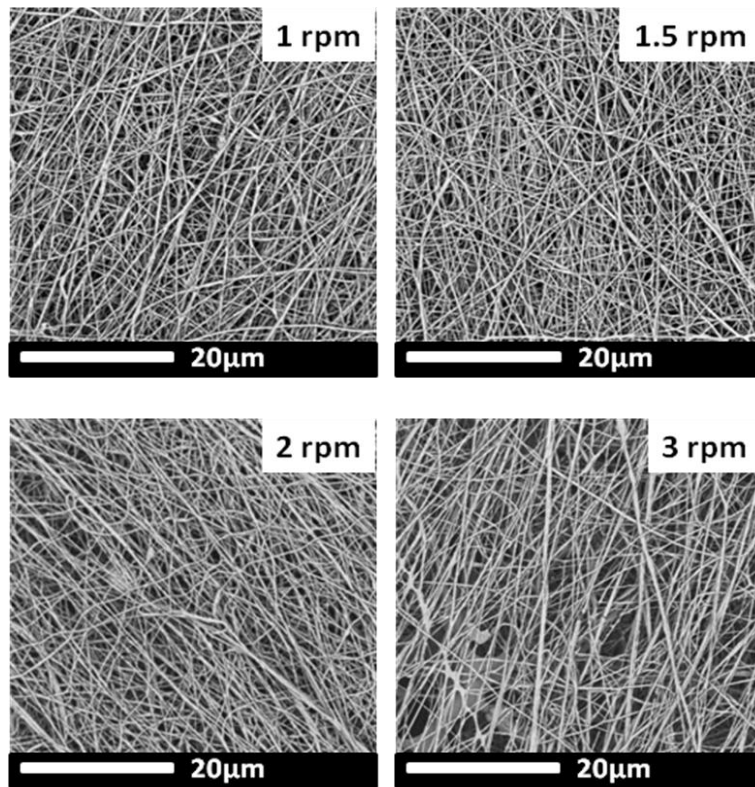
PEOT2 in various rpm:



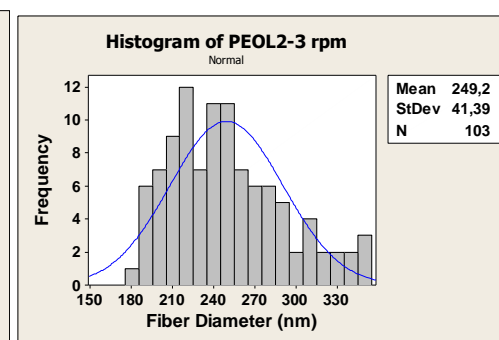
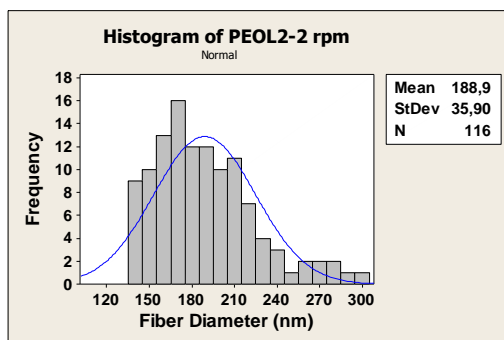
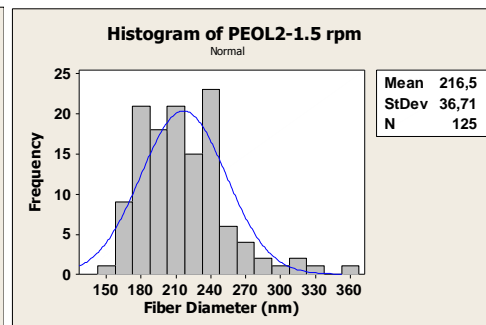
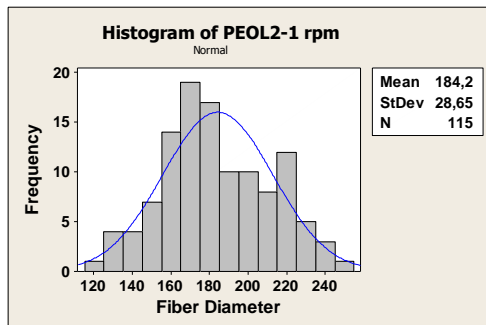
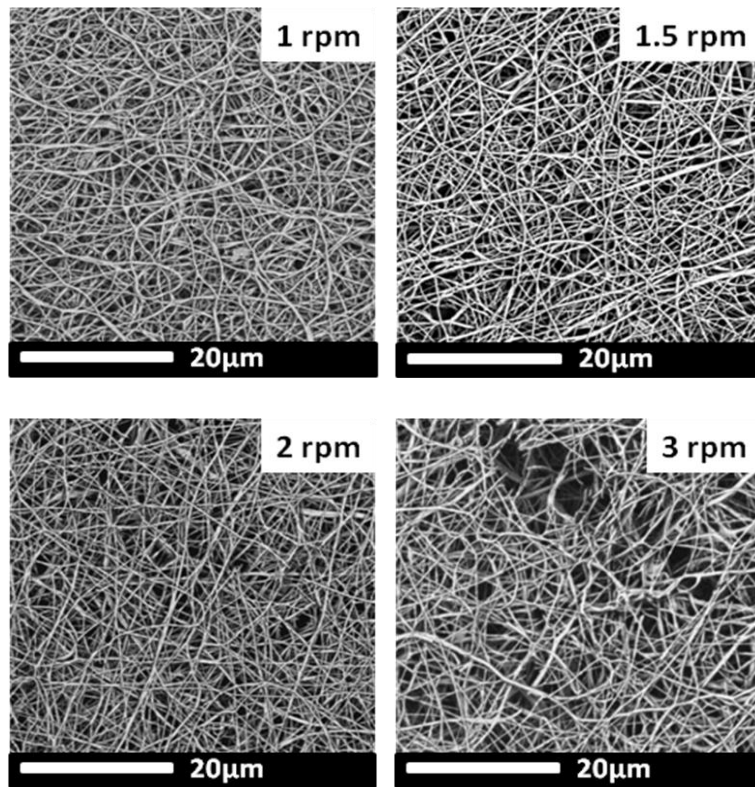
PEOT3 in various rpm:



PEOL1 in various rpm:



PEOL2 in various rpm:



PEOL3 in various rpm:

